

**Container Crystals for Microencapsulation:
Manufacturing and Application Potential**

Dissertation

zur Erlangung des
Doktorgrades der Ingenieurwissenschaften (Dr.-Ing.)

der

Naturwissenschaftlichen Fakultät I – Biowissenschaften –

der Martin-Luther-Universität
Halle-Wittenberg,

vorgelegt

von Frau Dipl.-LebChem. Julia Seidel

geb. am 05.06.1989 in Annaberg-Buchholz

Gutachter:

Prof. Dr.-Ing. Dr. h.c. Joachim Ulrich

Prof. Dr. Gerard Coquerel

Prof. Dr. Hans Roggendorf

Tag der öffentlichen Verteidigung

Mittwoch, 17. Mai 2017

Acknowledgement

An erster Stelle möchte ich mich bei Herrn Prof. Dr.-Ing. Dr. h.c. Joachim Ulrich, meinem Doktorvater, für die Bereitstellung des interessanten Themas bedanken, wobei ich die Freiheiten und das mir damit entgegengebrachte Vertrauen bei dessen Bearbeitung immer zu schätzen gewusst habe. Ich danke Ihnen auch für Ihre stets offene Tür und die Gelegenheit mit Fragen und Problemen zu Ihnen zu kommen. Einen besonderen Dank möchte ich Ihnen an dieser Stelle auch für die vielen Gelegenheiten zu Tagungsteilnahmen und Forschungsaufenthalten aussprechen, welche mir viele schöne Momente aber auch wertvolle Erfahrungen eingebracht haben.

I am grateful to Prof. Dr. Gerard Coquerel who kindly agreed to assess my dissertation and even came all the way from Rouen to Halle to join my defense. Further I would like to thank you for creating the opportunity for me to participate in a great research exchange at the University of Rouen. It was a great time for me where I learned a lot and enjoyed the benefits of your laboratory equipment. Further, I would like to thank Emilie Bobo who took good care for me in all situations during my stay in Rouen from valuable scientific discussions organizing an accommodation to. Another big thank you goes to the entire working group of the SMS lab, especially Lina, Grace, Valerie and Morgan.

Ein großes Dankschön gilt auch Herrn Prof. Dr. Roggendorf, meinem dritten Gutachter. Weiterhin möchte ich Herrn Prof. Dr. Wehrspohn, der sich bereiterklärt hat, den Prüfungsausschuss zu leiten, sowie den übrigen Teilnehmern des Prüfungsausschusses Herr Prof. Dr. Neubert und Frau Prof, Dr. Dailey danken.

Für die Darstellung eines Dissertationsthemas ist es unerlässlich auf die Ergebnisse anderer Autoren zurückzugreifen. Da in diesem Fall das Aussehen anderer Kristalle von großer Bedeutung ist, wurden einige Aufnahmen von anderen Autoren mit eingebaut, um auf deren für diese Arbeit so bedeutenden Ergebnisse aufbauen zu können. Ich danke Herrn Dr. Nordhoff, Herrn Prof. Dr. Ulrich sowie Herrn Prof. Coquerel für die Erlaubnis von ihnen veröffentlichte Bilder zu verwenden. Weiterhin danke ich den Verlagen Elsevier, ACS Publications und dem Wiley-VCH Verlag für die Erlaubnis, die in dieser Dissertation verwendeten Aufnahmen kostenfrei verwenden zu dürfen. Die Quellen der von anderen Autoren veröffentlichten Abbildungen sind jeweils in den Bildunterschriften angegeben.

I would like to thank Prof. Reeves and Dr. Zoltan Aigner from the University of Szeged who allowed me to stay at their institute for three weeks. My thanks also go to Klara and Piroshka who supported me so well in the lab. I would like to thank the DAAD/MÖB who financed this exchange project.

My thanks go to Leila Nemdili for the joint project on the solubility investigations of citric acid. It was my pleasure to work with on this topic. Further, I would like to thank Prof. Koutchoukali for enabling this research exchange.

Ein weiterer Dank geht an das Prorektorat für Forschung und wissenschaftlichen Nachwuchs der Martin-Luther-Universität Halle-Wittenberg, welche mir zweimal durch die Bewilligung von Frauenfördermitteln die Teilnahme an Fachtagungen finanziell ermöglicht hat.

An dieser Stelle möchte ich auch meinen ehemaligen Diplom- und Bachelorstudenten Josefine Skrypek, Melanie Meißner und Karim Awad meinen besonderen Dank aussprechen. Jeder von euch war mir eine sehr große Hilfe bei der Bearbeitung des Themas. Karim, dir möchte ich besonders für die Zeit, die du in die Entwicklung verschiedener Methoden zur Salizylsäureanalytik investiert hast und die vielen generierten Stoffdaten danken. Ich danke dir, Melanie, für die deine endlose Ausdauer beim Kristallnadeln ausmessen am Mikroskop, du warst da wirklich ausgesprochen fleißig. Josefine, dir danke ich für dein Engagement und Durchhaltevermögen bei der Suche nach geeigneten Materialien und entsprechenden Nachweismethoden zum Kristalle befüllen, ich weiß, dass das nicht immer einfach war. Neben den generierten Daten danke ich euch insbesondere für die gemeinsame Zeit, in der auch ich viel dazu gelernt habe.

I would like to thank my ‚HiWi‘-students Christiane and Svitlana who worked motivated and hard for me at the lab, as well. It was my pleasure to work with you.

My thanks also go to my voluntary interns Karnpitcha and Gloria for their interest in the topic and the diligent and motivated work. I really enjoyed working with you.

Ein besonderer Dank gebührt meinen Kollegen in der TVT, die mir zum einen ein sehr angenehmes Arbeitsumfeld geboten haben, sich zum anderen aber auch immer Zeit genommen haben, z.B. für fachliche Diskurse, der Suche nach Geräten oder Chemikalien, die „noch irgendwo sein müssten“, oder dem Lösen von IT-Problemen. Dafür ein dickes Dankeschön an Ronny, Sandra, Kristin und Felix. Weiterhin möchte ich mich bei Anne, Julchen, Martha, Patrick, Haihao, Miaomiao, Xiaoxi, Franzi, Steffi, Jiting, Dr. Sun, Mohammed, Maryam, Ahmed, Claudia, Frau Höser und Gerhard für die unvergessliche Zeit danken.

Die Ehre der letzten Danksagung gebührt meinem Mann, der mich in jeder erdenklichen Weise unterstützt hat.

Table of Contents

1. Introduction	1
2. State of the art.....	2
2.1 Crystallization	2
2.1.1 Solubility, supersaturation and phase diagram	2
2.1.2 Nucleation and crystal growth	3
2.2 Encapsulation by means of crystalline container systems.....	4
2.2.1 Sodium-2-ketogulonate anhydrate	5
2.2.2 Glucose anhydrate.....	5
2.2.3 Sodium acetate	6
2.2.4 Carbamazepine.....	7
2.2.5 Theophylline.....	8
2.3 Mechanism of cavity formation	8
2.3.1 Solvent-mediated phase transformation	8
2.3.2 Mass transport by means of sublimation and/or capillarity.....	11
2.3.3 Formation of inclusions	11
2.4 Influence of gases in the solution on crystallization and inclusion formation	13
3. Motivation	15
4. Materials and methods	17
4.1 Materials.....	17
4.1.1 Salicylic acid	17
4.1.2 Further materials.....	19
4.2 Experimental Methods.....	19
4.2.1 Saturation curve.....	19

4.2.2	Solubility and MZW	20
4.2.3	Growth rate	21
4.2.4	Dissolution rate	23
4.2.5	Degassing	24
4.2.6	Determination of SA solubility in EtOH-water-mixtures	25
4.2.7	Microscopic observations of SA crystals growing during antisolvent crystallization	26
4.2.8	Investigations of experimental parameters on crystal and inclusion sizes .	27
4.2.9	Filling of SA container crystals	31
4.3	Calculations	32
4.3.1	Hansen Solubility Parameters (HSP)	32
5.	Results	37
5.1	Crystallization behavior of SA depending on the presence of dissolved gases	37
5.1.1	Saturation curve	37
5.1.2	Solubility and MZW	37
5.1.3	Growth rate	38
5.1.4	Dissolution rate	40
5.1.5	Determination of HSP for SA and nitrogen in pure solvents	41
5.1.6	Estimation of gas solubility in dependence on SA mole fraction	41
5.2	Solubility of SA in solvent mixtures	43
5.2.1	Solubility of SA in EtOH-water-mixtures	43
5.2.2	Comparison between measured and literature data	44
5.2.3	Model development for SA solubility in solvent-water-mixtures	46
5.2.4	Verification of the HSP solubility prediction model	48
5.2.5	Solubility predictions by means of HSP	49

5.3	Investigations on inclusion containing crystals	50
5.3.1	Single crystal growth observed from antisolvent crystallization.....	51
5.3.2	Shapes of inclusions	53
5.3.3	First enquiry on the effects of experimental parameters on crystal and inclusion sizes	55
5.3.4	Second enquiry on the effects of experimental parameters on crystal and inclusion sizes	61
5.4	Encapsulation of foreign substances inside container crystals	69
5.4.1	Copper sulfate.....	69
5.4.2	Ascorbic acid.....	69
6.	Discussion.....	70
6.1	Finding a model substance.....	70
6.2	Crystallization behavior of SA depending on the presence of dissolved gases	72
6.2.1	Saturation curve, solubility, MZW and crystal growth rate	72
6.2.2	Effects of solution degassing on dissolution rate	73
6.3	Stability of SA crystals in dependence on solvent compositions	74
6.3.1	SA solubility in EtOH-water-mixtures	74
6.3.2	Development of a solubility prediction model for SA in EtOH-water-mixtures	75
6.3.3	Valuation of the used HSP model	76
6.4	Investigations on inclusion containing crystals	77
6.4.1	Effect of growth rates on inclusion formation	77
6.4.2	Investigations on the effects of experimental parameters on the crystal and inclusion sizes	79
6.5	Preparation of filled container crystals of SA	85
6.5.1	Model system SA-AA.....	86

6.5.2	Experimental parameters chosen for preparation of container crystals	87
6.5.3	Potential of inclusion containing SA crystals for application as container crystals	87
7.	Conclusions	90
8.	Summary.....	92
9.	Zusammenfassung	94
10.	Abbreviations and symbols	96
10.1.1	Abbreviations	96
10.1.2	Latin symbols	97
10.1.3	Greek symbols	97
10.1.4	Indices	97
11.	References.....	99
12.	Appendix.....	112

List of Figures

- Fig. 2.1:** Exemplary phase diagram under isobaric conditions; a) Designation of sections of the diagram; b) Events of cooling crystallization illustrated in the phase diagram.17
- Fig. 2.2:** Types of nucleation [Mul01].17
- Fig. 2.3:** Dehydration of SKGM in methanol. Formation of needle-shaped crystals can be observed [Nor99b].19
- Fig. 2.4:** Sodium acetate trihydrate crystals generated by dropping saturated aqueous solution into a) Dry methanol and b) Dry methanol colored with brilliant blue solution [Sch11b].21
- Fig. 2.5:** SEM pictures of carbamazepine crystals from evaporative crystallization: a) Carbamazepine from toluene, b) Carbamazepine dihydrate from methanol [Edd10]. c) Carbamazepine dihydrate crystals generated by means of solvent-mediated phase transformation [Ulr13].21
- Fig. 2.6:** Hollow crystals of theophylline monohydrate a) Grown by means of evaporative crystallization from water (SEM image) [Edd10] and b, c) Prepared by solvent-mediated phase transformation (b: SEM image, c: OM image) [Ulr13].22
- Fig. 2.7:** Mechanism of hollow whisker growth by means of solvent exchange as proposed by Mallet et al. [Mal04]. The ambient antisolvent leads to an increase of the internal pressure of the crystal, especially, close to defects, which results in the formation of droplets of the crystal's material in the incorporated solvent. Due to the high pressure the dissolved material is pushed through the defects outwards and recrystallizes in contact with the antisolvent as tubular whiskers.23
- Fig. 2.8:** Dependence of the internal diameter of SKGA crystal needles on the water content in methanol [Det10b].24
- Fig. 2.9:** Illustrated inclusion formation modeled by Perry et al. [Per13] for the case study salicylic acid: a) Initial crystal growth; b) Initiation of inclusion formation due to limited diffusion and, thus, limited material flux; c) Continued growth with cavity; d)

Closure of inclusion caused by partial dissolution of inner edges and material flux to crystal edges.	26
Fig. 4.1: Molecular structure of SA.	31
Fig. 4.2: a) Solubility of SA in acetone (∇), ethyl acetate (\diamond), methanol (\square), acetic acid (\triangle), acetonitrile (\circ) and water (\times) [Nor06]b) 3D-illustration of SA crystals with labeled faces [Per13].	32
Fig. 4.3: Experimental procedure to determine the saturation curve. Solution with crystals was kept at constant temperature until solution concentration became constant. Solution was removed carefully and its mass fraction was measured by means of refractometer.	34
Fig. 4.4: a) Schematically drawn US setup. It was used to determine solubility and nucleation lines as well as growth and dissolution rates; b) Measure principle of the US probe is based on determining the time a signal transmitted through the solution takes until it is received after a defined distance [Sei17].	34
Fig. 4.5: a) Progression of US velocity-time and temperature-time plots in dependence on experimental procedure. b) Mass fraction-time plot as provided from US velocity-time plot and US velocity-mass fraction calibration, initial (w_0) and final mass (w^*) fraction can be read from the curve.	35
Fig. 4.6: Evaluation of growth rate experiments: a) Convert US velocity to concentration profile which provides initial and final mass fractions as well as their difference (Δw); b) The moment of seed addition is set to zero to fit the w - t -curve.	36
Fig. 4.7: a) Theoretically expected dissolution curve with increasing mass fraction over time; b) US velocity-time plot as revealed during crystal dissolution; c) Mass fraction plotted over time, initial (w_0) and final (w^*) mass fractions as well as dissolution time (Δt) are marked.	38
Fig. 4.8: Scheme of degassing unit. Gases are removed from the initial solution by means of vacuum (300 mbar) through a gas permeable membrane.	38
Fig. 4.9: Setup for determination of solubility of SA in ethanol-water mixtures [Sei16].	40

- Fig. 4.10:** Experimental setup for microscopic observations of SA crystal growth by means of an antisolvent method; a) Sample preparation; b) Microscopic pictures were taken each 5 s; c) Pictures of SA crystal during growth.41
- Fig. 4.11:** Experimental setup for generation of SA crystal needles by means of antisolvent crystallization.41
- Fig. 4.12:** a) Microscopic image of prepared SA container crystals; b) measurement of length and width of the total crystal; c) Measurement of length and width of the inclusion.42
- Fig. 5.1:** a) Saturation curves of SA in MeOH in degassed (∇) and non-degassed solutions (\blacksquare); b) The measured data are complemented by literature data ($*$) published by [Nor06].51
- Fig. 5.2:** Results of solubility and MZW measurements by means of US method for heating rates of a) 2 K h^{-1} ; b) 5 K h^{-1} ; c); 10 K h^{-1} and d) 15 K h^{-1} . The mean values as well as the 95% confidence interval of the curves are depicted.52
- Fig. 5.3:** Growth rates measured at a) $10 \text{ }^\circ\text{C}$ and b) $30 \text{ }^\circ\text{C}$ for degassed and non-degassed solutions.53
- Fig. 5.4:** Progression of US velocity during crystal growth (section 2 in Fig. 4.5b) are completed by number of crystals (RawCounts), D10 crystal length and D90 crystal length measured by ORM.53
- Fig. 5.5:** Dissolution rates of SA in MeOH at a) $10 \text{ }^\circ\text{C}$ and b) $30 \text{ }^\circ\text{C}$ plotted against saturation degree.55
- Fig.5.6:** Dependency of oxygen solubility in methanolic SA solutions on the SA mole fraction based on HSP-SA/[Han07] (Δ) and HSP-SA-ps (\bullet).56
- Fig. 5.7:** Mole fraction solubility of oxygen and nitrogen in SA-MeOH solutions, depending on SA concentration; a) Whole range; b) Saturation mole fraction of SA in MeOH at 10 and $30 \text{ }^\circ\text{C}$ are highlighted.56
- Fig. 5.8:** a) Ternary phase diagram of SA in EtOH and water, measured at $20 \text{ }^\circ\text{C}$; b) Increased section illustrates SA solubility in mass fraction range below 15% SA and 50% EtOH.58

- Fig. 5.9:** Molefraction solubility of SA in EtOH-water-mixtures. Measured data (at 20 °C) are compared to literature data by Matsuda et al. (at 25 °C) [Mat09]; a) Full data range; b) Range of measured data is increased.59
- Fig. 5.10:** Predicted mole fraction solubility of SA in EtOH-water-mixtures based on HSP-SA/ps; a) Full data range; b) Range of measured data is increased.60
- Fig. 5.11:** Predicted data for HSP-SA/ew show good accordance to the literature data [Mat09]; a) Full data range; b) Range of measured data is increased.61
- Fig. 5.12:** Solubility predictions for SA in EtOH-water-mixtures using HSP-SA/ew. Measured data and predictions from HSP-SA/ps are depicted for comparison; a) Full data range; b) Range of measured data is increased.62
- Fig. 5.13:** Literature [Mat09] and predicted data for SA solubility in MeOH-water-mixtures; a) Full data range; b) Range of measured data is increased.63
- Fig. 5.14:** Predicted solubility for SA in water-iso-propanol. a) Mole fraction solubility; b) Mass fraction solubility.64
- Fig. 5.15:** Predicted solubility for SA in water-glycerol-mixtures. a) Mole fraction solubility; b) Mass fraction solubility.64
- Fig. 5.16:** a) Growth rates of (001) crystal face over time for the crystal that is depicted in b-e) Over time.65
- Fig. 5.17:** a) Face growth rate of crystal shown in b) Sections of growth fluctuation are reflected in the thickness of the observed inclusion.66
- Fig. 5.18:** SA crystal containing two funnel-shaped inclusions. a) Since the inclusions already were formed when the measurement could be started b) Only the closure of the inclusions could be observed.67
- Fig. 5.19:** One crystal can even contain inclusions of different types.69
- Fig. 5.20:** Exemplary results of the first, parameter screening step of this enquiry are shown: a) Sample 1-11; b) Sample 1-15; c) Sample 1-16.70
- Fig. 5.21:** a) For each sample of this second step the applied w and IR are summarized. The schematically illustrated crystals are based on the median values for crystal and

inclusion sizes. The illustration allows comparing inclusion and crystal ratios between samples. b) Schematic legend of boxplots as used to describe the results.	71
Fig. 5.22: Prepared crystals show low agglomeration degree and a high particle size distribution; a) Sample 2-6; b) Sample 2-9; c) Sample 3-2.	72
Fig. 5.23: Measured data for a) Crystal length [μm] and b) Crystal volume [μm^3] in dependence on w and IR (second step).	72
Fig. 5.24: Illustration of a) Relative inclusion amount (RIA) [%] and b) Absolute inclusion volume (AIV) [μm^3] in dependence on w and IR (second step).	73
Fig. 5.25: Experimental conditions and median crystal and inclusion sizes of the third step for a) 10 °C and b) 35 °C solution temperature (T_S). The orientation of depicted crystals represents the stirring rate (SR) which is defined exemplarily for Samples 3-4 (250 rpm: ↗) and 3-2 (600 rpm: ↘).	74
Fig. 5.26: Measured data for a) Crystal length [μm] and b) Crystal volume [μm^3] in dependence on solution temperature, degassing and stirring rate (step 3). The experimental conditions for each samples are given in Fig. 5.25.	74
Fig. 5.27: Illustration of a) Relative inclusion amount (RIA) [%] and b) Absolute inclusion volume (AIV) [μm^3] in dependence on temperature (T_S), degassing and stirring rate (third step).	75
Fig. 5.28: Schematic illustration of inclusion containing crystals reflect the median dimensions of all crystals measured in each sample show the effects of stirring rate (SR) at different mass fractions (w) of SA in EtOH.	76
Fig. 5.29: Measured values for crystal sizes in a) Length and b) Volume plotted against the mass fraction (w) of the SA solution for stirring rates (SR) of 100 rpm (white boxes) and 350 rpm (gray boxes).	77
Fig. 5.30: a) Relative (RIA) and b) Absolute (AIV) inclusion amounts of crystals in dependence on mass fraction (w) of the used SA solution (x-axis) and the stirring rate (SR; white boxes: 100 rpm; gray boxes: 350 rpm).	77

- Fig. 5.31:** Schematic illustration of median crystal and inclusion dimensions in dependence on the performance of seeding for different SA mass fractions (w) of the ethanolic solution.78
- Fig. 5.32:** Crystal dimensions expressed in a) Length and b) Volume in dependence on the performance of seeding (white boxes: No seeding; gray boxes: Seeding) plotted against SA mass fraction (w) of the solution.78
- Fig. 5.33:** Measured values for a) Relative and b) Absolute inclusion amounts depending the performance of seeding (white boxes: No seeding; gray boxes: Seeding) plotted against SA mass fraction of the solution.79
- Fig. 5.34:** Illustration of median crystal and inclusion dimensions depending on the direction of injection (water injected into SA solution 'AS>S': White boxes; SA solution injected into water 'S>AS': Gray boxes) at different temperatures and for solution mass fractions (w) of 8 and 15% SA in EtOH.79
- Fig. 5.35:** Crystal dimensions in a) Length and b) Volume depending on the direction of injection (white boxes: Water injected into solution 'AS>S'; gray boxes: Solution injected into water 'S>AS') plotted against the temperature of antisolvent crystallization using solution mass fraction $w=8\%$80
- Fig. 5.36:** a) Relative and b) Absolute inclusion amounts of crystal prepared by injecting water into the solution (white boxes) or solution into the water (gray boxes) plotted against the crystallization temperature of the antisolvent crystallization using a solution mass fraction of 8%.81
- Fig. 5.37:** Crystal dimensions in a) Length and b) Volume in dependence on the injection direction of the antisolvent crystallization (white boxes: Water injected into the solution 'AS>S'; gray boxes: Solution injected into water 'S>AS') plotted against the temperature, SA mass fractions of $w=15\%$ were used.81
- Fig. 5.38:** a) Relative and b) Absolute inclusion amount in crystal depending on the injection direction (water injected into solution 'AS>S': White boxes; solution injected into water 'S>AS': Gray boxes) plotted against crystallization temperature, $w=15\%$82

- Fig. 6.1:** SA amounts that are available for container crystals (at 25 °C) depend on solubility of SA in ambient medium and, thus, on solvent composition, exemplarily illustrated for EtOH-water-mixtures containing 2% SA.**88**
- Fig. 6.2:** Mechanisms to describe the formation of liquid inclusions; a) Diffusion-limited formation of funnel-shaped inclusions of SA [Per13]; b) Observation of macro steps on crystalline surface after induced growth rate enhancement [Sai99]; c) Formation of liquid inclusions depending on the face growth rate [Bob15]; d) Crystal from microscopic growth rate measurements which contains different inclusions.**92**
- Fig. 6.3:** a) Mass transfer coefficients for surface integration (k_r , ■) and volume diffusion step (k_d , ▼) plotted against temperature; b) Dominating mechanisms for growth of SA crystal faces [Per13].**97**
- Fig. 6.4:** Solubility of oxygen and nitrogen in ethanol in dependence on the water amount predicted by means of the HSP model. The gas solubility is decreasing with increasing water content.**97**

List of Tables

Tab. 2.1: Exemplary substances that are reported to form hollow whiskers by solvent-induced phase transformation.	11
Tab. 4.1: Physical properties of SA.	17
Tab. 4.2: Further materials that were used in this thesis.	19
Tab. 4.3: Solubility data for oxygen and nitrogen in MeOH expressed as Ostwald coefficient ($V_{\text{gas}}/V_{\text{MeOH}}$). Based on literature data for saturation solubility [Kre46] the amount of oxygen and nitrogen that remains in solution after degassing at 300 mbar was calculated.	25
Tab. 4.4: Variable conditions of experimental design in first step of parameter identification. Additionally (parameter abbreviations) as well as [units] are given.	29
Tab. 4.5: Variable parameters as performed in step 2.	29
Tab. 4.6: Variable parameters as performed in step 3.	30
Tab. 4.7: HSP for SA, oxygen and nitrogen as provided by [Han00, Han07]. These parameters are based on calculations and estimations based on substance similarities.	33
Tab. 4.8: Solubility data of SA in several pure solvents at 25 °C and the HSP of these solvents from [Han00].	34
Tab. 4.9: Mole fraction solubility of SA in different EtOH-water-mixtures as published by [Mat09].	35
Tab. 4.10: Solubility data for nitrogen in pure solvents 25 °C and solvent HSP [Han00].	36
Tab. 5.1: Results for HSP determination and $\log x-R_g$ -relation for SA and nitrogen.	41
Tab. 5.2: Mole fraction solubility for oxygen and nitrogen at 25 °C in pure methanol, literature and calculated values.	43
Tab. 5.3: HSP for SA determined based on solubility in pure solvents and in EtOH-water-mixtures.	47

Tab. 5.4: An overview of the observed inclusion shapes is presented by schematically illustrations and microscopic images.	54
Tab. 6.1: Overview of the effects of experimental parameters on particle sizes of different APIs as described in literature; Increase: ↗, Decrease: ↘. The effects shown in the table are quite generalized, thus, it should be pointed out that all effects occur within limited ranges.	81
Tab. 6.2: Definitions of mass transfer coefficients k from temperature for surface integration and volume diffusion step as well as the corresponding Arrhenius activation energies E [Lew15].	82
Tab. 6.3: Literature data on the effects of experimental parameters on the inclusion sizes; Increase: ↗, Decrease: ↘.	84
Tab. 12.1: SA mass fraction of saturated solutions measured at different temperatures.	112
Tab. 12.2: Nucleation and solubility temperatures depending on solution mass fraction of SA in MeOH measured by means of US-technique using heating rates of 2 K h^{-1}	112
Tab. 12.3: Nucleation and solubility temperatures depending on solution mass fraction of SA in MeOH measured by means of US-technique using heating rates of 5 K h^{-1}	113
Tab. 12.4: Nucleation and solubility temperatures depending on solution mass fraction of SA in MeOH measured by means of US-technique using heating rates of 10 K h^{-1}	113
Tab. 12.5: Nucleation and solubility temperatures depending on solution mass fraction of SA in MeOH measured by means of US-technique using heating rates of 15 K h^{-1}	114
Tab. 12.6: Growth rates of SA in MeOH measured at $10 \text{ }^\circ\text{C}$	115
Tab. 12.7: Growth rates of SA in MeOH measured at $30 \text{ }^\circ\text{C}$	115
Tab. 12.8: Dissolution rates of SA in MeOH measured at $10 \text{ }^\circ\text{C}$	116

Tab. 12.9: Dissolution rates of SA in MeOH measured at 30 °C.	116
Tab. 12.10: Experimental values of water, EtOH and SA content from investigations of SA solubility in EtOH-water-mixtures.	117

1. Introduction

Microencapsulation is a field of growing interest for a variety of applications. The idea of microencapsulation is based on the encapsulation of a substance and its release under defined conditions, e.g. after a certain time or external effects, like temperature or pressure exposure or pH changes, e.g. [Lor98, Tsu01, Gou04, Sim07, Che08, Riz13]. Potential applications range from epoxy coatings whose weathering and scratch resistance could be improved by modifying them with nanoparticles [Sim05], increased handling safety for pesticides [Tsu01] to drug delivery systems for pharmaceutical applications, e.g. [Lor98, Ben99, Wan06, Riz13, Fre15]. Further, the use of microencapsulation for food and cosmetic applications with focus on protecting reactive, volatile or sensitive ingredients, e.g. flavors or vitamins, or masking unpleasant tastes are discussed in literature, e.g. [Kir91, Ben99, Udd01, Gou04, Fre15]. Even the expansion of cosmetic benefits to textiles by imparting encapsulated cosmetic or pharmaceutical agents into fabrics is in focus of research [Nel02, Che08].

There are described both many different potential applications for microencapsulation and many procedures to prepare them. On the one hand, there are several technologies to prepare microcapsules, like spray drying, spray cooling, centrifugal coextrusion, extrusion, fluidized bed, coacervation and RESS (rapid expansion of supercritical solutions), e.g. [Lor98, Gou04, Ben06]. On the other hand, the development of suitable carrier materials is in focus of encapsulation research. Such carrier systems can be liposomes, cyclodextrines, lipospheres, bi-layer membranes, alginates, polysaccharide based materials, polymers or carbon nanotubes as described, e.g. by [Lor98, Gou04, Ben06, Wan06, Fre15].

According to the high variety of potential applications the development of microencapsulation techniques is a research topic of high interest. The number of developed technologies might be expanded by crystallization. Such an approach was described by Dette et al. [Det10b] and first results could be presented by Schuster et al. [Sch10] and Ulrich et al. [Ulr13]. However, more research needs to be performed in order to verify the applicability of these techniques for potential industrial uses.

2. State of the art

2.1. Crystallization

Crystallization is a thermal separation process that is commonly used as purification process. It is based on the conversion of a liquid, gaseous or amorphous state into an ordered solid phase. The revealed crystals are solid state with a regularly three-dimensional lattice structure which consists of atoms, ions or molecules [Gra97].

2.1.1 Solubility, supersaturation and phase diagram

The solubility of a substance in a solvent is a thermodynamic value that depends on concentration, temperature and pressure. In Fig. 2.1a an exemplary phase diagram under isobaric conditions is depicted. The solubility curve represents the amount of solute that is soluble in a solvent under equilibrium conditions. If the system leaves the equilibrium state, e.g. by supercooling, a driving force, termed as supersaturation S , is created and the system enters the metastable state. The driving force is defined by Eq. 2.1 where C_0 is the initial concentration of the solution and C^* reflects the saturation solubility at the same temperature [Kak12a].

$$S = \frac{C_0}{C^*} \quad 2.1$$

The width of this metastable zone is defined by the appearance of nuclei which is represented in the phase diagram by the nucleation curve. Since this curve is not based on thermodynamic values it actually does not belong in a phase diagram. However, due to its practical meaning for crystallization it is established to depict it in the phase diagram. The position of the nucleation curve can be affected by process conditions, e.g. cooling rate, stirring rate, sample size or presence, type and amount of particles inside the solution [Gra97, Mul01, Mye02, Rod99].

In Fig. 2.1b the crystallization process for a cooling crystallization is illustrated in the phase diagram. In the beginning the process parameters (C_0 , T_0) provide stable conditions for the initial solution. By means of temperature decrease (to T^*) the metastable zone is entered, where the solution's state is termed as 'supercooled', and

passed through until nucleation occurs. Depending on further temperature decrease and crystal growth rate the crystals grow until an equilibrium state (C^*) is reached.

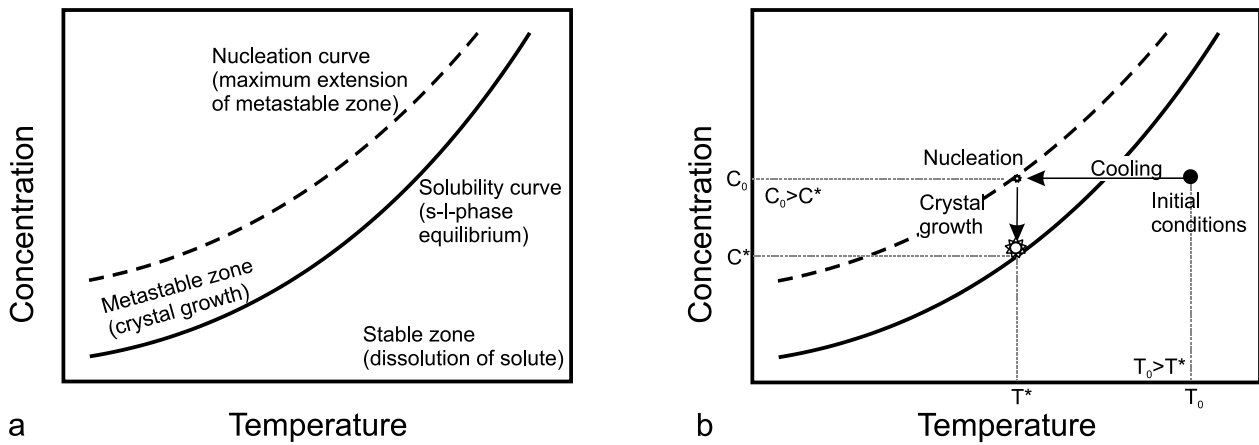


Fig. 2.1: Exemplary phase diagram under isobaric conditions; a) Designation of sections of the diagram; b) Events of cooling crystallization illustrated in the phase diagram.

Besides changes in temperature or pressure there are more possibilities to create a supersaturation. On the one hand, there is the possibility of increasing the solute’s concentration by solvent removal, e.g. by evaporation or freeze out. On the other hand, the solute’s solubility can be decreased, e.g. by the adjustment of pH value, the addition of solvent or can be induced by a chemical reaction [Mul01, Lew15].

2.1.2 Nucleation and crystal growth

If a driving force is created the vital condition for crystallization is nucleation. This initiation of crystallization can be structured as shown in Fig. 2.2 [Mul01].

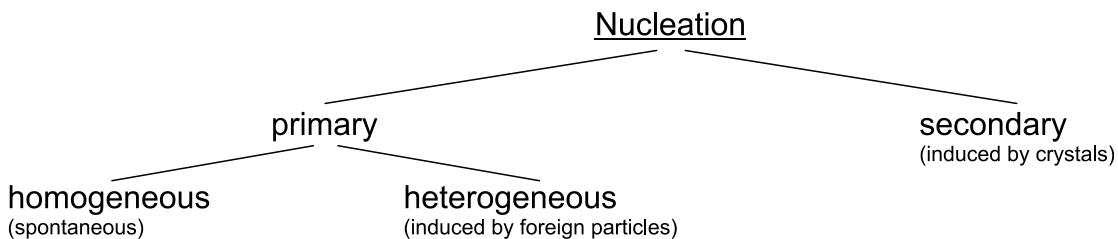


Fig. 2.2: Types of nucleation [Mul01].

Homogenous nucleation happens hardly at sample volumes larger than 100 μL and, thus, is of negligible practical interest. Usually solutions contain some impurities, e.g. dust particles or bubbles, which offer a surface of interface that decreases the energy barrier for nuclei formation. This heterogeneous type of nucleation usually happens if no secondary nucleation is induced by adding seed crystals of the solute material to a supersaturated solution. Secondary nucleation or ‘seeding’ is commonly applied in

industrial crystallization since it allows the performance of the process under low supersaturations and, thus, moderate growth rates which results in better adjustment of morphology and higher purities [Mye02, Mul01, Rod99].

As soon as nuclei are present they start growing to macroscopic crystals depending on the driving force. The growth mechanism can be structured into two steps as follows. First, the solute material has to be transported from the solution to the crystal surface (diffusion step). There, the material can either adsorb to this surface or can be transported diffusion controlled within the boundary layer to a growth site. Secondly, the material is incorporated into the crystal lattice (surface integration step) [Mul01, Mye02, Lew15]. The rate of the growth mechanism, which depends on the temperature, can be limited either by the diffusion or the incorporation step. Between crystal faces the limiting factor and also the growth rates can vary [Per13]. This variation of growth rates of different crystal faces defines the overall crystal shape since the fastest growing faces disappear [Til91, Bob15].

2.2. Encapsulation by means of crystalline container systems

The idea of using hollow crystals as encapsulation technique in pharmaceutical industry is presented, e.g. by Schuster et al. [Sch10] and picked up by Dette et al. [Det10b] and Ulrich et al. [Ulr13]. In these case studies the generation of hollow container crystals caused by a hydrate-anhydrate or anhydrate-hydrate transition using the APIs carbamazepine and theophylline [Ulr13] as well as D-glucose [Det10b, Sch10] as container substances is described. This encapsulation technique is discussed to increase the shelf life of enclosed drugs and offers the possibility of retarded drug release by a slow dissolution of the container material. A further suggestion to use crystalline container systems in pharmaceutical products could be the incorporation of bitter tasting drugs into the container crystals and, thus, an unpleasant taste could be masked. Besides pharmaceuticals another potential field of application could be the generation of food additives. Exemplarily, flavors could be encapsulated inside such container crystals and be released when crystals are chewed [Ulr13].

Several studies on the generation of hollow crystals are already published and a summary of the used substances and methods will be given.

2.2.1 Sodium-2-ketogulonate anhydrate

Sodium-2-ketogulonate anhydrate (SKGA) is a very well investigated model substance in the field of hollow crystal generation and is described in numerous studies, e.g. [Jon06, Det07, Det10a, Det10b, Sch11a, Wac11, Det12]. Sodium-2-keto-L-gulonic acid has industrial meaning as precursor material for ascorbic acid production. If it is suspended in methanol it transforms from the monohydrate form (SKGM) to the anhydrate form (SKGA) under the appearance of needle shaped crystals as depicted in Fig. 2.3 [Nor99b]. Later, it was discovered that the grown crystal needles were hollow [Jon06, Det07] which made it interesting for research.

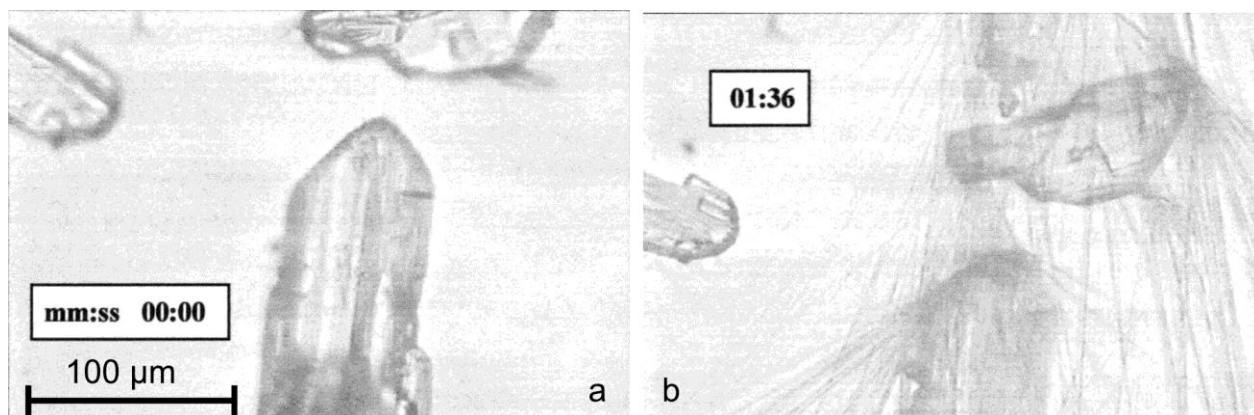


Fig. 2.3: Dehydration of SKGM in methanol. Formation of needle-shaped crystals can be observed [Nor99b].

Sodium-2-keto-L-gulonic acid had an important meaning for the investigations of the mechanism that takes place during solvent mediated phase transformations (Chapter 2.3.1) and the formation of crystal tubes, e.g. [Det10a, Det10b, Sch11a]. However, no proof was reported on that the generated crystal tubes could be filled and closed.

2.2.2 Glucose anhydrate

Dette et al. [Det10b] and Schuster et al. [Sch10] described the idea of using closed crystalline tubes as container systems for pharmaceutical substances. As container substance glucose was used. When glucose monohydrate crystals were suspended in dry methanol at 25 °C for 30 min a solvent mediated phase transformation was induced and hollow anhydrate crystals were generated. After filtration the needle shaped glucose anhydrate crystals were dried for 2 h at 60 °C. During this drying step the crystals' tips sealed. Based on this experimental procedure, crystalline containers could be filled with

ibuprofen and rhodamine 6G solutions by dissolving these substances in the dry methanol before the phase transformation happened.

In case of glucose anhydrate crystals filled with ibuprofen the glucose anhydrate needles were investigated under the microscope according to their size and the enclosed ibuprofen amount was quantified [Sch10]. The average outer diameter of the crystal needles was 2.55 μm and the average length was determined to be 22 μm . Based on these results the cavity dimensions were estimated. A cavity diameter of 1.27 μm and a cavity length of 20 μm were assumed. This led to an expected cavity volume of 25.4 μm^3 , in which up to $1.2 \cdot 10^{-11}$ g ibuprofen could be enclosed theoretically. In order to quantify the ibuprofen amount, 100 mg of crystals were dissolved in 1 mL methanol and measured by means of UV spectroscopy. The ibuprofen concentration of washed crystal needles was determined to be 0.361 mmol L^{-1} . This corresponds to an ibuprofen amount of 1.13 wt-% in 100 mg glucose anhydrate crystals. Due to the comparison between the theoretical and determined ibuprofen amount it was concluded that only approx. 1% of the theoretical possible amount could be enclosed inside the glucose anhydrate crystals.

2.2.3 Sodium acetate

Sodium acetate was chosen as another model system to illustrate the possibility of generating hollow crystal tubes which can be filled and closed [Sch11b]. Crystal containers of sodium acetate trihydrate were generated as in case of glucose monohydrate [Sch10] by dropping a saturated sodium acetate solution into dry methanol [Sch11b]. As a results needle-shaped crystals containing a hollow interior and sealed tips could be observed (Fig. 2.4a). For better visualization the tubes were crystallized in an ethanolic brilliant blue solution which resulted in a blue colored enclosed liquid (Fig. 2.4b).

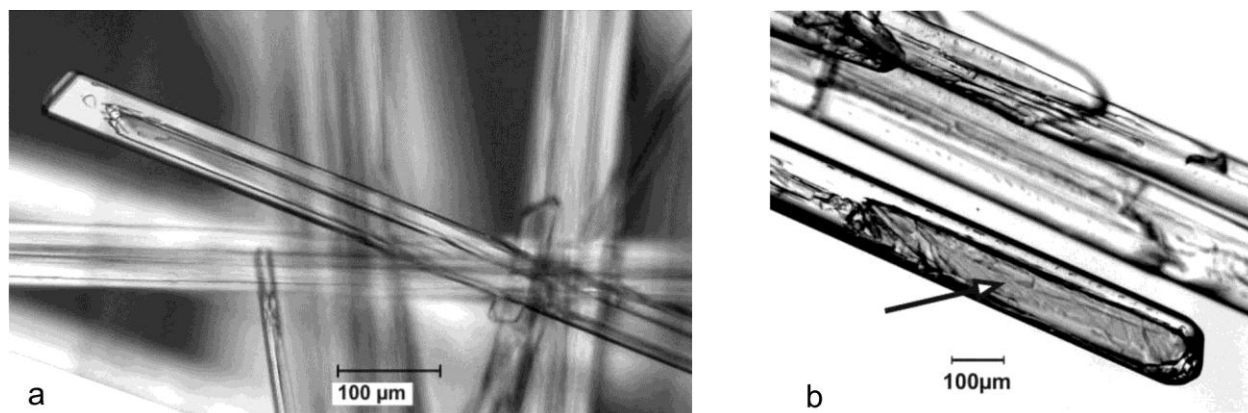


Fig. 2.4: Sodium acetate trihydrate crystals generated by dropping saturated aqueous solution into a) Dry methanol and b) Dry methanol colored with brilliant blue solution [Sch11b].

2.2.4 Carbamazepine

Eddleston and Jones [Edd10] prepared hollow tubular crystals of carbamazepine form II and carbamazepine dihydrate by means of evaporative crystallization. Carbamazepine was crystallized as hollow hexagonal rods from toluene (Fig. 2.5a). The pore diameter ranged along its length from 2 to 10 μm . Carbamazepine dihydrate crystals that grew from methanol (Fig. 2.5b) are described to have a rectangular cross section and the pore diameters range from 5 to 25 μm [Edd10].

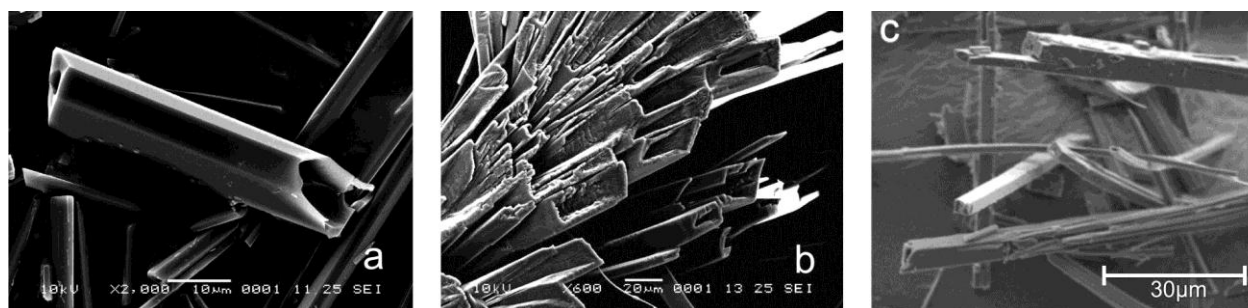


Fig. 2.5: SEM pictures of carbamazepine crystals from evaporative crystallization: a) Carbamazepine from toluene, b) Carbamazepine dihydrate from methanol [Edd10]. c) Carbamazepine dihydrate crystals generated by means of solvent-mediated phase transformation [Ulr13].

Ulrich, Schuster and Stelzer [Ulr13] chose carbamazepine for their studies, e.g. [Sch11b, Sch13], on the use of hollow crystals as coating materials in pharmaceutical industry. By means of a solvent mediated phase transformation the generation of hollow carbamazepine dihydrate crystal needles was observed (Fig. 2.5c).

2.2.5 Theophylline

Tubular crystals of theophylline monohydrate were prepared by Eddleston and Jones [Edd10] using evaporative crystallization from water. The crystals with an approximate rectangular cross section showed pore diameters between 2 and 10 μm (Fig. 2.6a).

It was shown by Ulrich et al. [Ulr13] and Schuster [Sch13] that hollow needle-shaped crystals of theophylline monohydrate can be generated by means of solvent-mediated phase transformation as well (Fig. 2.6b, c). Therefore, theophylline anhydrate was suspended in water, heated up and cooled down again. The tubes could be filled with rhodamine 6G solution and its release was observed after breaking the crystal.

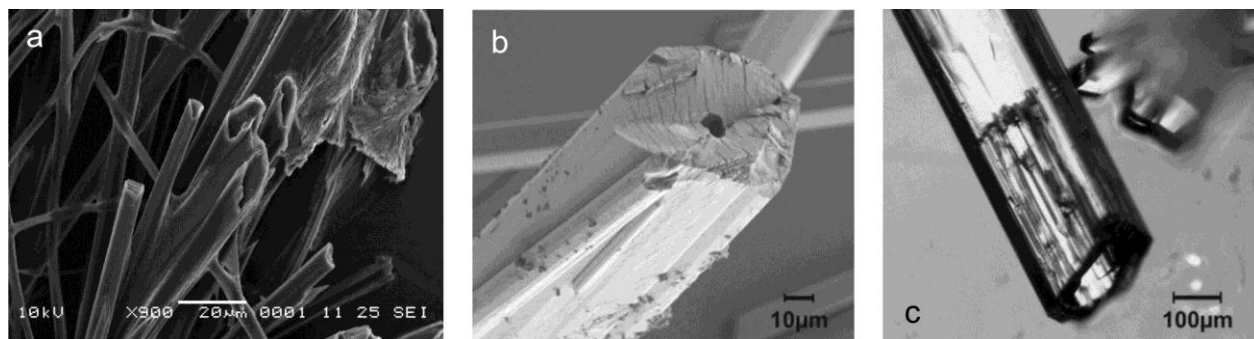


Fig. 2.6: Hollow crystals of theophylline monohydrate a) Grown by means of evaporative crystallization from water (SEM image) [Edd10] and b, c) Prepared by solvent-mediated phase transformation (b: SEM image, c: OM image) [Ulr13].

2.3. Mechanism of cavity formation

As mentioned above many studies where hollow crystals were generated used the mechanism of solvent-mediated phase transformation. But there are other mechanisms described in literature to form hollow crystals or those that contain cavities or inclusions. An overview over known mechanisms is given in this subchapter.

2.3.1 Solvent-mediated phase transformation

Prerequisite for the solvent-mediated or solvent-induced phase transition is that a substance exists in more than one solid phase, like polymorphs (appearance in different modifications) or solvates (incorporation of solvent into the crystal lattice) [Car85]. The basic principle of the phase transition is that one solid structure changes into another solid structure in order to minimize the free energy of the system. This can occur, on the one hand, in a complete transformation in a solid state when the molecules or atoms of

a metastable solid rearrange internally. On the other hand, there is a solvent involved which leads to the dissolution of the metastable form while the stable form can nucleate and grow independently from solution [Car85].

This secondly mentioned mechanism in context of tubular crystal growth named as solvent-induced phase transformation is described in details by Mallet et al. [Mal04]. In their study the formation of hollow whiskers of dexamethasone acetate (DMA) by means of a solvent exchange mechanism was investigated. DMA solvates of DMSO and DMF (incorporated solvents) were generated and these crystals were immersed into the antisolvent phase water at room temperature. After a few minutes a large number of whiskers (needle like crystals) could be observed on the surface of the initial crystal, especially at its corners, edges and defects. By means of XRPD analysis it was found that the whole initial solvate crystal of DMA was transformed to a huge number of needle shaped sesquihydrate crystals within a few minutes. The occurring mechanism was investigated by interrupting the transformation process after 30 s and analyzing the crystals by means of SEM. The observations led to the assumption that the transformation happens through an inward moving interface and can be described as destructive-reconstructive process and is illustrated in Fig. 2.7.

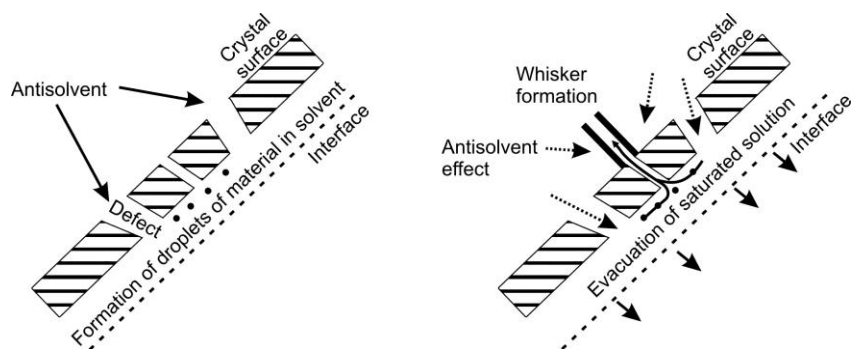


Fig. 2.7: Mechanism of hollow whisker growth by means of solvent exchange as proposed by Mallet et al. [Mal04]. The ambient antisolvent leads to an increase of the internal pressure of the crystal, especially, close to defects, which results in the formation of droplets of the solute in the incorporated solvent. Due to the high pressure the dissolved material is pushed through the defects outwards and recrystallizes in contact with the antisolvent as tubular whiskers.

Based on this model Mallet et al. [Mal04] developed an experimental setup in order to prove this hypothesis. A saturated solution of DMA in DMSO was injected by means of a syringe through a glass filter into water as antisolvent phase. This spray-in-antisolvent-method revealed in a large number of hollow, needle shaped crystals and, thus, the proposed mechanism can be seen as proven.

There are more studies available where similar observations were made using other model substances. Especially, the transformation of SKGM to SKGA (Chapter 2.2.1) under the formation of needle shaped crystals is well described in literature [Nor99a, Bec01, Det10a, Det10b, Car12]. The numerous investigations of this model substance led to important results to help understanding this mechanism. Dette et al. [Det10a, Det10b] reported that the internal diameter of the needle crystals can be influenced by the type of antisolvent and its water amount (Fig. 2.8).

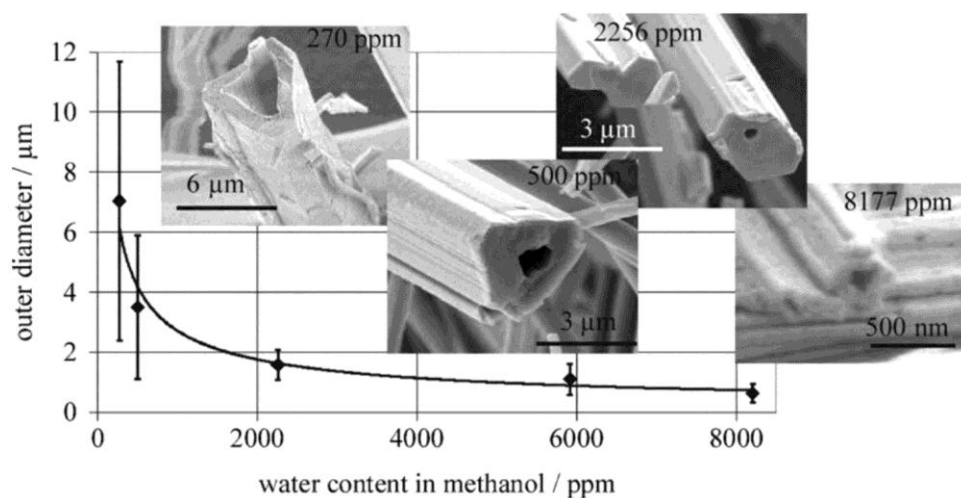


Fig. 2.8: Dependence of the internal diameter of SKGA crystal needles on the water content in methanol [Det10b].

This approach was taken up by Wachsmuth et al. [Wac11] who could further decrease the needle dimensions (to 500 nm outer diameter) by using single crystals of SKGM for needle generation. This concept allowed further clarification of the nucleation of SKGA and confirmed the assumptions made by Mallet et al. [Mal04] that needle growth starts close to defects in crystal surfaces. Schuster et al. [Sch11b] and Schuster [Sch13] used a new technique to generate SKGA needles. Therefore, an aqueous solution of SKGM was dropped into dry methanol. This method led to an increased ratio of hollow needle-shaped crystals while the induction time for the transition could be reduced significantly.

One example where hollow crystals were investigated according to their potential for pharmaceutical uses is given by Paulino et al. [Pau13]. In this study an antisolvent-method to produce hollow crystals of deflazacort monohydrate was used with the aim to improve the dissolution behavior of this poorly water-soluble drug. It was found that the generation of hollow crystal tubes (without stirring) led to a great acceleration of the dissolution rate compared to usually used methods for dissolution improvement, e.g.

micronization. Even though, a phase transformation is not mentioned explicitly the described observations are in good reliability with those made by Schuster in case of SKGM/SKGA (Chapter 2.2.1) or theophylline monohydrate (Chapter 2.2.5) [Sch13].

Further examples of both organic and inorganic substance that are described to form hollow needle-like structures by means of solvent-mediated phase transformation are summarized in Tab. 2.1.

Tab. 2.1: Exemplary substances that are reported to form hollow whiskers by solvent-induced phase transformation.

Organic substances		Inorganic Substances	
D-glucose anhydrate	[Det09]	Barium chloride anhydrate	[Nor99b, Det09]
Sodium acetate trihydrate	[Sch11b, Ulr13, Sch13]	Calcium chloride anhydrate	[Det09]
Theophylline monohydrate	[Ulr13, Sch13]	Copper sulfate anhydrate	[Nor99b, Det09]
Nitrofurantoin monohydrate	[Wik08]	Sodium sulfate anhydrate	[Nor99b, Det09]
Caffeine hydrate	[Wik08]		
Carbamazepine dihydrate	[Wik08, Sch11b, Ulr13, Sch13]		

2.3.2 Mass transport by means of sublimation and/or capillarity

Such a chimney-like growth as described above (Fig. 2.7) cannot only be observed in case of solvent-mediated phase transformation. Martins et al. [Mar11] described for several compounds (glycine, salicylic acid, saccharin, barbital, phenobarbital, various hydantoin derivatives, succinic acid, caffeine, theophylline anhydrate, acetanilide and acetamide) comparable observations when the substances were heated on a Kofler bench. This led to the growth of crystal tubes from the heated material (powder or single crystals) upwards. The mechanism is described to be based on heat dissipation combined with matter transport caused by sublimation and/or capillarity effects. Thus, the material melts due to the induced heat and the convection leads to the transportation of the material upwards, which recrystallizes in a similar chimney-like mechanism.

This study demonstrates that hollow crystal structures can be generated without the need of a phase transformation. Even substances without the affinity to form polymorphs or solvates, like salicylic acid, could be crystallized in a hollow, whisker-like shape.

2.3.3 Formation of inclusions

Inclusions are one kind of impurities that are incorporated into the lattice of the host crystal. Besides these three-dimensional or phase defects, which can be solid, liquid or gaseous, zero-, one- and two-dimensional surface defects exist as well [Zha99]. In the

context of 3D or macroscopic defects very often inclusions containing a liquid and a gaseous phase can be observed.

The mechanism of cavity or inclusion formation is based on a fast growth of crystal faces [e.g. Den66, Wil77, Sai99, Mik05, Zha05, Edd10, Wal11a, Per13, Cao13, Bob15, Bob16a]. This can lead to the fast growth of the crystal edges while the growth in the center of the crystal face is inhibited due to a limited flux of material (Fig. 2.9a and b). This effect is continuing since the faster the crystal edges grow the deeper gets the occurring indent (Fig. 2.9c). The appearance of this type of crystal growth can be observed, e.g. in case of cooling crystallization with [Den66, Zha05] and without [Cao13] the presence of solvent as well as in evaporative crystallization [Nor06, Edd10]. The inhibition of the growth at the center of the crystal faces is discussed to be induced by a limited diffusion [Edd10, Cao13, Per13] which can be caused or intensified by the adsorption of foreign particles or even gas bubbles [Wal11a]. In several studies it is discussed that a critical crystal size is necessary to observe the formation of inclusions [Den66, Wil77, Cao13, Bob16b].

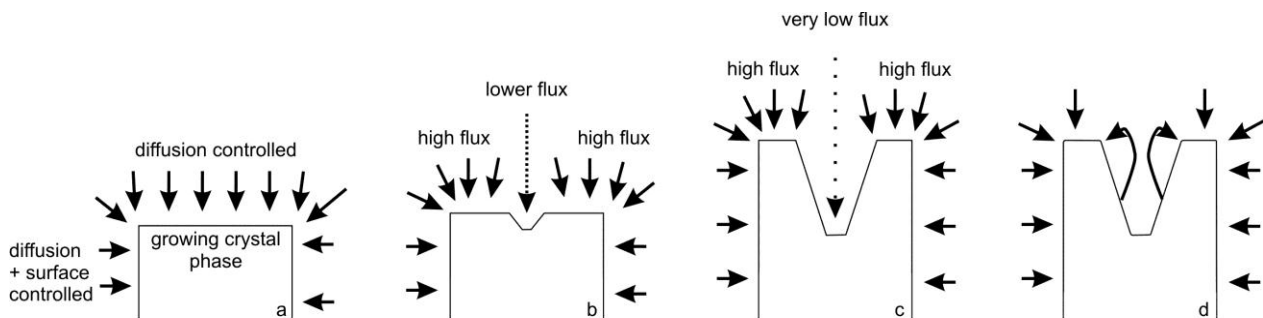


Fig. 2.9: Illustrated inclusion formation modeled by Perry et al. [Per13] for the case study salicylic acid: a) Initial crystal growth; b) Initiation of inclusion formation due to limited diffusion and, thus, limited material flux; c) Continued growth with cavity; d) Closure of inclusion caused by partial dissolution of inner edges and material flux to crystal edges.

In case of crystallization from solution it can be observed that the formed cavities close over and thus liquid inclusions that can be described as pockets of saturated solution [Zha05]. The reason for this phenomenon might be found in a decrease of growth rates by the end of the crystallization process [Den66, Bob16a]. Another explanation might be that due to equilibrium conditions the inner edges (inclusion edges) dissolve followed by diffusion toward the crystal edges where the material recrystallizes and, thus, the inclusion is closed [Per13] (Fig. 2.9d).

2.4. Influence of gases in the solution on crystallization and inclusion formation

Usually the influence of dissolved gases is hardly part of interest for studies on crystallization. However, as mentioned above gases are discussed to play a role in case of inclusion formation and, thus, an overview over known effects of dissolved gases or gas bubbles on crystallization behavior will be summarized.

The effect of gas bubbles on the nucleation was investigated, e.g. by Wohlgemuth et al. [Woh09, Woh10]. In their studies it could be shown that the surfaces of gas bubbles that were bubbled into a supersaturated solution could act as nucleation center and initiate a heterogeneous nucleation mechanism.

Huang et al. [Hua16] investigated the effects of solutions saturated with single gases (air, oxygen, nitrogen and carbon dioxide) or degas the solutions on the solubility, the MZW and the growth rates. As a result it was demonstrated that the dissolved gases can have a considerable influence on the solubility and the MZW of the used substances epsomite ($\text{MgSO}_4 \cdot 7 \text{H}_2\text{O}$), diammonium phosphate, glycine and citric acid. In case of epsomite an effect of the dissolved gases on the growth rates was described as well.

An effect of dissolved gases (hydrogen, helium, argon, nitrogen, oxygen, air, nitrous oxide and carbon dioxide) on the growth rates was reported by Waldschmidt et al. [Wal11a], too. In that study it could clearly be shown that oxygen-containing gases resulted in high growth rates for the model substance ciclopirox while the presence of oxygen-free gases or degassing the solution decelerated the crystal growth rates drastically. As a consequence the formation of liquid inclusions appeared to be distinctly more intense when solutions were saturated with oxygen-containing gases than in presence of oxygen-free gases. Furthermore, it is discussed that oxygen-containing gases might adsorb to the rough surfaces of the growing crystals and, thus, promote the inclusion formation additionally. The meaning of dissolved gases on the formation of inclusions was supported by proving the presence of the appropriate gases in the bubbles inside the liquid inclusions [Wal11b, Bob16a]. By means of Raman spectroscopy it could be shown that such bubbles contain not only gaseous solvent but even ambient gases, e.g. nitrogen. In case of crystals grown from solutions enriched

with single gases, e.g. oxygen or nitrogen, the specific gas was analyzed in remarkable high amounts in the occurring bubbles inside the inclusions.

3. Motivation

Microencapsulation is a growing research field and due its wide range of potential applications, especially, in the field of foods and cosmetics, new technologies to extend the possibilities are of great interest. Such a new technology for microencapsulation might be found in the use of crystals that contain liquid inclusions which can be seen as kind of pocket.

In literature a few case studies presenting filled container crystals using different materials can be found [Det10b, Sch10, Sch11b, Sch13, Ulr13]. The concept of using hollow crystals as encapsulation systems could successfully be proven by those results. The mechanism to prepare those container crystals was based on a solvent-mediated phase-transformation [Mal04, Jon06, Det07, Det10b, Wac11, Sch13].

Considering, however, the use of crystalline encapsulation materials for industrial application there are still open questions that need to be answered. First of all, the encapsulation potential of such container crystals has not been evaluated, yet, and hardly any study quantified the amount of encapsulated substance. The hollow crystals made in the previous studies consist of metastable solvates whose stability, e.g. under storage conditions, was not considered. The applied methods to prepare these container crystals were based on laborious conditions in small lab scale, e.g. dropping solution into small quantities of antisolvent or positioning each crystal needle separately in the drying oven to seal the tips. Moreover, in these basic research studies no agitation was applied. Without doubt such a procedure is not feasible for industrial purposes. As a last important point which is not discussed in literature as intense as necessary is the applicability of container crystals in potential products with regard to the amount of container crystals that can be added to a product.

The aim here is to answer the above mentioned questions and leave the field of pure basic research toward an application-oriented research that paves the way for the industrial production of crystalline encapsulation systems. Therefore, a model substance with a high affinity to form liquid inclusions, that is stable under storage conditions and that offers possible applications, preferably in the field of foods or cosmetics, will be chosen. Since most food and cosmetic products are based on water as solvent a low

water solubility of the model substance is preferred. In order to prepare a scale up from lab conditions to industrial conditions a stirred tank need to be used for the crystallization process. Another important step is to verify the application of inclusion containing crystals as encapsulation materials by quantifying the inclusion amounts, e.g. by means of optical microscopy, and the amount of encapsulated substance. Considering the later application in a product, the conditions that ensure the stability of the container crystals, e.g. against dissolution, need to be defined.

The effect of dissolved gases on the crystallization behavior is another point in the focus of this work. Dissolved gases are described to affect the growth rates and inclusion formation [Wal11a] as well as the solubility [Hua16] and the nucleation [Woh09]. Since these aspects were investigated separately by different authors using different substance there is no case study that considers the effects of dissolved gases on solubility, MZW, growth and dissolution behavior for the same substance. Thus, it will be investigated here using again the chosen model substance as case study.

4. Materials and methods

4.1. Materials

4.1.1 Salicylic acid

As model substance that fulfills the proposed claims (Chapter 3) salicylic acid (SA) was chosen because of its high affinity to form liquid inclusions and its low water solubility [Nor06]. The properties of this dermatological and cosmetic agent (Fig. 4.1) which is also known as ortho-hydroxybenzoic acid or 2-hydroxybenzencarboxylic acid (IUPAC) are summarized below. For this study SA ($\geq 99\%$) purchased from Carl Roth (Germany) was used.

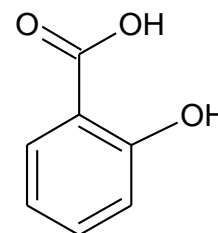


Fig. 4.1: Molecular structure of SA.

4.1.1.1 Physical and crystal properties

The physical properties of SA are summarized in Tab. 4.1. Solubility data of SA in several organic solvents and water are depicted in Fig. 4.2a.

Tab. 4.1: Physical properties of SA.

Property	Value	
Appearance	White crystalline powder or as needlelike crystals	[Kaw84, Ras92, Gfd07]
Density	1.443 g cm ⁻³	[CIR03, IFA16c]
Melting point	159 °C	[IFA16c]
Sublimation temperature	76 °C	[IFA16c]
pH	95-134 °C	[Jon60]
	2.4 (saturated aqueous solution)	[Ras92, IFA16c]

Salicylic acid crystallizes usually as prismatic needles or rod shaped crystals [Bla01, Nor06, Hat12, Per13]. The crystals grow in a monoclinic space group which points to an intense anisotropic behavior of growing crystal faces [Prz15]. Investigations about growth and dissolution mechanisms of single crystal faces revealed that (001) face (Fig. 4.2b) grows and dissolves diffusion controlled and mass transport effects dominate at this face. Growth and dissolution of (110) and ($\bar{1}10$) faces are characterized by both surface integration and diffusion controlled mechanisms and, thus, material transport happens much slower than in case of a purely diffusion controlled mechanism as in case of (001) face [Per13].

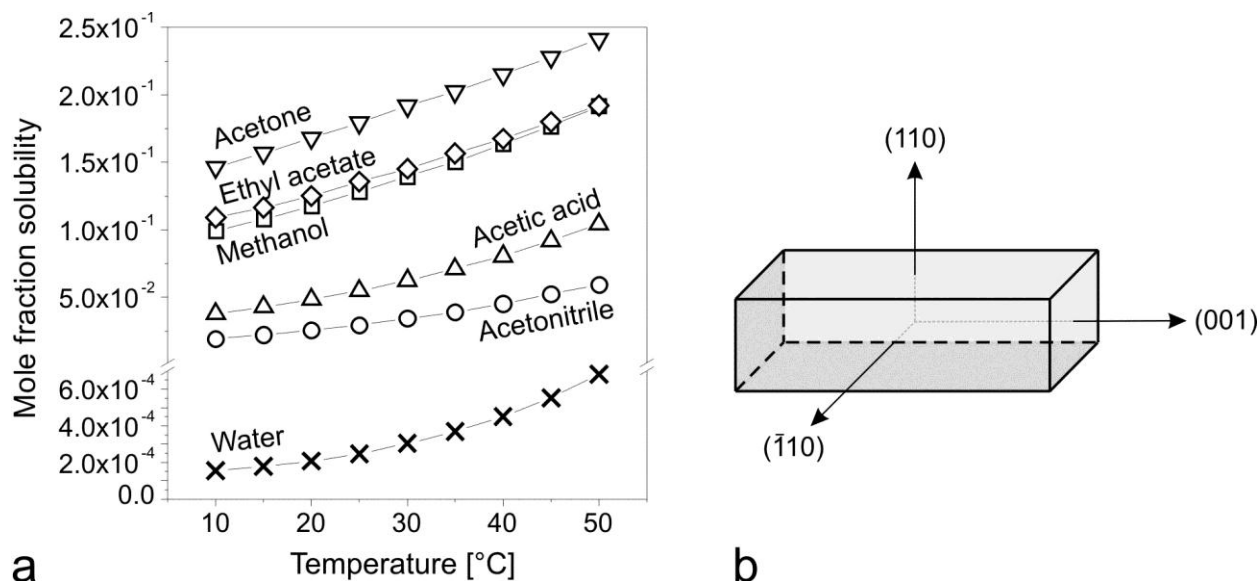


Fig. 4.2: a) Solubility of SA in acetone (∇), ethyl acetate (\diamond), methanol (\square), acetic acid (Δ), acetonitrile (\circ) and water (\times) [Nor06]. b) 3D-illustration of SA crystals with labeled faces [Per13].

Besides the above mentioned morphology which is usually observed and described in literature Xu et al. [Xu06] were able to generate SA crystallites with different morphologies. Therefore, SA crystals were prepared by means of a neutralization method in presence of additives referred to as organic modifiers (e.g. polyvinyl pyrrolidone, citric acid). Due to FT-IR measurements it could be proven that the additives had no effect on the chemical composition of the crystals. However, significant changes in the morphology from bar-like to leaf-like or chrysanthemum-like shapes were observed.

4.1.1.2 Applications

SA can be found naturally in willow leaves and has been used as analgesic since approximately 400 BC [Nor06, Ras92]. Nowadays, SA is mainly used as precursor for acetyl salicylic acid (Aspirin) production [Mon06], but it finds applications as active agent itself. In low concentrations (up to 0.5%) it is used as preservative for cosmetic products [Eur09]. As active agent for cosmetic skincare products SA concentrations of up to 2% can be applied, e.g. in antiacne, antidandruff as well as hair- and skin-conditioning treatment. Considering pharmacological or dermatological applications higher concentrations (>10%) of this keratolytic agent (removal of dead skin cells) can be used in the local treatment of psoriasis, eczema, neurodermatitis and the removal of corns, calluses and warts [CIR03, Leb99].

4.1.1.3 Toxicity

In high concentrations dermal SA exposure causes skin irritations and skin peeling. However, the active effect of SA treatment is described to happen only in upper epidermis but not in the deeper layers, thus, neither the skin thickness nor its degeneration are affected adversely [CIR03]. Acute SA intoxication (salicylism) appears at blood concentrations of 45-65 mg% which can be reached by oral intake and manifests itself by dizziness, tinnitus, impaired hearing and headaches [Pas12]. Further detailed information about the properties, applications, metabolism and toxicity of SA and its derivatives can be found in [CIR03].

4.1.2 Further materials

Beside SA further materials were applied which include solvents, foreign substances the container crystals were filled with and those that were of analytical purpose (Tab. 4.2). Moreover, deionized water was used.

Tab. 4.2: Further materials that were used in this thesis

	Substance	Producer	Purity
Solvents	Methanol	Carl Roth GmbH & Co. KG, Karlsruhe	≥99%
	Ethanol	Carl Roth GmbH & Co. KG, Karlsruhe	≥99.8%
Filling materials	L(+)-Ascorbic acid	Merck KGaA, Darmstadt	≥99.7%
	Copper sulfate pentahydrate	Riedel-de Haën AG, Seelze	≥99%
Analytically used substances	Iron(III)chloride hexahydrate	Fluka Chemie AG, Neu Ulm	99.0-102%
	Iodine standard solution	Merck KGaA, Darmstadt	-
	9910 Titrisol® (0.05 mol L ⁻¹)		
	Hydrochloric acid	Carl Roth GmbH & Co. KG, Karlsruhe	37%
	Sodium thiocyanate	Carl Roth GmbH & Co. KG, Karlsruhe	≥98%

4.2. Experimental Methods

4.2.1 Saturation curve

One possibility to determine the solubility curve of a substance is by determining its concentration in a saturated two phase (s, l) system at a defined temperature. In order to differentiate the solubility curves that were prepared using this method from those using another method (Chapter 4.2.2) the revealed curves will be termed as 'saturation curves'. Therefore, solutions that were supersaturated at the aimed temperatures were prepared, filled into 2 mL plastic tubes and placed into a heating block (25-30 °C) or a centrifuge (5-20 °C) using 5 K temperature steps from 5-30 °C. After 10 min some seed

crystals were added and the tubes were kept at constant temperature. It was found that one hour was enough to reach a constant mass fraction of the solution. Thus, after one hour the supernatant solution was separated very carefully by means of a 1 mL Eppendorf pipette (Fig. 4.3) and filled into a 1.5 mL plastic tube. The mass fraction of this solution was measured by means of a refractometer (RE40 by Mettler-Toledo, Schwerzenbach, Switzerland) at 35 °C using an external calibration. At each temperature six samples were prepared and measured [Sei17].

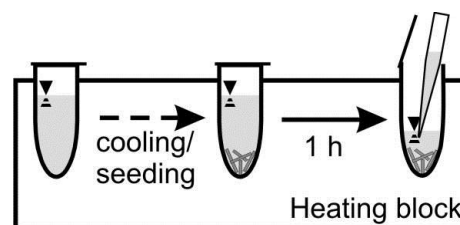


Fig. 4.3: Experimental procedure to determine the saturation curve. Solution with crystals was kept at constant temperature until solution concentration became constant. Solution was removed carefully and its mass fraction was measured by means of refractometer.

4.2.2 Solubility and MZW

The use of an ultrasound (US) based method as described in literature, e.g. [Oma99, Hel12, Hua1], offers the possibility to measure the solubility line and the nucleation curve and, thus, to determine the metastable zone width (MZW). This method is based on measuring the time a transmitted signal needs to pass a defined distance through the solution (Fig. 4.4b). The revealed US velocity of the solution can be understood as temperature dependent substance property since it depends on the adiabatic compressibility and the density of the liquid only [Oma99].

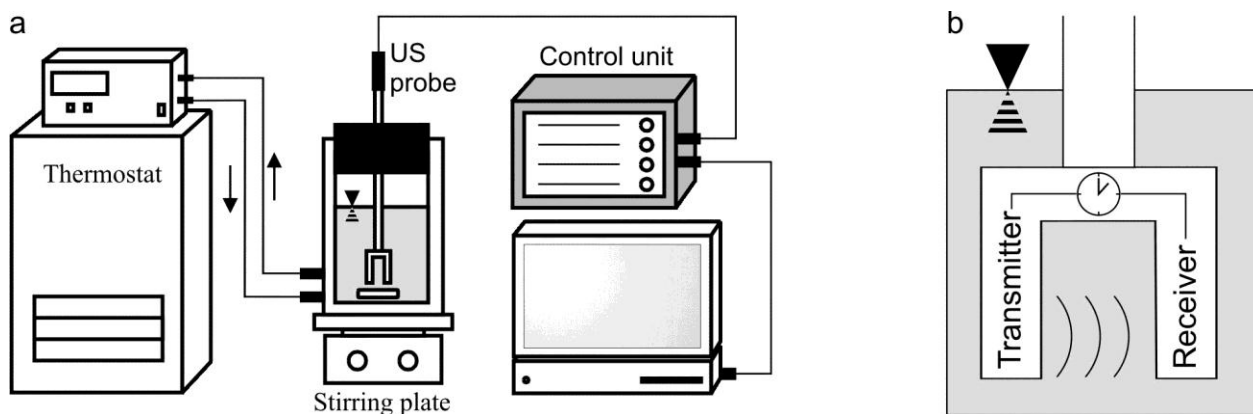


Fig. 4.4: a) Schematically drawn US setup as used to determine solubility and nucleation lines as well as growth and dissolution rates; b) Measure principle of the US probe is based on determining the time a signal transmitted through the solution takes until it is received after a defined distance [Oma99].

The experimental setup consisted of a double jacketed vessel that was temperature controlled by means of a thermostat and on top of a stirring plate. The ultrasonic probe

(LiquiSonic, Sensotech, Magdeburg, Germany) was positioned in the medium as can be seen in Fig. 4.4a. To determine nucleation and solubility point of a solution with a known mass fraction a temperature cycle (cooling and heating step) was run. In this study mass fractions from 32-42% SA in MeOH and heating/cooling rates of 2, 5, 10 and 15 K h⁻¹ were used.

4.2.3 Growth rate

The growth rates were measured by means of a desupersaturation method. This method is based on measuring the decrease of the supersaturation which is represented by the decrease of the solution's concentration during crystal growth [Oma99, Tav79].

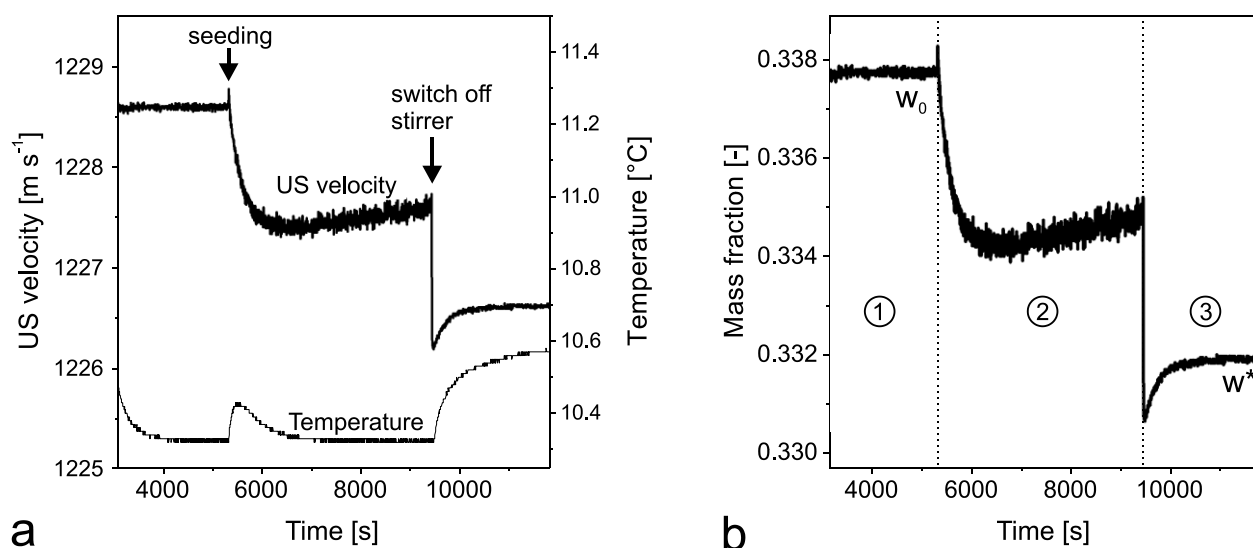


Fig. 4.5: a) Progression of US velocity-time and temperature-time plots in dependence on experimental procedure. b) Mass fraction-time plot as provided from US velocity-time plot and US velocity-mass fraction calibration, initial (w_0) and final mass (w^*) fraction can be read from the curve.

The growth rate of SA in MeOH was investigated using the US setup in Fig. 4.4a. Growth rates were measured under isothermal conditions at both 10 and 30 °C. 200 mL of a filtered solution that was slightly supersaturated at the aimed temperature was kept 5 K above the aimed temperature for 30 min to ensure a homogenous solution without any crystals. Then, the solution was cooled down to the aimed temperature in 30 min and kept at this temperature for further 45 min to reach stable values for both temperature and US velocity (Fig. 4.5b, section 1). When this condition was reached for at least 20 min 0.500 ± 0.001 g seed crystals of the sieve fraction 80-100 μm were added to the solution (Fig. 4.5a). One hour after the seed crystals were added, the stirrer was switched off to allow the grown crystals to settle (Fig. 4.5a).

Since there is a temperature dependent but linear relation between concentration and US velocity [Oma99] a US velocity-mass fraction calibration at 10 and 30 °C could be performed. Due to this calibration the US velocity-time curve (Fig. 4.5a) could be converted to a mass fraction-time curve (Fig. 4.5b) where the initial (w_0 , section 1) and final (w^* , section 3) mass fraction of SA in the solution can be read directly from the diagram.

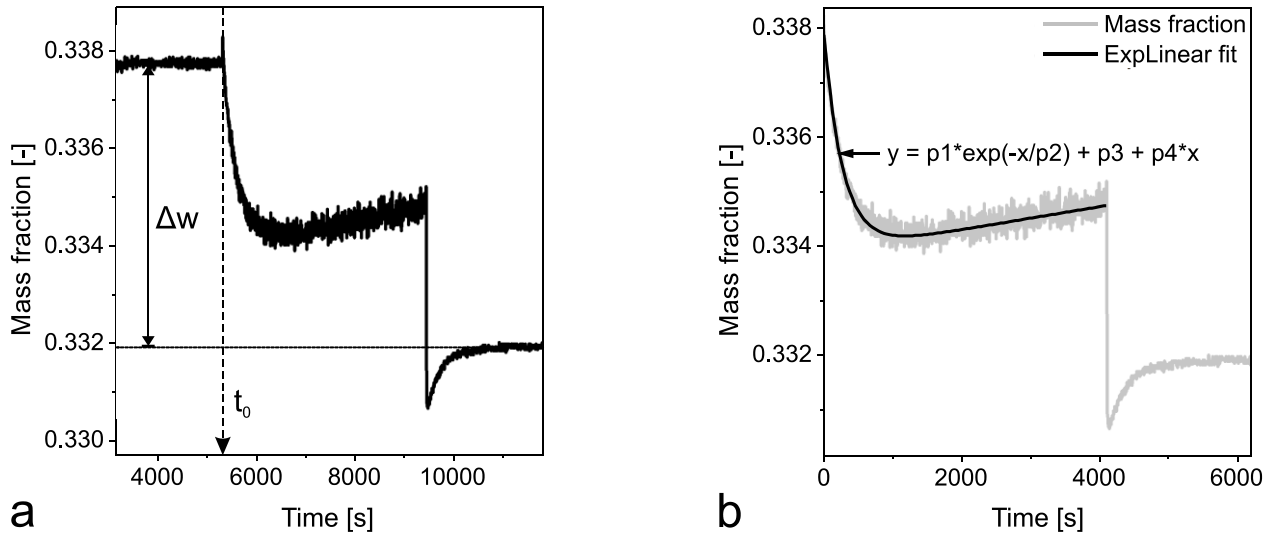


Fig. 4.6: Evaluation of growth rate experiments: a) Convert US velocity to concentration profile which provides initial and final mass fractions as well as their difference (Δw); b) The moment of seed addition is set to zero to fit the w - t -curve.

It should be pointed out that the US velocity reflects both the liquid and the solid phase of a suspension. In the liquid phase the US velocity depends on density and adiabatic compressibility and, thus, on concentration and temperature. In the presence of solid particles suspension density and particle size additionally affect the US velocity [Say02]. For that reason only in sections 1 and 3 (Fig. 4.5b) where no crystals disturb the measurement the curve can be interpreted according to the mass fraction of the solution. In section 2 where the actual crystal growth happens, the US signal is spread by the suspended crystals which is evidenced by the obviously higher fluctuations. However, the growth rates can be determined from this curve section in which exponential and linear curve character overlap. Under the condition of setting the moment of seeding to zero the curve can be fit according to Eq. 4.1 as illustrated in Fig. 4.6. This fit provides the time constant (p_2) of the growth and thus, the growth rate can be calculated as described in Eq. 4.2. This procedure will be discussed in details in Chapter 5.1.3.

$$y = p_1 \cdot e^{-\frac{x}{p_2}} + p_3 \cdot p_4 x \quad 4.1$$

$$G = \frac{m_{sol}}{m_{seed}} \cdot \frac{V_{0,seed}}{A_{0,seed}} \cdot \frac{\Delta w}{p_2} \quad 4.2$$

In order to clarify what happens in the suspension of growing crystals where solution and suspension effects overlap a 3D-ORM probe (APAS 14, by Sequip S&E GmbH, Germany) was added to the setup. This 3-dimensional optical reflectance measurement technique allows an inline measurement of the particle size distribution [Hel12, Mos14, Mos15].

4.2.4 Dissolution rate

The US device (Fig. 4.4) was used to determine dissolution rates. Undersaturated solutions were kept at 10 or 30 °C, 10 g crystals (160-200 µm) were added and the time until crystals were dissolved completely was determined.

The mass fraction increase that happens during crystal dissolution should theoretical be shaped as shown in Fig. 4.7a. Based on this curve the dissolution rates could be determined by means of a time constant similarly as described above. Such an evaluation would provide the dissolution rates in the commonly used unit $m s^{-1}$. However, the US method provides ‘dissolution curves’ as depicted in Fig. 4.7b. When crystals are added the US velocity first decreases, then increases sharply and finally decreases again until it reaches a constant value. This progression can be explained by the overlapping effects of a suddenly increased suspension density and its decrease during crystal dissolution. For that reason no time constant could be determined in case of dissolution. Alternatively, the overall time of crystal dissolution (Δt) was determined from the graph. By means of the initial (w_0) and final (w^*) mass fractions that were calculated from the US velocity (Fig. 4.7c) and the overall dissolution duration the dissolution rates will be expressed by the change of mass fraction over time plotted against saturation degree of the solution.

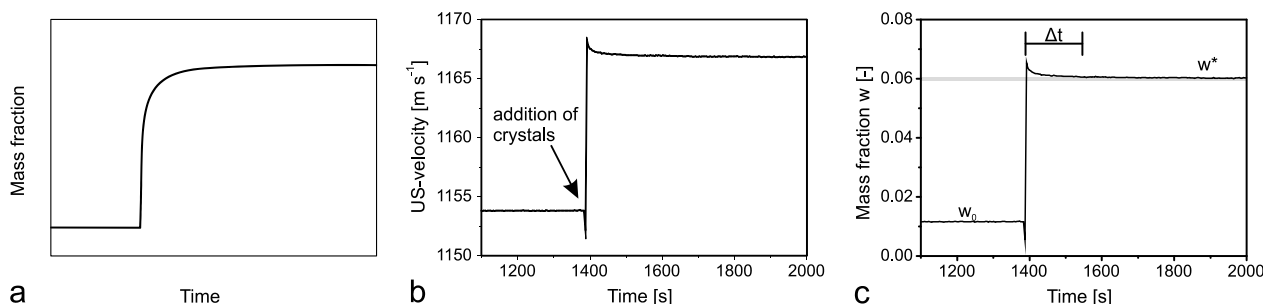


Fig. 4.7: a) Theoretically expected dissolution curve with increasing mass fraction over time; b) US velocity-time plot as revealed during crystal dissolution; c) Mass fraction plotted over time, initial (w_0) and final (w^*) mass fractions as well as dissolution time (Δt) are marked.

4.2.5 Degassing

As described in Chapter 2.4 dissolved gases can affect the crystallization in different ways, e.g. promote nucleation [Woh09, Woh10] or dramatically reduce growth rates [Wal11a]. In order to investigate a possible effect of dissolved gases on crystallization of SA saturation curve, solubility, MZW as well as growth and dissolution rates were determined for both air saturated and degassed solutions.

Solutions were degassed using the degasser DE01 (by M2-Automation, Berlin, Germany) which contains a gas permeable membrane tube in a vacuum cell with defined pressure of 300 mbar (Fig. 4.8). When the prepared solution is pumped slowly (1 mL min^{-1}) through this tube the dissolved gases are removed from the solution.

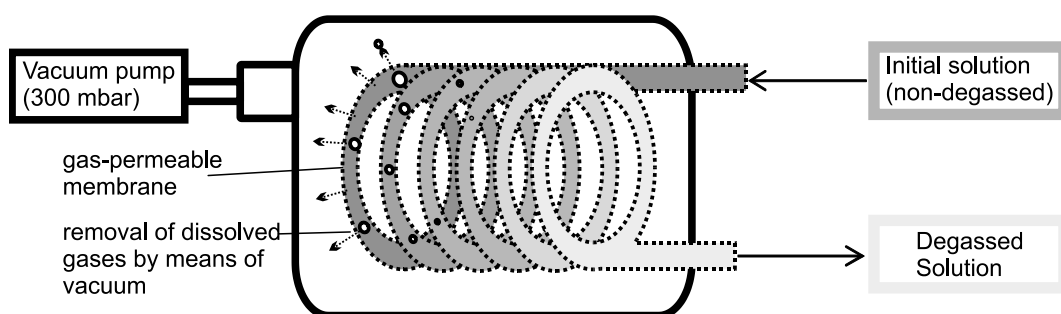


Fig. 4.8: Scheme of degassing unit. Gases are removed from the initial solution by means of vacuum (300 mbar) through a gas permeable membrane.

The mechanism of solvent degassing is based on Henry's law which describes the directly proportional relation between the partial pressure of the gas and its soluble amount in the liquid [Hen03]. Thus, if the ambient pressure of the liquid is reduced the gas amount is reduced by the same ratio. Exemplarily, the solubility for oxygen and nitrogen for 1 bar and 0.3 bar ambient pressure are noted in Tab. 4.3. All experiments concerning saturation curve, solubility, MZW, growth and dissolution rates were run

using both degassed and non-degassed solutions. Since changes in ambient pressure would affect the thermodynamics of the system all experiments were run under normal pressure.

Tab. 4.3: Solubility data for oxygen and nitrogen in MeOH expressed as Ostwald coefficient ($V_{\text{gas}}/V_{\text{MeOH}}$). Based on literature data for saturation solubility [Kre46] the amount of oxygen and nitrogen that remains in solution after degassing at 300 mbar was calculated.

Temperature [°C]	Oxygen		Nitrogen	
	Saturation solubility [Kre46] [-]	Amount after degassing [-]	Saturation solubility [Kre46] [-]	Amount after degassing [-]
-25	0.243	0.072	0.144	0.042
0	0.245	0.072	0.153	0.045
25	0.248	0.073	0.165	0.049
50	0.255	0.076	0.177	0.052

4.2.6 Determination of SA solubility in EtOH-water-mixtures

One aim of this thesis is to define the solvent composition which enables the presence of SA crystal containers in a potential product without their dissolution. Therefore, the solubility of SA in solvent mixtures which can be seen as miscibility gap in a ternary system needs to be investigated. Exemplarily, the SA solubility in EtOH-water-mixtures will be focused on. The used experimental setup consisted of six 30 mL double jacketed vessels with screw caps and stirring bars inside. The vessels were positioned on top of a multipoint magnetic stirring plate and connected to a thermostat. In order to determine the solubility curve of SA in the solvent mixtures solutions of SA in ethanol (different concentrations) were prepared and kept at 20 °C (Fig. 4.9). Then water was added until crystals appeared. After waiting for 30 min to ensure complete crystal growth the initial solution was dropped very slowly into the turbid solution until the crystals just dissolved. At this point samples were taken to analyze the solutions' compositions at the solubility points. For the solubility determination in pure water and pure EtOH saturated solutions were prepared and kept at 20 °C. The amounts of water and SA were determined as described below.

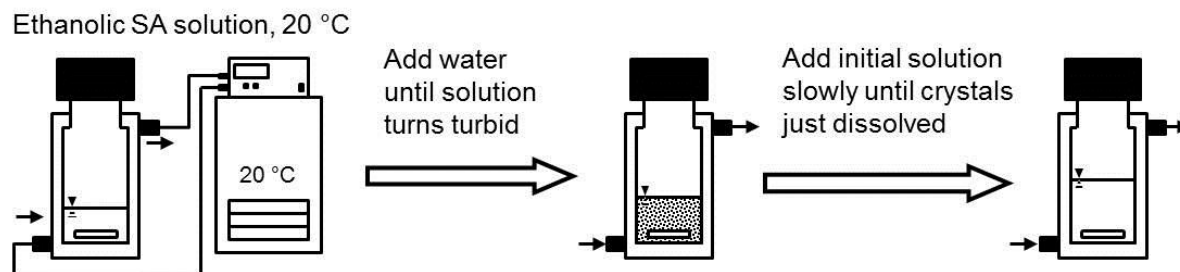


Fig. 4.9: Setup for determination of solubility of SA in ethanol-water mixtures [Sei16].

The water content was measured by means of Karl-Fischer titration (V 30 Volumetric KF Titrator, Mettler Toledo AG Analytical, Schwerzenbach, Switzerland). SA was quantified as iron(III)-complex using a spectrophotometric method. Therefore, 1.0 mL of a hydrochloric 0.8 M iron(III)chloride solution was mixed with 0.5 mL ethanol and 50 μ L of the sample solution. The absorption of the resulting brown solution was measured at a wavelength of 531 nm (Specord 40 spectrophotometer by Analytik Jena, Jena, Germany). For quantification an external calibration was used [Sei16].

Due to the assumption of Eq. 4.3 the amount of the third component ethanol could be calculated from the determined SA and water amounts using Eq. 4.4.

$$w_{SA} + w_{water} + w_{EtOH} = 1 \quad 4.3$$

$$w_{EtOH} = 1 - w_{SA} - w_{water} \quad 4.4$$

4.2.7 Microscopic observations of SA crystals growing during antisolvent crystallization

In order to investigate the crystal growth of SA crystals in situ during antisolvent crystallization a small petri dish (diameter 1 cm) was filled with 300 μ L distilled water and approx. 70 μ L of 8% ethanolic SA solution were injected into the water (Fig. 4.10a). The solution was covered in order to avoid nucleation on the surface of the solution. Crystal growth was observed by means of optical microscope (Nikon Eclipse LV100 with CCD camera) and pictures were taken each 5 s (Fig. 4.10b, c).

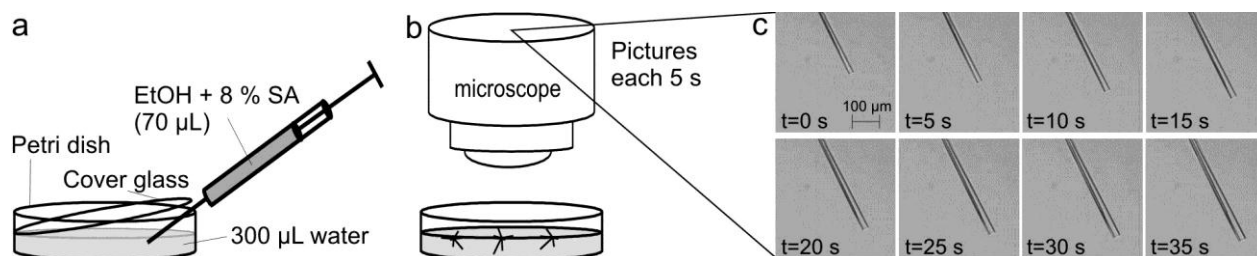


Fig. 4.10: Experimental setup for microscopic observations of SA crystal growth by means of an antisolvent method; a) Sample preparation; b) Microscopic pictures were taken each 5 s; c) Pictures of SA crystal during growth.

This method allows determining the growth rates of single crystals in situ during antisolvent crystallization by measuring the change of crystal size over time as presented by Bobo et al. [Bob15].

4.2.8 Investigations of experimental parameters on crystal and inclusion sizes

Two inquiries were performed in order to investigate the influencing parameters on crystal and inclusion sizes in case of SA using an antisolvent crystallization method with water as antisolvent and methanol (first enquiry) or ethanol (second enquiry) as solvents. Besides the used solvents some different parameters were investigated in both enquiries.

4.2.8.1 General crystallization procedure

Crystals were generated by injecting the antisolvent water into the stirred solution by means of a dosage device. The experimental setup is depicted schematically in Fig. 4.11.

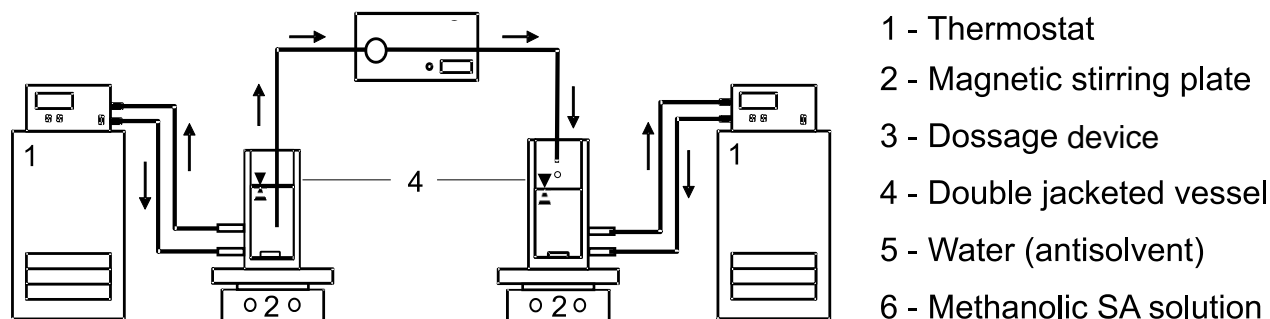


Fig. 4.11: Experimental setup for generation of SA crystal needles by means of antisolvent crystallization.

The prepared crystals were filtered and dried, first at a vacuum oven at 40 °C and about 700 mbar for 24 h, then uncovered at room temperature until complete drying. For all

experiments in general the same procedure of crystal preparation was used. The variation of the parameters will be described in Chapters 4.2.8.3 and 4.2.8.4.

4.2.8.2 Quantification of crystal and inclusion sizes by means of OM

The prepared and dried crystals were measured using an optical microscope (Keyence VHX-500FD), as illustrated in Fig. 4.12, in length and width of the total crystals as well as length and width of the inclusions. Intense microscopic investigations showed that SA crystals own a nearly quadratic base and the inclusions are formed like round channels. According to the assumption that all crystals respectively inclusions reflect these observations the data were used to calculate the volume of the total crystals and the inclusions. In case of crystals containing more than one inclusion up to three inclusions were measured and their sum was taken into account for further evaluations.

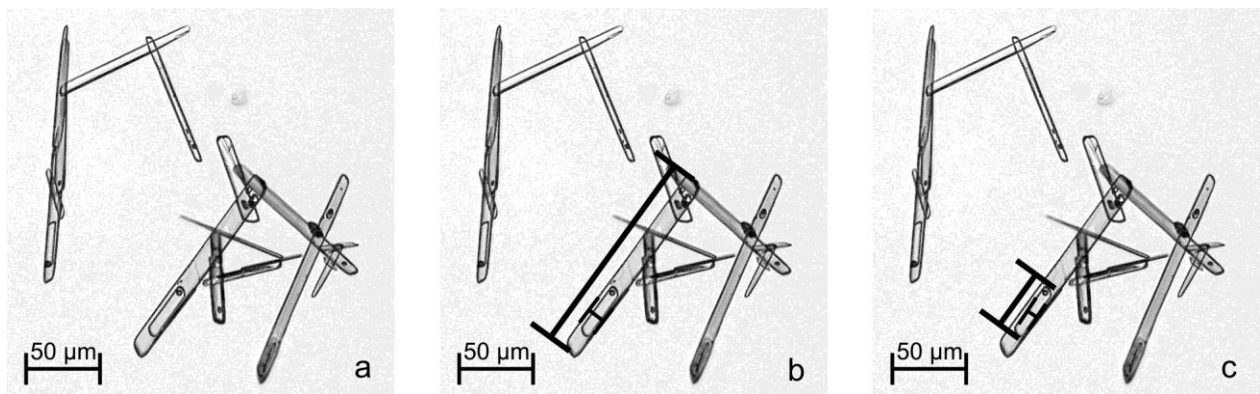


Fig. 4.12: a) Microscopic image of prepared SA container crystals; b) measurement of length and width of the total crystal; c) Measurement of length and width of the inclusion.

4.2.8.3 First enquiry on the effects of experimental parameters on crystal and inclusion sizes

In this first enquiry [Sei15] on the experimental parameters that might influence the inclusion formation methanol was chosen as solvent. Three steps were performed in order to identify parameters that might be of interest for inclusion formation (first step) and two further steps to investigate the parameters of interest in more details.

For this first enquiry an experimental design method was applied by means of the software Statistica (by StatSoft Inc.). Based on this method the experiments for all three steps were designed and, as far as possible, evaluated.

Step 1: Parameter screening

The first step was a screening step where a high number of parameters was investigated in order to find the most important ones and to ensure that e.g. sample size or the use of a colorant have no influence. In Tab. 4.4 the investigated parameters and the used values are summarized.

After this first step some parameters were kept constant. Those were the solution temperature which was fixed at 35 °C and the solution-water-ratio where a value of 1:4 was used for following experiments. Moreover, neither solution nor water was colored after this first step.

Tab. 4.4: Variable conditions of experimental design in first step of parameter identification. Additionally (parameter abbreviations) as well as [units] are given.

Parameter			Low value	High value
Mass fraction solution	(w)	[%]	8	25
Stirring rate	(SR)	[rpm]	250	600
Injection rate	(IR)	[mL min ⁻¹]	5	20
Temperature of SA solution	(T_S)	[°C]	10	35
Temperature of antisolvent	(T_{AS})	[°C]	10	35
Gas content of SA solution	(gas_S)	[-]	Degassed (-)	Non-degassed (+)
Gas content of SA antisolvent	(gas_{AS})	[-]	Degassed (-)	Non-degassed (+)
Volume of SA solution	(V_S)	[mL]	10	40
Ratio SA solution: water	(S/AS)	[-]	1:2	1:6
Colorant in SA solution	(col_S)	[-]	No (-)	Yes (+)
Colorant in antisolvent	(col_{AS})	[-]	No (-)	Yes (+)

Step 2: Influence of mass fraction, injection rate and solution volume

At the second step three different values of w , IR and V_S (Tab. 4.5) were chosen to investigate in more details how they affect the generation of liquid inclusions in SA crystals. The other parameters SR=250 rpm and T_S =10 °C were kept constant for all experiments and neither solution nor antisolvent degassing was performed.

Tab. 4.5: Variable parameters as performed in step 2.

Parameter	Sample No.								
	2-1	2-2	2-3	2-4	2-5	2-6	2-7	2-8	2-9
w [w-%]	8	8	8	14,5	14,5	14,5	25	25	25
IR [mL min ⁻¹]	4	12	20	4	12	20	4	12	20
V_S [mL]	30	70	50	70	50	30	50	30	70

Step 3: Influence of stirring rate, solution temperature and gas content of solution and antisolvent

At the third step the influence of gas content in solution and water as well as the solution temperature and the stirring speed on crystal and inclusion sizes were focused on (Tab. 4.6). $w=8\%$, $IR=16 \text{ mL min}^{-1}$ and $V_S=50 \text{ mL}$ were kept constant.

Tab. 4.6: Variable parameters as performed in step 3.

Parameter	Sample No.							
	3-1	3-2	3-3	3-4	3-5	3-6	3-7	3-8
SR [rpm]	250	600	600	250	600	250	250	600
T_S [°C]	10	10	10	10	35	35	35	35
Gas _S	-	-	+	+	-	-	+	+
Gas _{AS}	-	+	-	+	-	+	-	+

4.2.8.4 Second enquiry on the effects of experimental parameters on crystal and inclusion sizes

The effects of experimental parameters were investigated in a second enquiry using ethanolic SA solution and water as antisolvent. The same setup as depicted in Fig. 4.11 was chosen. In these experiments only single parameters were varied, contrary to the experiments of the first enquiry where an experimental design was applied.

Effect of mass fraction and stirring rate

The effects of solution mass fraction w and stirring rate SR were repeatedly investigated in the second enquiry in order to verify the effect of these two parameters which are described in literature to be of high interest for crystal and inclusion sizes, e.g. [Den66, Zha05, Kim09].

The crystallization was performed at 20 °C and the antisolvent was injected into the solution with $IR=15 \text{ mL min}^{-1}$. Of both w (4%, 8%, 15%) and SR (0 rpm, 100 rpm, 350 rpm) each three different values were used which results in nine experiments that were performed. For all experiments 70 mL SA solution were used. The amount of antisolvent was generally set to 200 mL. However, in case of $w=4\%$ this antisolvent amount was too low to reach nucleation, thus, for these experiments 300 mL antisolvent were used.

Effect of seeding

The effect of seeding on crystal and inclusion sizes was investigated for three different w (4%, 8%, 15%) as well. General conditions were same as described above (20 °C, 70 mL solution, IR=15 mL min⁻¹, antisolvent amount of 200 or 300 mL depending on w). SR=350 rpm was applied. Seed crystals (0.5 g, sieve fraction 200-240 μm) were added after 90 mL water was injected into the solution.

Effect of injection direction

As one parameter that is hardly investigated in case of antisolvent crystallization the effect of the injection direction was investigated as last parameter of this second enquiry. Contrary to all previously described experiments the injection direction was changed from the injection of antisolvent into the solution (AS>S) to injecting the solution into the antisolvent (S>AS). This parameter was investigated for $w=8%$ and $w=15%$ and each at temperatures of 10, 20 and 35 °C. $V_S=70$ mL, IR=15 mL min⁻¹ and the amount of water (200 mL) were kept constant as described above.

4.2.9 Filling of SA container crystals

The final aim of this study is to prepare container crystals which can be filled with another substance ('foreign substance'). The filling procedure was applied by adding the foreign substance to the antisolvent. During crystal growth and inclusion formation the solution containing the foreign substance will be enclosed inside the crystals' inclusions. Two test foreign substances were chosen in order to prove the filling of container crystals qualitatively and quantitatively.

4.2.9.1 Copper sulfate

As first test substance which offers the possibility of a solid qualification copper sulfate was chosen. The crystallization was performed by injecting 80 mL of an 8% SA solution with 20 mL min⁻¹ into 200 mL antisolvent which contained 5% of copper sulfate pentahydrate. Both liquids were kept at 10 °C and the batch was stirred with 200 rpm. The prepared crystals were filtered and rinsed until the light blue color of the copper sulfate disappeared. The dried crystals were dissolved in pure EtOH and the copper ions were identified qualitatively. Therefore a spatula tip of potassium ferricyanide is

added to the solution. As first positive result a brown precipitation appears which is separated by means of centrifugation. This separated brown precipitation can be dissolved in a few mL of concentrated ammonia solution which results in a blue ammonia-copper complex. The blue color of the solution represents a second positive result of copper present in dissolved container crystals [Ger01].

4.2.9.2 Ascorbic acid

The second foreign substance that was chosen for encapsulation experiments was ascorbic acid. This substance is highly UV-sensitive and, thus, needs protection which could be provided by encapsulation inside SA container crystals [Kir91]. The crystallization procedure was same as described above using 5% aqueous ascorbic acid solution as antisolvent. The rinsed and dried crystals (8 g) were dissolved in an EtOH-water-mixture (85:50, v:v) in order to get 38 g solution. This solution was cooled on ice in order to improve the equivalence point and after adding a few drops of sulfuric acid the solution was titrated using a 0.005 M iodine standard solution until the solution color changed from colorless to yellow [Yos01].

4.3. Calculations

4.3.1 Hansen Solubility Parameters (HSP)

The HSP model is described in details by Hansen [Han00, Han07]. It is based on the use of three solubility parameters δ which are generally defined as seen in Eq. 4.5 where E [J] represents the liquid cohesion energy which is divided by the molar volume V_m [cm³ mol⁻¹].

$$\delta = (E/V_m)^{1/2} \quad 4.5$$

By means of three parameters (δ_D , δ_P , δ_H) describing dispersion interactions (D), dipole interactions (P) and hydrogen bonding interactions (H) the molecule properties are described simply and comprehensively. To determine the solubility of one component in another Eq. 4.6 can be used, where R_a [MPa^{1/2}] can be understood as the distance of the HSP of both components in a 3D-diagram. The lower the R_a value the higher is the similarity between the molecules and, thus, the better is the solubility.

$$R_a^2 = 4(\delta_{D2} - \delta_{D1})^2 + (\delta_{P2} - \delta_{P1})^2 + (\delta_{H2} - \delta_{H1})^2 \quad 4.6$$

In case of mixed solvents Eq. 4.7 is used to determine the HSP ($\bar{\delta}_D$, $\bar{\delta}_P$, $\bar{\delta}_H$) of the mixture. In this equation $\bar{\delta}_{i,1,2}$ represent the respective HSP and $\varphi_{1,2}$ stands for the volume fraction of the pure components in the mixture. These values will be used in Eq. 4.6 as solvent parameters.

$$\delta_i = \varphi_1 \delta_{i1} + \varphi_2 \delta_{i2}, \quad i \in \{D, P, H\} \quad 4.7$$

For this work the HSP for oxygen, nitrogen and SA are of interest and for these substances literature data based on calculations and estimations according to group similarities are provided by [Han00, Han07] (Tab. 4.7). In this study the HSP model will be used to predict the solubility behavior of the substances in dependency on the solvent composition. Since the determination of R_a (Eq. 4.6) is not able to provide quantitative solubility data the relation between R_a and the mole fraction (x) of the substances has to be defined. This will be reached by determining the HSP for oxygen, nitrogen and SA as described below.

Tab. 4.7: HSP for SA, oxygen and nitrogen as provided by [Han00, Han07]. These parameters are based on calculations and estimations based on substance similarities.

	HSP-SA/[Han07]	HSP-Ox/[Han00]	HSP-Ni/[Han00]
$\bar{\delta}_D$	19.4	17.7	11.9
$\bar{\delta}_P$	10.1	0.0	0.0
$\bar{\delta}_H$	17.4	0.0	0.0

4.3.1.1 Determination of HSP

A detailed description about the determination of HSP from experimental solubility data is described by Sato et al. [Sat14] who determined the HSP for oxygen (HSP-Ox) based on an experimental study.

The HSP were determined by defining a relation between R_a and the mole fraction solubility by means of an equation system. This was solved under the condition that the correlation coefficient R (Eq. 4.8) reaches the maximum value. The values for $\bar{\delta}_D$, $\bar{\delta}_P$, and $\bar{\delta}_H$ for the solvents as well as the mole fraction solubility values were taken from literature.

To calculate the HSP Eq. 4.6 was used to determine R_a using literature data for the solvent HSP and as initial value for oxygen HSP [Han00]. As condition to determine the values for $\bar{\delta}_{D,Ox}$, $\bar{\delta}_{P,Ox}$, $\bar{\delta}_{H,Ox}$ the correlation coefficient R (Eq. 4.8) between the

logarithmic mole fraction solubility of oxygen and R_a was determined. The revealed equation system was solved by determining HSP-Ox in order to get the maximum value for correlation coefficient.

$$R = \frac{\sum_{j=1}^n (\log x_{Ox,j} - \overline{\log x_{Ox}})(R_{a,j} - \overline{R_a})}{\sqrt{\sum_{j=1}^n (\log x_{Ox,j} - \overline{\log x_{Ox}})^2 \cdot \sum_{j=1}^n (R_{a,j} - \overline{R_a})^2}} \quad 4.8$$

4.3.1.2 Determination of HSP for SA in pure solvents (HSP-SA/ps)

In order to determine the HSP for SA in pure solvents (HSP-SA/ps) the above described procedure was done using literature data for the solubility of SA in several solvents which are summarized in Tab. 4.8.

Tab. 4.8: Solubility data of SA in several pure solvents at 25 °C and the HSP of these solvents from [Han00].

Solvent	x_{SA}	$\log x_{SA}$	$\delta_{D,solvent}$	$\delta_{P,solvent}$	$\delta_{H,solvent}$	
Methanol	0.128	-0.893	14.7	12.3	22.3	[Nor06]
Acetonitrile	0.029	-1.531	15.3	18	6.1	
Acetic acid	0.055	-1.260	14.5	8	13.5	
Acetone	0.179	-0.747	15.5	10.4	7	
Water	0.0002	-3.607	15.5	16	42.3	
Ethyl acetate	0.136	-0.867	15.8	5.3	7.2	
Ethanol	0.139	-0.858	15.8	8.8	19.4	[Lim13]
1-Propanol	0.143	-0.845	16.0	6.8	17.4	
1-Butanol	0.148	-0.829	16.0	5.7	15.8	
1-Pentanol	0.155	-0.810	15.9	5.9	13.9	
1-Hexanol	0.158	-0.800	15.9	5.8	12.5	
1-Heptanol	0.160	-0.795	15.9	4.5	13.9	
Water	0.0002	-3.523	15.5	16	42.3	[Sha08]
Ethanol	0.139	-0.858	15.8	8.8	19.4	
Ethyl acetate	0.138	-0.860	15.8	5.3	7.2	
Water	0.0002	-3.699	15.5	16	42.3	[Pen06]
Ethanol	0.140	-0.855	15.8	8.8	19.4	
Ethyl acetate	0.114	-0.945	15.8	5.3	7.2	
Dioxane	0.312	-0.506	19.0	1.8	7.4	
Water	0.000	-3.523	15.5	16	42.3	[Mat09]
Methanol	0.122	-0.913	14.7	12.3	22.3	
Ethanol	0.145	-0.839	15.8	8.8	19.4	
Ethyl acetate	0.138	-0.859	15.8	5.3	7.2	
1.4-Dioxane	0.261	-0.583	19.0	1.8	7.4	

This table contains the HSP of the pure solvents [Han00], too. The equation system was solved by means of MS Excel Solver-function. Due to this procedure the HSP-SA/ps as well as the $\log x_{SA}-R_a$ -relation were calculated.

4.3.1.3 Determination of HSP for SA in EtOH-water-mixtures (HSP-SA/ew)

The HSP of SA in EtOH-water-mixtures (HSP-SA/ew) were determined as described above for HSP-SA/ps but instead of literature data for SA solubility in different solvents the data for SA solubility in EtOH-water-mixtures provided by Matsuda et al. [Mat09] were used (Tab. 4.9).

Tab. 4.9: Mole fraction solubility of SA in different EtOH-water-mixtures as published by [Mat09].

x_{H_2O}	x_{EtOH}	x_{SA}	x_{H_2O}	x_{EtOH}	x_{SA}
1	0	0.0003	0.6335	0.3665	0.0449
0.9671	0.0329	0.0004	0.5841	0.4159	0.0541
0.9269	0.0731	0.0007	0.5226	0.4774	0.0666
0.8821	0.1179	0.002	0.4513	0.5487	0.0781
0.8293	0.1707	0.0063	0.3686	0.6314	0.0981
0.7652	0.2348	0.0161	0.2596	0.7404	0.1178
0.7266	0.2734	0.026	0.1543	0.8457	0.1295
0.7101	0.2899	0.0294	0.145	0.855	0.145
0.6817	0.3183	0.0342	0	1	0.145

4.3.1.4 Determination of nitrogen HSP (HSP-Ni)

The same procedure was repeated for nitrogen under the conditions that polar molecule interactions are neglected ($\delta_p=0$) and that hydrogen bonding interactions are not more influential than dispersion interactions ($\delta_H \leq \delta_D$). Used literature data can be found in Tab. 4.10.

Tab. 4.10: Solubility data for nitrogen in pure solvents 25 °C and solvent HSP [Han00].

Solvent	x_{SA}	$\log x_{SA}$	$\delta_{D,solvent}$	$\delta_{P,solvent}$	$\delta_{H,solvent}$	
Water	1.37E-05	-4.862	15.5	16	42.3	
Methanol	2.54E-04	-3.595	14.7	12.3	22.3	[Tok75]
Ethanol	4.07E-04	-3.391	15.8	8.8	19.4	
1-Propanol	4.33E-04	-3.363	16	6.8	17.4	
2-Propanol	4.82E-04	-3.317	15.8	6.1	16.4	
Ethanol	3.99E-04	-3.399	15.8	8.8	19.4	
Methanol	2.99E-04	-3.524	14.7	12.3	22.3	[Kre46]
2-Propanol	5.23E-04	-3.281	15.8	6.1	16.4	
n-Butanol	5.03E-04	-3.298	16	5.7	15.8	
Acetone	5.92E-04	-3.228	15.5	10.4	7	

4.3.1.5 Estimation of oxygen and nitrogen solubility in dependence on SA mole fraction by means of Hansen Solubility Parameters (HSP)

The solubility of oxygen and nitrogen in dependence on the SA mole fraction was estimated by calculating R_a as defined in Eq. 4.6. As solvent parameters the mixing parameters of MeOH (from literature) and SA (calculated) as described in Eq. 4.7 were used under the assumption that SA-MeOH-solutions behave like solvent mixtures.

In case of estimating the oxygen solubility HSP and $\log x$ - R_a -relation as described by Sato et al. [Sat14] were used (Eq. 4.9). The prediction of nitrogen solubility was based on calculated HSP-Ni and $\log x$ - R_a -relation.

When Sato et al. [Sat14] investigated the solubility of oxygen in numerous organic solvents and determined HSP-Ox they described the relation between the mole fraction solubility of oxygen in the solvents and the R_a value as seen in Eq. 4.9. Due to this relation the oxygen amount in a solvent or solvent mixture can be calculated if R_a is known.

$$\log x_{O_2} = (-8.89 \cdot 10^{-2})R_a - 1.10 \quad 4.9$$

All solubility estimations refer to a temperature of 25 °C and 1 bar ambient pressure.

5. Results

5.1. Crystallization behavior of SA depending on the presence of dissolved gases

5.1.1 Saturation curve

The determined data points of saturation curves for SA in MeOH for both degassed and non-degassed solutions overlay perfectly as can be seen in Fig. 5.1a. In order to compare measured saturation curves with literature data those are completed in Fig. 5.1b. Experimental values are tabulated in Tab. 12.1.

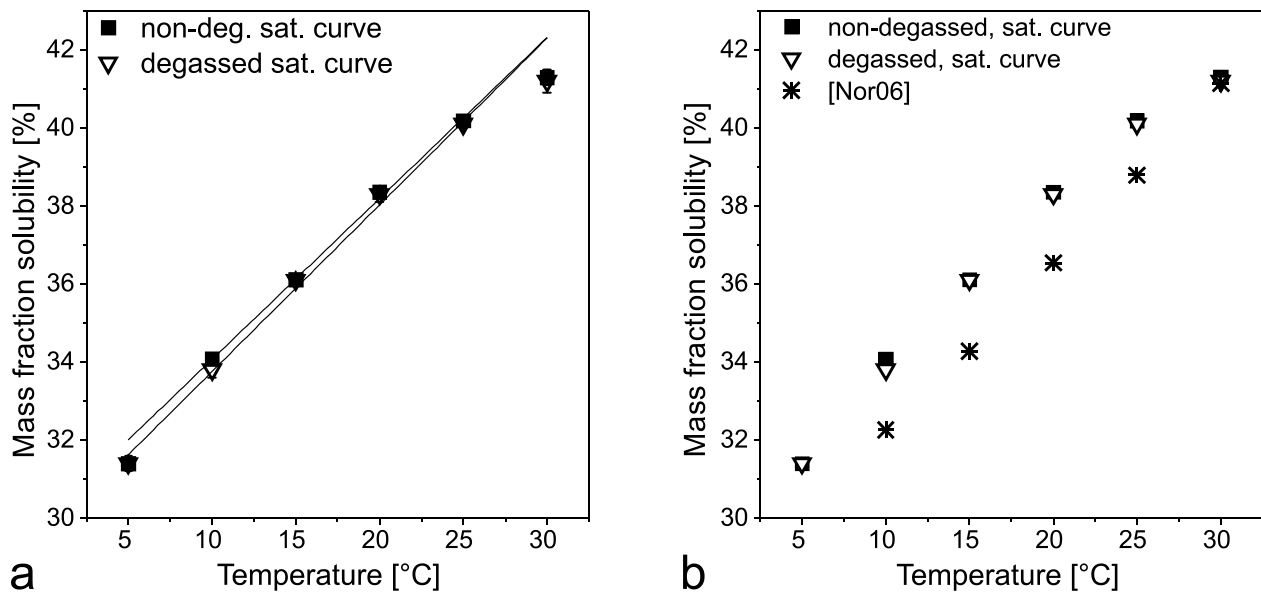


Fig. 5.1: a) Saturation curves of SA in MeOH in degassed (∇) and non-degassed solutions (\blacksquare); b) The measured data are complemented by literature data ($*$) published by [Nor06].

5.1.2 Solubility and MZW

Solubility and MZW were determined by means of US technique. The received results are depicted in Fig. 5.2. As can be seen for all heating rates (2, 5, 10 and 15 K h⁻¹) in case of the used model system SA in MeOH no effect of degassing on the solubility curve can be observed. Considering the nucleation curves degassing can affect a significant decrease of nucleation points at low temperatures (Fig. 5.2a and c) but this cannot always be observed clearly (Fig. 5.2b and d). Summarizing, no general effect of degassing on solubility curve could be found. Considering the MZW a tendency of

slightly enlarged MZW at lower temperatures can be observed if solutions were degassed. The measured values can be found in Tabs. 12.2-12.5.

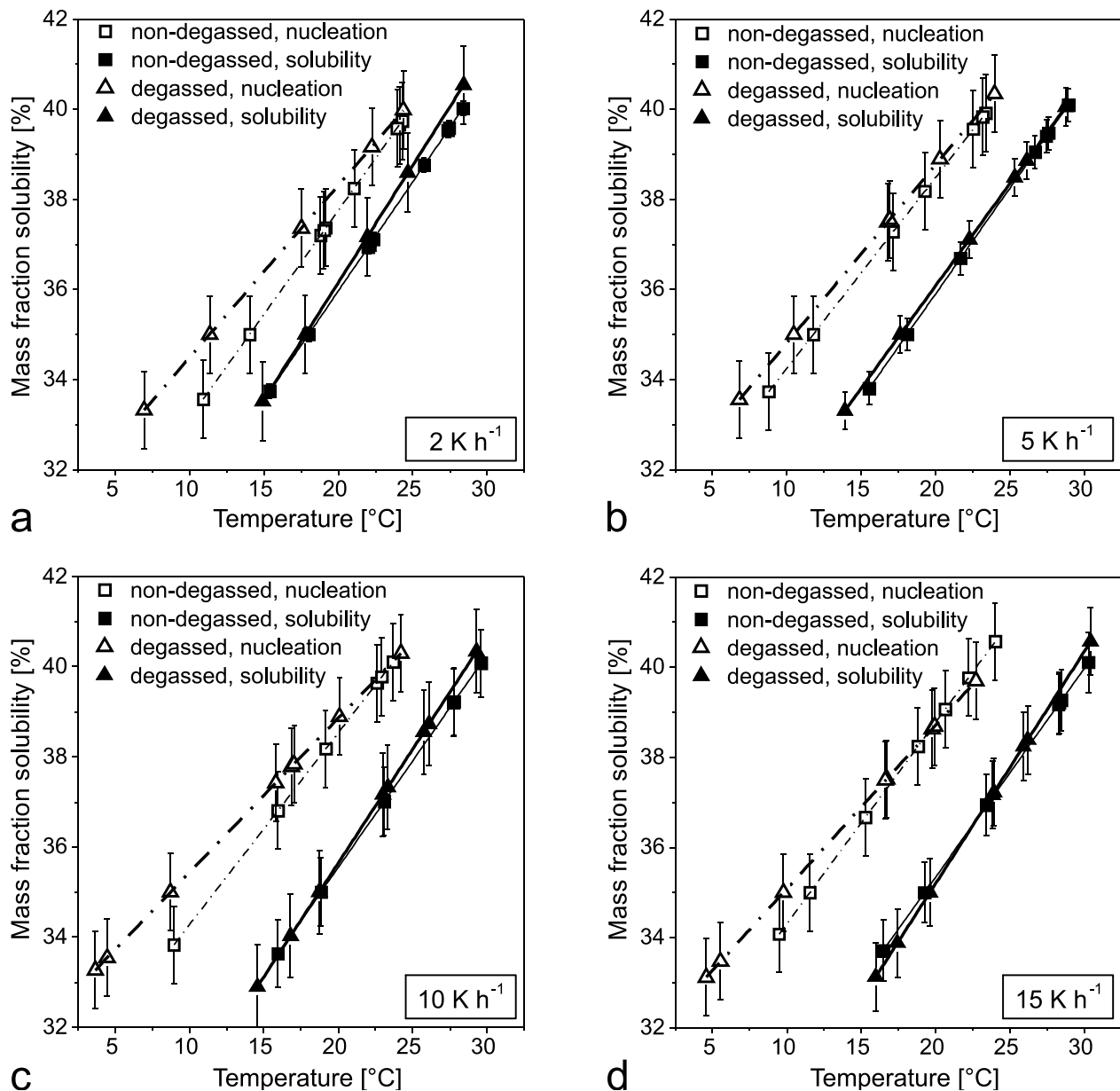


Fig. 5.2: Results of solubility and MZW measurements by means of US method for heating rates of a) 2 K h⁻¹; b) 5 K h⁻¹; c) 10 K h⁻¹ and d) 15 K h⁻¹. The mean values as well as the 95% confidence interval of the curves are depicted.

5.1.3 Growth rate

The results of growth rate measurements of degassed and non-degassed samples at both 10 and 30 °C by means of US setup are illustrated Fig. 5.3, the appropriate values are tabulated in Tabs. 12.6 and 12.7. The measured growth rates indicate that dissolved gases or their reduction do not influence the growth of SA crystals in MeOH.

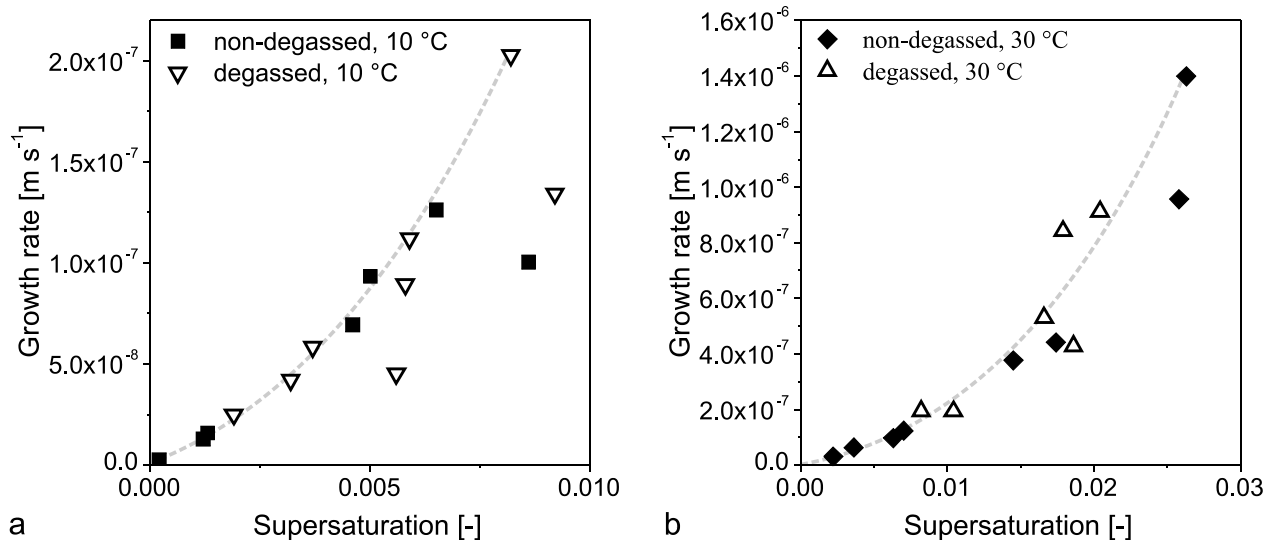


Fig. 5.3: Growth rates measured at a) 10 °C and b) 30 °C for degassed and non-degassed solutions.

The results of the ORM measurements which were performed in order to clarify the progression of the US curve during growth (section 2 in Fig. 4.5b) are illustrated in Fig. 5.4. There the 'desupersaturation curve' of the US velocity is completed by D10 and D90 values from crystal size distribution measurements as well as the counted number of crystals (RawCnt) received from ORM. Due to the needle like shape of the SA crystals D10 and D90 values were depicted instead of D50 distribution.

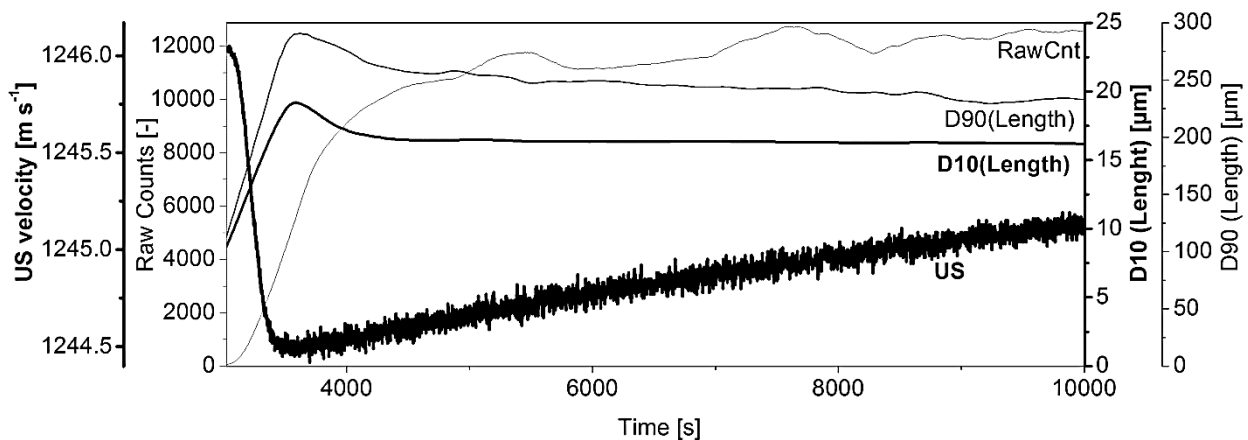


Fig. 5.4: Progression of US velocity during crystal growth (section 2 in Fig. 4.5b) are completed by number of crystals (RawCounts), D10 crystal length and D90 crystal length measured by ORM.

It can be seen that in the beginning the US signal decreases due to the change in solution density and parallel to that the crystals sizes (D10 and D90) increase. This supports the assumption that in the beginning of the desupersaturation the crystal growth takes place in length. This type of growth can be described by an exponential curve. Further, it can be seen that the number of determined crystals increases while the

crystal sizes decrease more and more which indicates the breakage of the crystals and/or the growth in number of crystals, e.g. due to high secondary nucleation [Bla01]. This effect is accompanied by a linearly increasing signal of US velocity which can be constituted by an increase in suspension density. Due to the overlap of the exponential character of growth in length and the linear character of growth in number of crystals the curve was fitted as described in Chapter 4.2.3.

Due to the dependence of the measurement on the used system, e.g. its refractive index, as well as the exact position of the probe and the flow behavior of the crystals this technique is more appropriate for comparative purposes than accurate crystal size measurements. In case of needle-shaped particles the measured crystal sizes are subject to intense fluctuations due to the particles' orientation to the focal point [Mos14]. For these two reasons this technique cannot provide reliable results for the particle sizes of needle-shaped SA crystals and, thus, it was only used for qualitative but not quantitative analysis of crystal growth rates in solution. However, the ORM technique is a useful tool to clarify the progression of the US-signal profile during crystal growth.

5.1.4 Dissolution rate

The dissolution rate was investigated at 10 and 30 °C as well. At 30 °C a shift indicating that SA crystals might dissolve slightly faster in degassed solution compared to non-degassed solution can be seen (Fig. 5.5b, Tabs. 12.8 and 12.9). If the temperature is decreased to 10 °C this shift is even more obvious and a clear difference between degassed and non-degassed samples can be seen (Fig. 5.5a). The data points for degassed solutions are approx. in the same range for 10 °C and 30 °C but in case of non-degassed solutions the dissolution is slower at 10 °C than at 30 °C. Since this T-effect can only be observed in presence of dissolved gases in the solution those gases are assumed to inhibit the dissolution.

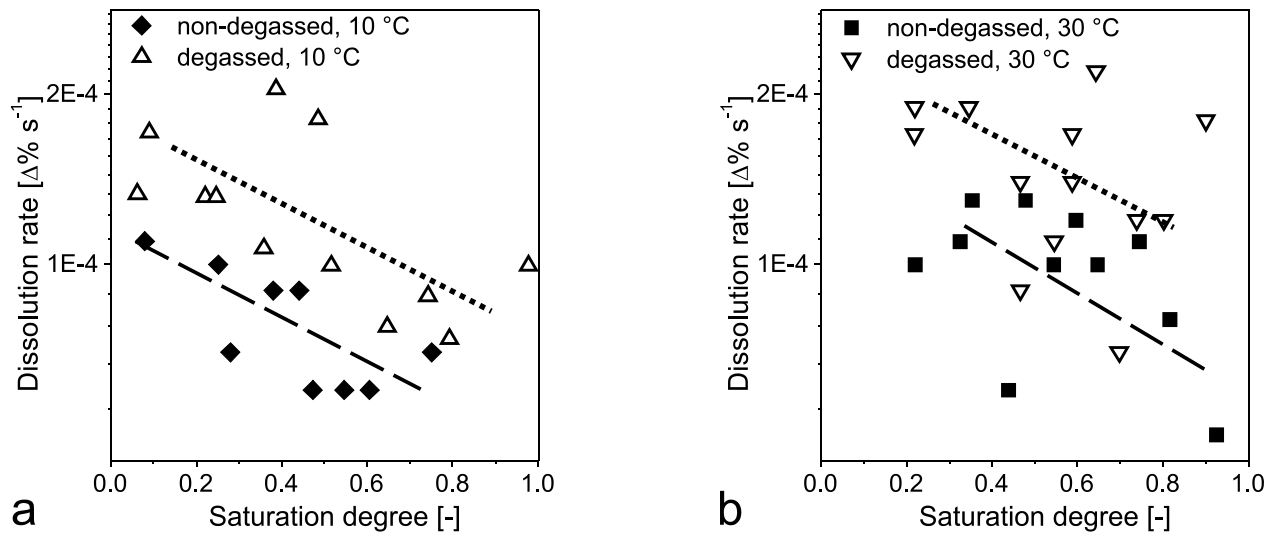


Fig. 5.5: Dissolution rates of SA in MeOH at a) 10 °C and b) 30 °C plotted against saturation degree.

5.1.5 Determination of HSP for SA and nitrogen in pure solvents

The HSP for SA (HSP-SA/ps) and nitrogen (HSP-Ni/ps) in pure solvents were determined in order to predict the solubility of dissolved gases, exemplarily oxygen and nitrogen, depending on the SA mole fraction. This information might help to explain the observed effect of degassing on the dissolution rate (Chapter 5.1.4).

The results from the determination of HSP-SA/ps and HSP-Ni/ps as well as their $\log x$ - R_a -relation can be found in Tab. 5.1.

Tab. 5.1: Results for HSP determination and $\log x$ - R_a -relation for SA and nitrogen.

	HSP-SA/ps	HSP-Ni/ps
$\bar{\sigma}_D$	22.8	7.0
$\bar{\sigma}_P$	11.9	0.0
$\bar{\sigma}_H$	12.5	7.0
	$\log x_{SA} = (-1.54 \cdot 10^{-1})R_a + 1.61$ 5.1	$\log x_{Ni} = (-7.33 \cdot 10^{-2})R_a - 1.74$ 5.2

5.1.6 Estimation of gas solubility in dependence on SA mole fraction

The oxygen solubility in dependence on SA amount in methanolic solution was predicted using HSP from literature (HSP-SA/[Han07]) and HSP determined in this work (HSP-SA/ps). As depicted in Fig. 5.6 the mole fraction solubility of oxygen for both HSP-SA values is decreasing with increasing SA mole fraction. In case of HSP-SA/ps the solubility decreases more steeply than in case of the literature HSP (HSP-SA/[Han07]).

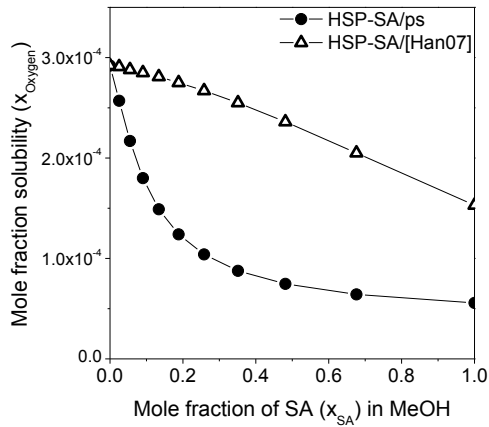


Fig.5.6: Dependency of oxygen solubility in methanolic SA solutions on the SA mole fraction based on HSP-SA/[Han07] (Δ) and HSP-SA-ps (●).

additionally to the HSP (δ_D , δ_P , δ_H) the x - R_a -relation which allows quantification of mole fraction solubility of SA if R_a is known. For that reason the HSP determined in this work are used for further solubility predictions.

The results for solubility estimations for oxygen and nitrogen in SA-MeOH solutions in dependence on the SA mole fraction are depicted in Fig. 5.7. Since there is no perfect miscibility between SA and MeOH the mole fractions of SA in saturated solutions as 10 and 30 °C are highlighted in Fig. 5.7b.

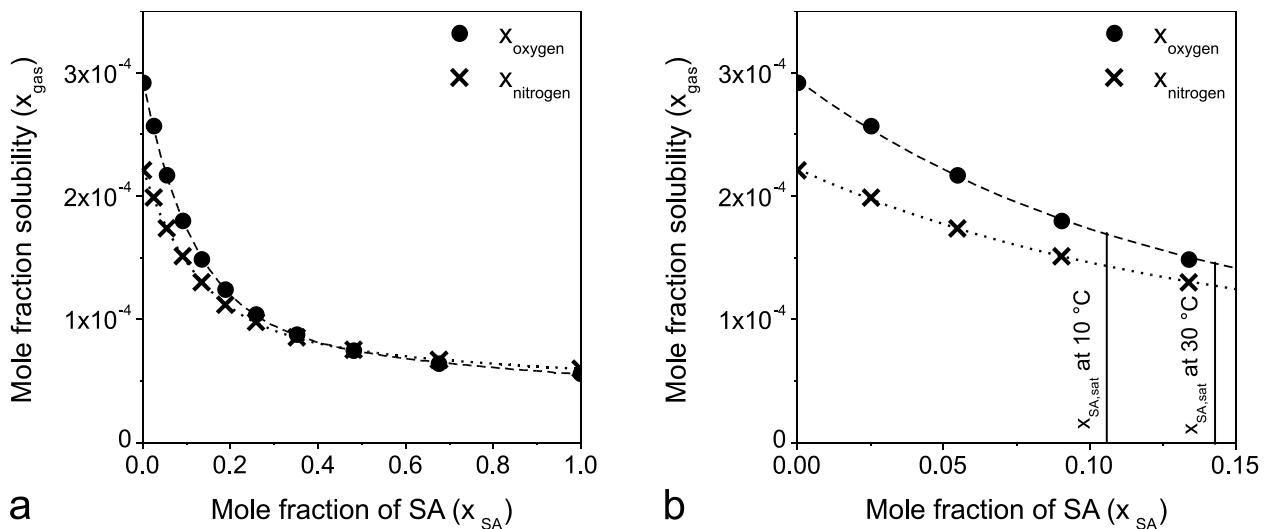


Fig. 5.7: Mole fraction solubility of oxygen and nitrogen in SA-MeOH solutions, depending on SA concentration; a) Whole range; b) Saturation mole fraction of SA in MeOH at 10 and 30 °C are highlighted.

It can be seen clearly in Fig. 5.7 that the solubility of both oxygen and nitrogen decrease with increasing amount of SA in solution. If the predicted solubility data of oxygen and

The differences in curve progression are not disagreeing with the HSP model. Hansen et al. [Han07] pointed out particularly that differences between modeled and experimental data can occur. These can be explained by the different methods to provide the HSP. Hansen et al. [Han07] calculated HSP for a wide range of organic compounds based on group contribution methods or similarities to related compounds. Contrary to that, in this study the determination of HSP-SA/ps was based on solubility data from literature. This method provided

nitrogen in pure MeOH are compared to literature data (Tab. 5.2) it is found that the calculated data are in quite good agreement with the literature data. Thus, this method is rated to provide reliable estimations for the solubility of oxygen and nitrogen in methanolic SA solutions.

Tab. 5.2: Mole fraction solubility for oxygen and nitrogen at 25 °C in pure methanol. Literature and calculated values.

		Mole fraction solubility in pure MeOH at 25 °C [-]	
		Oxygen	Nitrogen
Literature data	[Tok75]	$4.50 \cdot 10^{-4}$	$2.54 \cdot 10^{-4}$
	[Kre46]	$4.52 \cdot 10^{-4}$	$2.99 \cdot 10^{-4}$
Calculated value		$2.92 \cdot 10^{-4}$	$2.21 \cdot 10^{-4}$

5.2. Solubility of SA in solvent mixtures

In order to investigate the possibility of using SA container crystals as encapsulation systems for cosmetic or dermatological products their stability in such products has to be determined. In case of crystalline materials this means that the surrounding liquid has to be saturated with the same material to avoid the dissolution of the container crystals. Since SA crystals are used in the present study as encapsulation systems the SA solubility in dependence on the solvent composition was investigated. To reach this, the solubility of SA in EtOH-water-mixtures was determined experimentally and depicted in a ternary diagram. Moreover, a solubility prediction model based on literature data was developed which allows estimating the SA solubility in different solvent compositions.

5.2.1 Solubility of SA in EtOH-water-mixtures

The solubility of SA in EtOH-water-mixtures that was measured in this study is illustrated in Fig. 5.8 as ternary diagram while the measured values can be found in Tab. 12.10. The data points in this diagram represent the solubility curve of SA in EtOH-water-mixtures. In the area below this curve the solvent mixture is saturated with SA. Above this curve SA is undersaturated in the solvent phase and SA (container) crystals will dissolve.

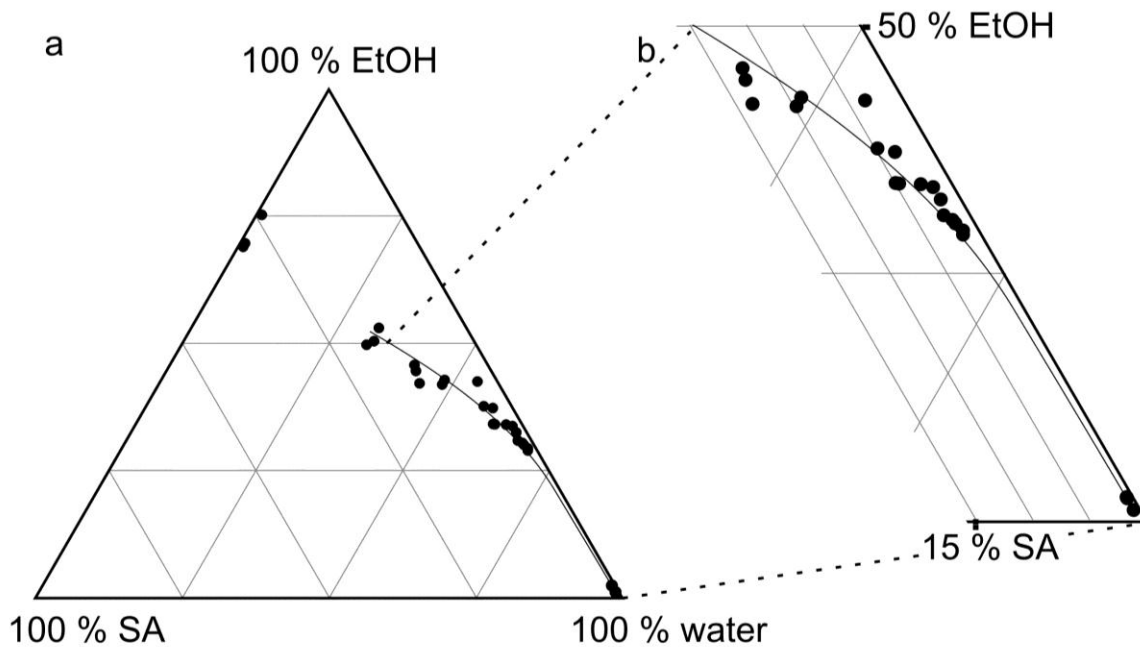


Fig. 5.8: a) Ternary phase diagram of SA in EtOH and water, measured at 20 °C; b) Increased section illustrates SA solubility in mass fraction range below 15% SA and 50% EtOH.

It should be mentioned that crystalline container materials are only stable in a saturated medium. As discussed in Chapter 4.1.1 the allowed upper amount of SA are 2% in cosmetic skincare products. Considering this amount the solvent compositions which enable minimum SA solubility should be chosen in order to reach the highest possible amount of container crystals for encapsulation.

5.2.2 Comparison between measured and literature data

The solubility of SA in EtOH-water-mixtures is described in literature by Matsuda et al. [Mat09]. These data as well as the data measured in this thesis are depicted in Fig. 5.9 where the SA mole fraction solubility (x_{SA}) is plotted against the mole fraction of EtOH in water (x_{EtOH}).

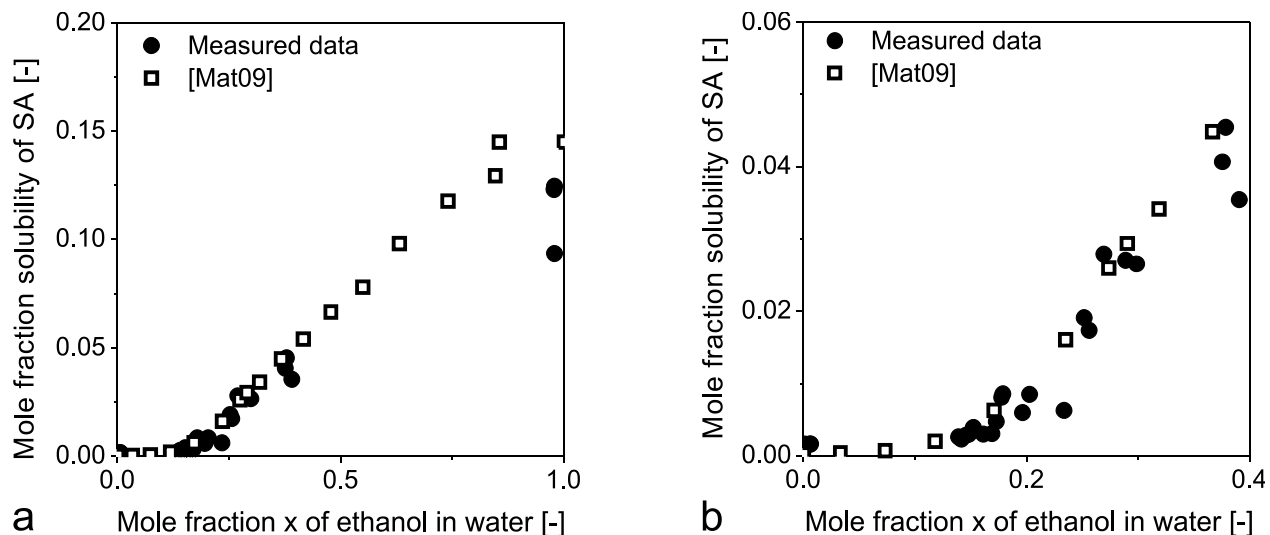


Fig. 5.9: Molefraction solubility of SA in EtOH-water-mixtures. Measured data (at 20 °C) are compared to literature data by Matsuda et al. (at 25 °C) [Mat09]; a) Full data range; b) Range of measured data is increased.

To determine the SA solubility in the binary solvent mixture Matsuda et al. [Mat09] first prepared the solvent mixtures and then added an excess amount of SA. After 24 h at 25 °C the SA concentration of the supernatant solutions was measured by means of HPLC. For each data point the average value of three measurements was used.

The solubility data measured in this study were generated by adding SA-EtOH-solution to water until crystals appeared. Afterwards the initial solution was dropped slowly into the ternary mixture until the crystals just dissolved. Due to this procedure it was not possible to get solubility data for EtOH mass fractions of <0.3 and >0.6 . That's why the data points for pure water and pure EtOH were determined as saturation concentrations. For all samples SA and water contents were determined analytically and based on these values the EtOH content was calculated. Each data point represents one measurement.

Both the experimental procedure and the inaccuracies of the analytical methods as well as the calculation of the EtOH amounts led to the variation of the data points. Moreover, it has to be pointed out that for this study the solubility of SA was determined at 20 °C. This explains the slight shift of SA solubility to lower values than the literature data which were measured at 25 °C. Nevertheless, a well acceptable accordance between measured and literature data was reached.

5.2.3 Model development for SA solubility in solvent-water-mixtures

For the development of a model to predict the solubility of SA in different solvent compositions the HSP-model was used. As described earlier the HSP for SA in pure solvents (HSP-SA/ps) were determined. These HSP values were used for solubility predictions of SA in EtOH-water-mixtures. The calculated results as well as the measured data can be seen in Fig. 5.10.

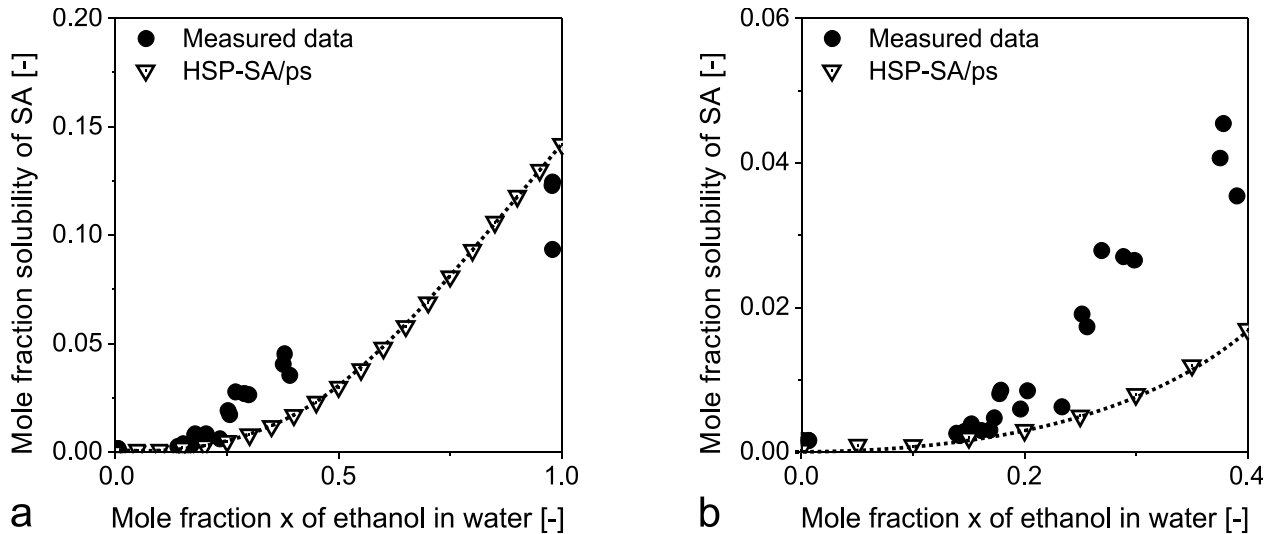


Fig. 5.10: Predicted mole fraction solubility of SA in EtOH-water-mixtures based on HSP-SA/ps; a) Full data range; b) Range of measured data is increased.

Only at low EtOH amounts (<0.2) the used model leads to acceptable results but with increasing EtOH content the prediction fits much less to the measured data. For that reason the determination of HSP-SA was repeated by using solubility data for SA in EtOH-water-mixtures (HSP-SA/ew) as published by Matsuda et al. [Mat09]. The calculated parameters for HSP-SA/ew are noted in Tab. 5.3. When HSP-SA/ew were determined it was found that a square root relationship resulted in much better correlation for the quantification equation than a logarithmic one as used in case of HSP-SA/ps.

Tab. 5.3: HSP for SA determined based on solubility in pure solvents and in EtOH-water-mixtures.

	HSP-SA/ps	HSP-SA/ew
δ_D^*	22.8	15.8
δ_P^*	11.9	16.7
δ_H^*	12.5	40.7
	$\log x_{SA} = (-1.54 \cdot 10^{-1})R_a + 1.61$ (5.3)	$\sqrt{x_{SA}} = (1.84 \cdot 10^{-2})R_a - 1.30 \cdot 10^{-2}$ (5.4)

In Fig. 5.11 the experimental data by [Mat09] as well as the values that were predicted using HSP-SA/ew including the associated x_{SA} - R_a -relation (Eq. 5.4) are illustrated. A very good agreement between literature data and predicted values is reached.

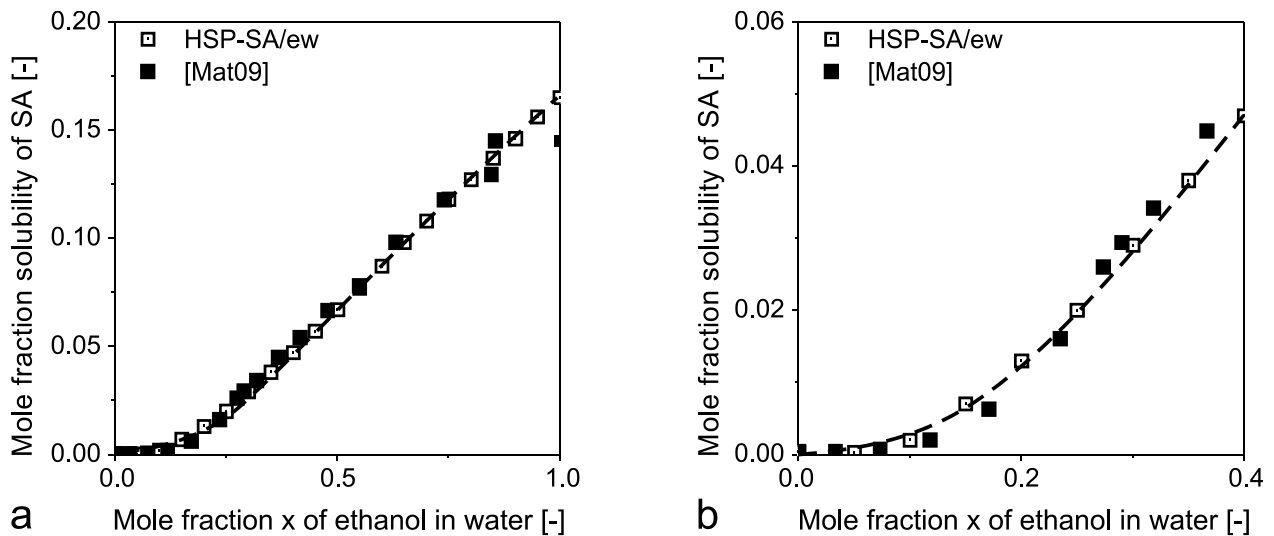


Fig. 5.11: Predicted data for HSP-SA/ew show good accordance to the literature data [Mat09]; a) Full data range; b) Range of measured data is increased.

The comparison between measured data and the values predicted on HSP-SA/ew and HSP-SA/ps are depicted in Fig. 5.12. There, it can be seen that the predictions based on HSP-SA/ew fit better to the measured results than the values predicted on HSP-SA/ps. At EtOH mass fractions around 0.2 the determined SA solubility data are between the predicted values of both models.

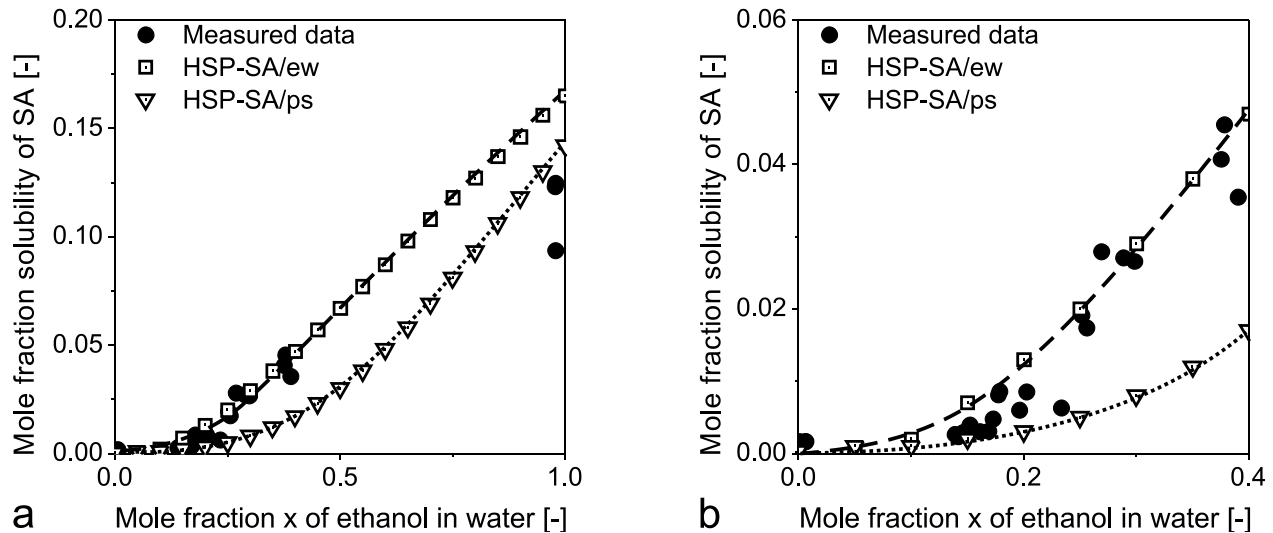


Fig. 5.12: Solubility predictions for SA in EtOH-water-mixtures using HSP-SA/ew. Measured data and predictions from HSP-SA/ps are depicted for comparison; a) Full data range; b) Range of measured data is increased.

5.2.4 Verification of the HSP solubility prediction model

The developed solubility prediction model is verified in order to determine the model accuracy in case of solvent-water-mixtures where another solvent than EtOH was used. Since Matsuda et al. [Mat09] provided SA solubility data for MeOH-water-mixtures, too, this system is used for verification and the accuracy of the prediction can be assessed. The results of the solubility prediction for MeOH-water-mixtures based on HSP-SA/ew and HSP-SA/ps are illustrated in Fig. 5.13.

In this example, where MeOH is used as second solvent component, literature data and predicted data show quite good correlation at MeOH amounts up to a mole fraction of 0.2. In this range the predictions based on HSP-SA/ps and HSP-SA/ew lead to similar results. If the MeOH amount increases further the predicted values reflect the measured values less and less accurate the higher the MeOH content gets. Comparing the accuracy of the two used models it can be seen that predictions based on HSP-SA/ew fit better than those based on HSP-SA/ps. However, due to the good accordance between measured and predicted data at low MeOH and SA amounts the used model is assessed to lead to acceptable results. Considering the in general better fit of predictions based on HSP-SA/ew compared to those based on HSP-SA/ps further predictions that include solvent-water-mixtures are based on HSP-SA/ew.

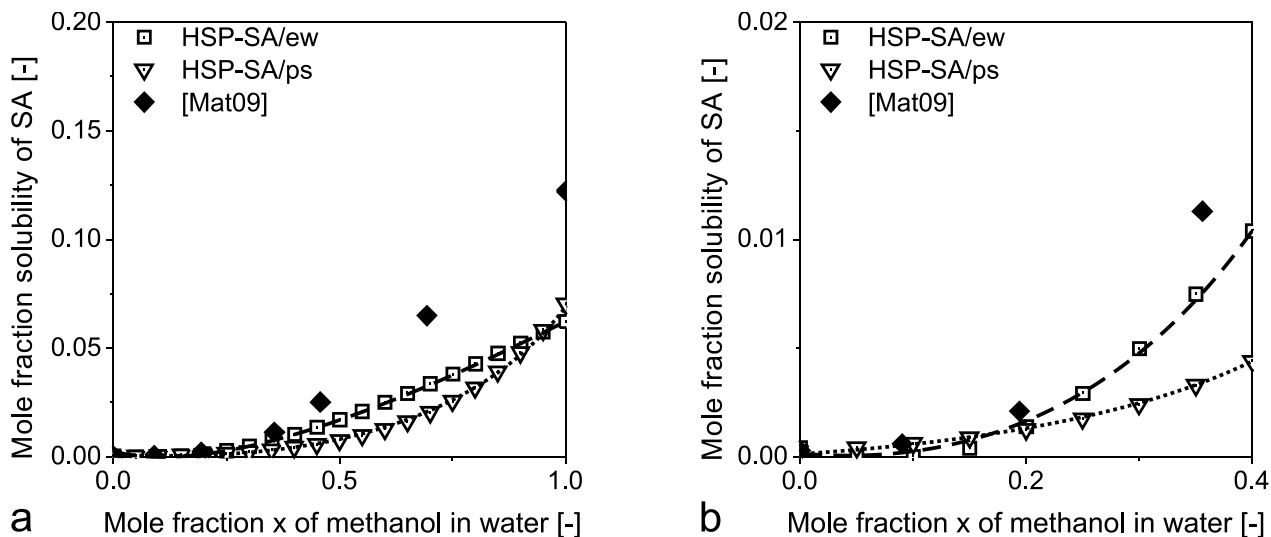


Fig. 5.13: Literature [Mat09] and predicted data for SA solubility in MeOH-water-mixtures; a) Full data range; b) Range of measured data is increased.

5.2.5 Solubility predictions by means of HSP

The reason for the development of the previously described solubility prediction model is to predict the SA solubility in other solvents, especially, solvent mixtures with a high amount of water without the need of available solubility data from literature. This should allow estimating the stability of SA container crystals in potential products in dependence on the used solvent composition. Since a wide range of skincare products are based on water as solvent the predictions are focused on water containing solvent mixtures.

As solvents which are widely used in skincare products iso-propanol and glycerol were chosen exemplarily [Fin05]. The predicted solubility data for SA in the solvent-water-mixtures are illustrated as both mole fraction and mass fraction solubility as can be seen in Fig. 5.14 for i-propanol-water mixtures and in Fig. 5.15 for glycerol-water-mixtures.

In Fig. 5.14b it can be seen well that in case of i-propanol-water-mixtures up to a mass fraction of 0.2 (20%) i-propanol can be used without changing the solubility of SA in the solvent mixture significantly. Thus, i-propanol can be used in products in moderate amounts without the risk of decreasing the available amounts of container crystals.

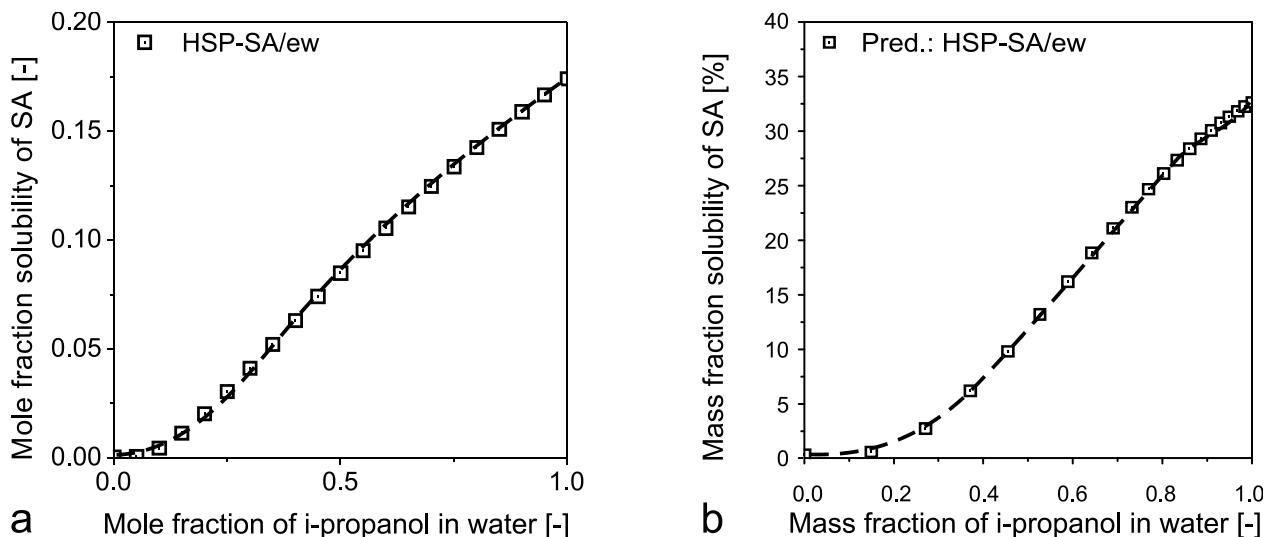


Fig. 5.14: Predicted solubility for SA in water-iso-propanol. a) Mole fraction solubility; b) Mass fraction solubility.

In case of glycerol-water-mixtures (Fig. 5.15) a glycerol mass fraction of 0.1 can be used without a change of SA solubility in the mixture.

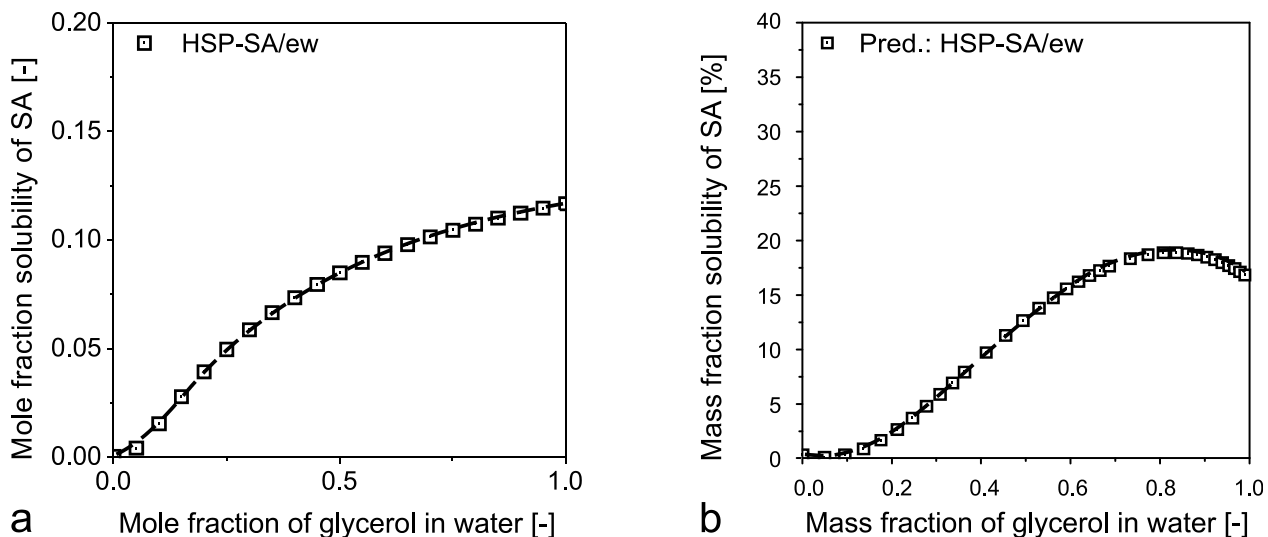


Fig. 5.15: Predicted solubility for SA in water-glycerol-mixtures. a) Mole fraction solubility; b) Mass fraction solubility.

It can be summarized that in general SA container crystals can tolerate the presence of organic solvents in moderate amounts. For practical applications experimental verifications of the predicted results should be performed.

5.3. Investigations on inclusion containing crystals

It is one important aim of this study is to prepare container crystals. Therefore, it is important to investigate the mechanisms of their formation and how to manipulate the

experimental parameters in order to reach maximum amounts of inclusion volume which will allow estimating the encapsulation potential.

5.3.1 Single crystal growth observed from antisolvent crystallization

As described Chapter 2.3 in context of cavity or inclusion formation several kinds and mechanisms to explain this phenomenon are reported in literature. In order to clarify the mechanism that takes place in this particular case where SA is crystallized in an antisolvent process the growth of single crystals was observed under the microscope. The results of these investigations will be given for two exemplary cases.

5.3.1.1 Slow growing crystal

As a first example a slowly growing crystal is chosen. The growth rate in length of the exemplary crystal is depicted in Fig. 5.16a. The images taken of this crystal over time can be seen in Fig. 5.16b-e. In the beginning of the measurement ($t=0$) the crystal growth was about $1.7 \cdot 10^{-7} \text{ m s}^{-1}$ and decreased distinctly. As can be seen in Fig. 5.16b-e the observed crystal has some tiny defects but no macroscopic inclusions were formed.

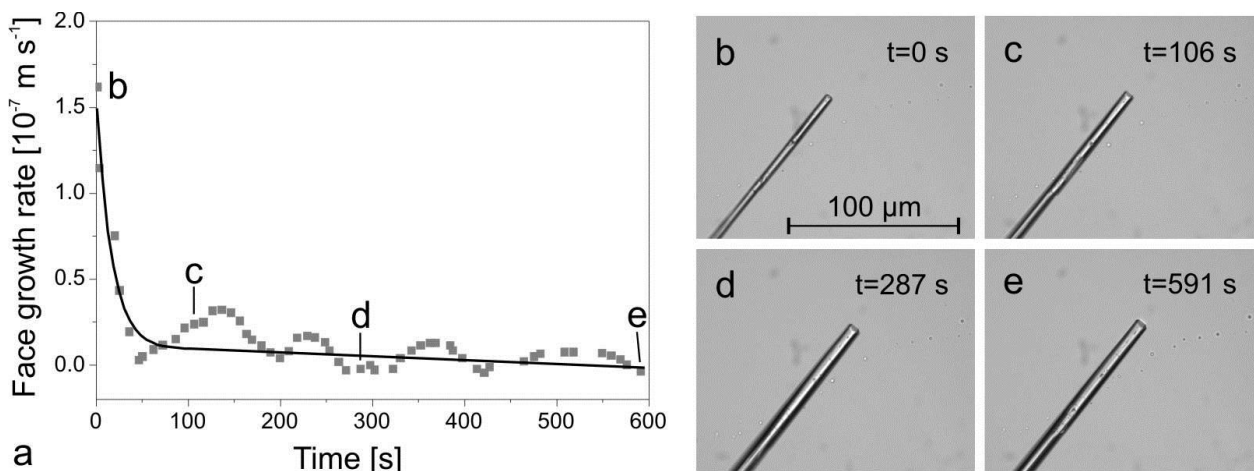


Fig. 5.16: a) Growth rates of (001) crystal face over time for the crystal that is depicted in b-e) Over time.

5.3.1.2 Fast growing crystal

In the second example a fast growing crystal was chosen. The growth rate of its (001) face is plotted over time (Fig. 5.17a). It should be pointed out that $t=0$ represents the moment the crystal was in focus of the microscope and the measurement could be started. In Fig. 5.17b the appropriate crystal is shown. As can be seen in the growth rate-time-graph (Fig. 5.17a) the growth rate of the observed face is characterized by

distinct fluctuations. The points of particular high and low growth rates are marked by arrows which are linked to the arrows in Fig. 5.17b. Considering the first sudden but distinct increase in the growth rate (arrow 1) it could be observed that at this point a flat bottom was formed (Fig. 5.17b, arrow 1). Thereafter, a decrease in growth rate can be observed (Fig. 5.17a, arrow 2) which leads to the reduction of the inclusion's width (Fig. 5.17b, arrow 2). This phenomenon can be observed for several further times.

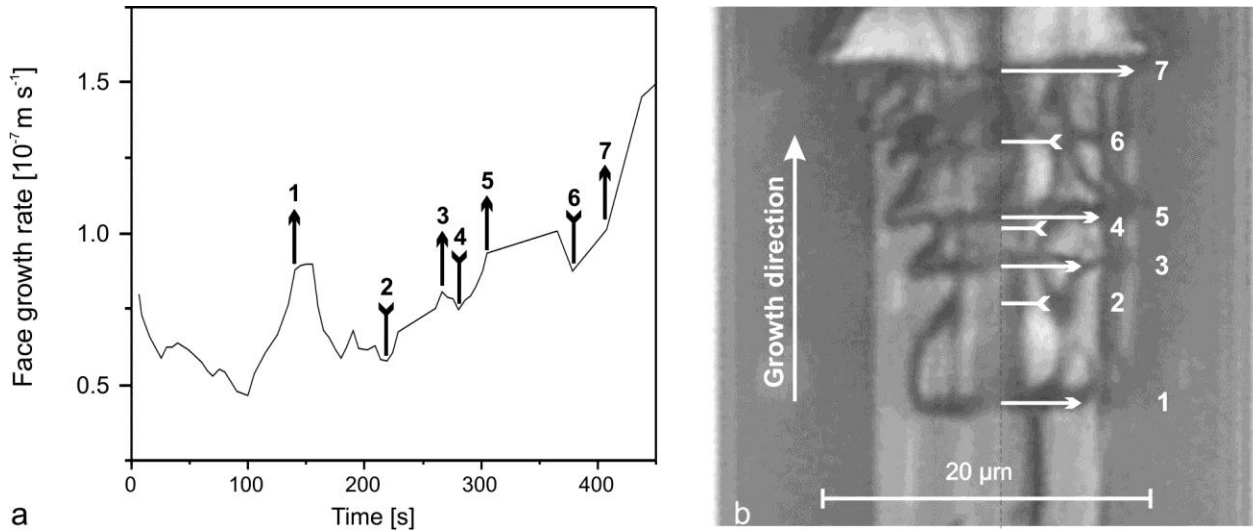


Fig. 5.17: a) Face growth rate of crystal shown in b) Sections of growth fluctuation are reflected in the thickness of the observed inclusion.

5.3.1.3 Closure of inclusions

Besides the importance of the face growth rate on the formation of inclusions the sealing of the inclusions is a further issue in inclusion formation and was observed. This 'healing' process was observed in case of a crystal that contains symmetrical funnel-shaped inclusions (Fig. 5.18). Since the crystal was discovered too late the growth rates during the formation of this type of inclusions could not be determined. As illustrated in Fig. 5.18 the complete 'healing' of the open inclusions happens quite fast (78 s). Due to the inaccuracies of the measurement the growth rate during this step could not be quantified. However, the observations show that such a closure of inclusions takes only a few minutes for SA crystals.

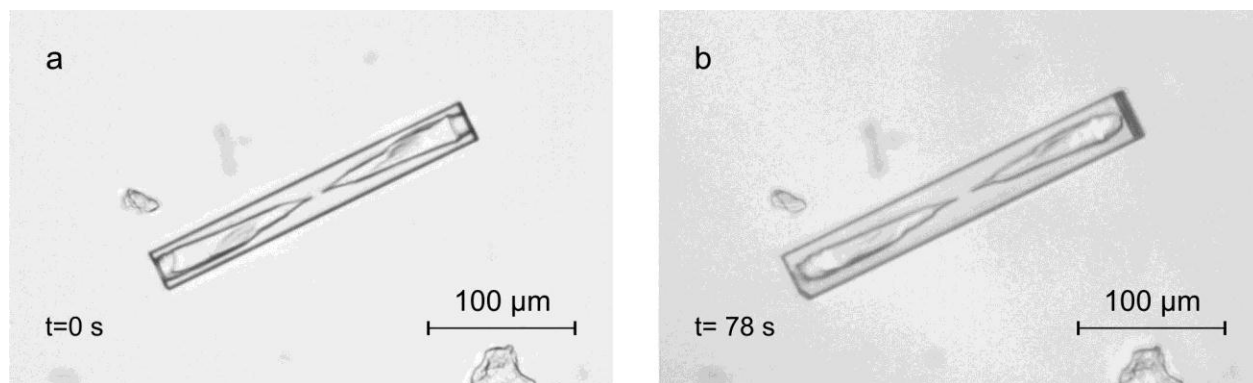


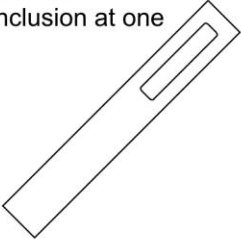
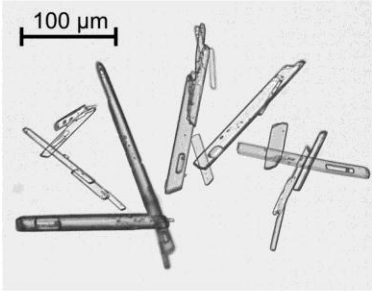
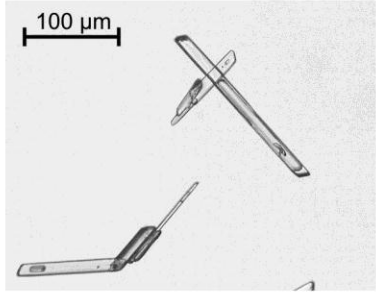
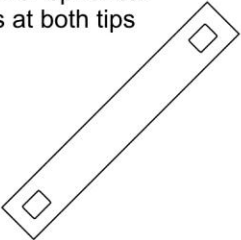
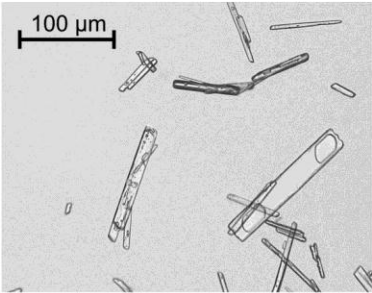
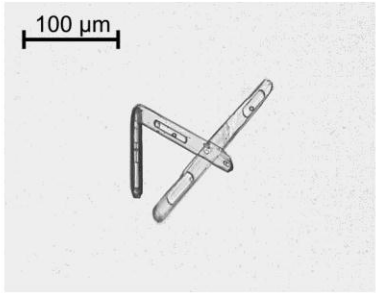
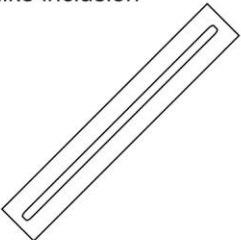
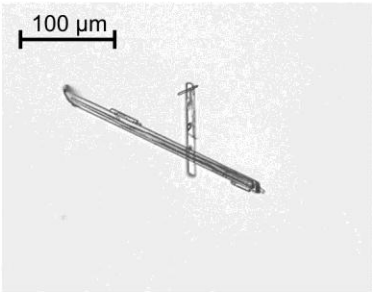
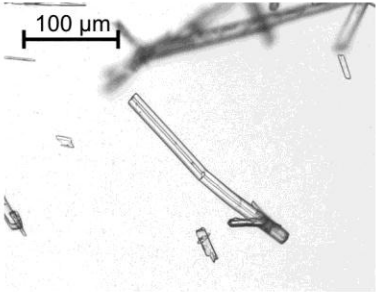
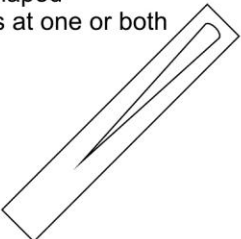
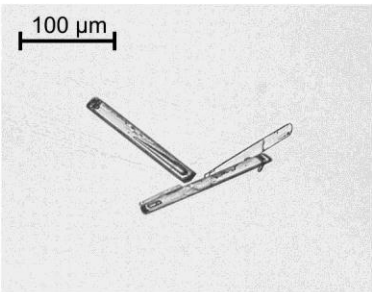
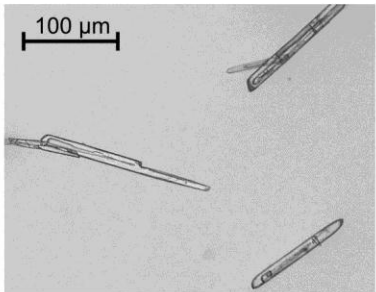
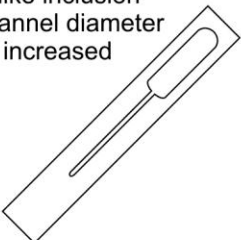
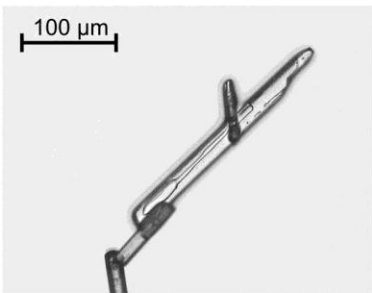
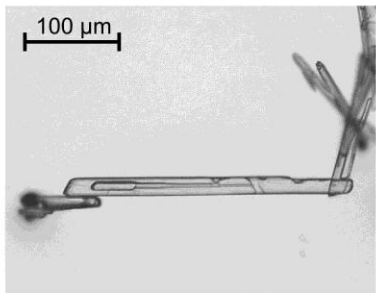
Fig. 5.18: SA crystal containing two funnel-shaped inclusions. a) Since the inclusions already were formed when the measurement could be started b) Only the closure of the inclusions could be observed.

The method that was applied for the microscopic investigations of crystal growth during static antisolvent crystallization offers the possibility to observe the growth of single crystals. In some cases growth rates of single faces could be determined and compared to the appearance of the growing crystal. The results of these experiments show that a relation between growth rate fluctuations and inclusion formation or shaping can be observed. Moreover, it could be shown that by means of this static antisolvent method inclusions of different shapes can be formed.

5.3.2 Shapes of inclusions

The intense microscopic investigations performed using the crystals prepared during the first enquiry on the effects of experimental parameters on crystal and inclusion sizes led to interesting results according to the shape of the formed inclusions. In the crystals from stirred antisolvent crystallization processes the formation of different types of shapes of inclusions was exposed as illustrated schematically and shown by microscopic images in Tab. 5.4.

Tab. 5.4: An overview of the observed inclusion shapes is presented by schematically illustrations and microscopic images.

Type of inclusion shape	Microscopic images	
<p><u>Type 1:</u> Single cylindrical or spherical inclusion at one tip</p> 		
<p><u>Type 2:</u> Cylindrical or spherical inclusions at both tips</p> 		
<p><u>Type 3:</u> Channel-like inclusion</p> 		
<p><u>Type 4:</u> Funnel-shaped inclusions at one or both tips</p> 		
<p><u>Type 5:</u> Channel-like inclusion where channel diameter suddenly increased</p> 		

It occurs that some crystals contain different types of inclusions (Fig. 5.19) and a smooth transition between different types can be observed. As can be seen in Fig. 5.19a where the crystal contains a small spherical inclusion (type 1) and a larger one that could be interpreted as funnel-like (type 4) or a channel-like inclusion with increasing diameter (type 5).

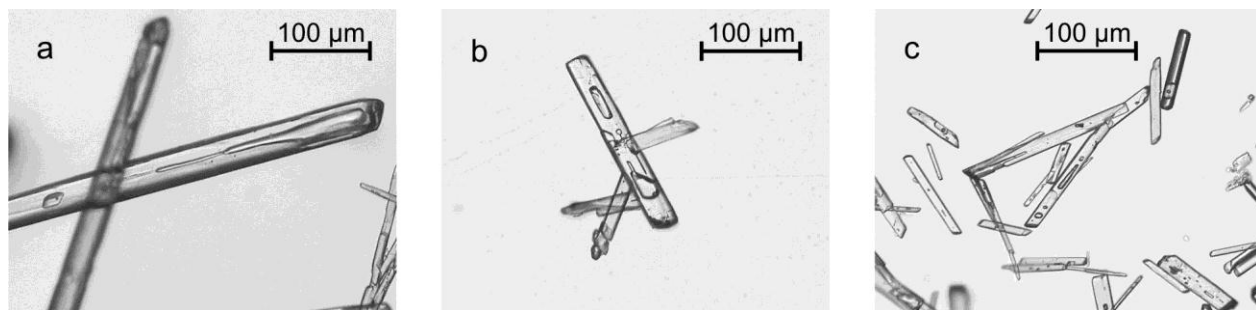


Fig. 5.19: One crystal can even contain inclusions of different types.

For the current enquiries only the sizes of crystals and inclusions were of interest and, thus, no statistical recording was carried out about the frequency of the occurrence of the different types of inclusions. According to the observations type 1 appeared slightly more often than the types 2, 4 and 5, while the channel like inclusions (type 3) were hardly observed.

5.3.3 First enquiry on the effects of experimental parameters on crystal and inclusion sizes

In this first enquiry the effects of experimental parameters on SA container crystals grown from antisolvent crystallization were investigated. This first enquiry consisted of three steps: the experimental parameters which might affect the crystal and inclusion sizes first were identified and, secondly, the effects of single parameters were determined in more details. For the antisolvent crystallization the antisolvent water was injected into a methanolic SA solution.

5.3.3.1 1. Step: Parameter screening

Due to the high number of investigated parameters and the partially bad crystal shapes as well as the high agglomeration degree of many samples it was not possible to get meaningful data for crystal and inclusion dimensions from microscopic investigations (see Fig. 5.20). Thus, the evaluation of the experimental results by means of Statistica

could not be applied and the decision about further parameter investigations need to be based on the OM images. Due to those results the parameters solution mass fraction (w), injection rate (IR), solution volume (V_S), solution temperature (T_S), stirring rate (SR) and gas content in both water and solution were chosen as parameters that needed to be investigated in more details.

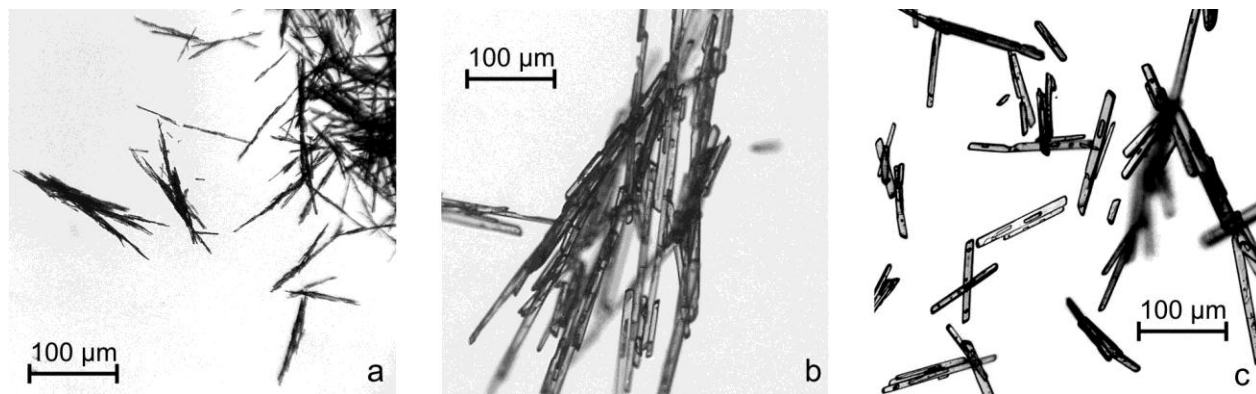


Fig. 5.20: Exemplary results of the first, parameter screening step of this enquiry are shown: a) Sample 1-11; b) Sample 1-15; c) Sample 1-16.

Even though, no effect of the colorant could be observed for further experiments only uncolored solutions were used. The ratio between solution and antisolvent neither had an observable effect. To ensure possibly high yields and reduce experimental time a solution-antisolvent ratio of 1:4 was chosen for further experiments.

Based on the results of this first step the experimental parameters for steps 2 and 3 were chosen as described in Chapter 4.2.8. The aim of this enquiry is to identify the parameters which are of interest for the formation of liquid inclusions and to adjust the experimental procedure in order to reach maximum inclusion amounts in the crystals.

5.3.3.2 2. Step: Influence of solution mass fraction, injection rate and solution volume

In the second step the parameters mass fraction (w), injection rate (IR) and solution volume (V_S) were varied in order to identify their influences on the generation of container crystals that own maximum possible inclusion amounts.

In this step the revealed container crystals were much better defined and showed in general much less agglomeration. This allowed applying Statistica for the evaluation of the experiments. It was found that the solution volume had negligible effects on the amount of inclusions inside the crystals. Thus, the effects of w and IR will be focused on.

For a better visualization the experimental parameters are according to w and IR for each sample summarized in Fig. 5.21a. Moreover, the median crystal and inclusion sizes are illustrated based on the measured results. For easier illustration all inclusions are depicted as type 1 inclusion although different inclusion shapes were observed as described in more details in Chapter 5.3.2.

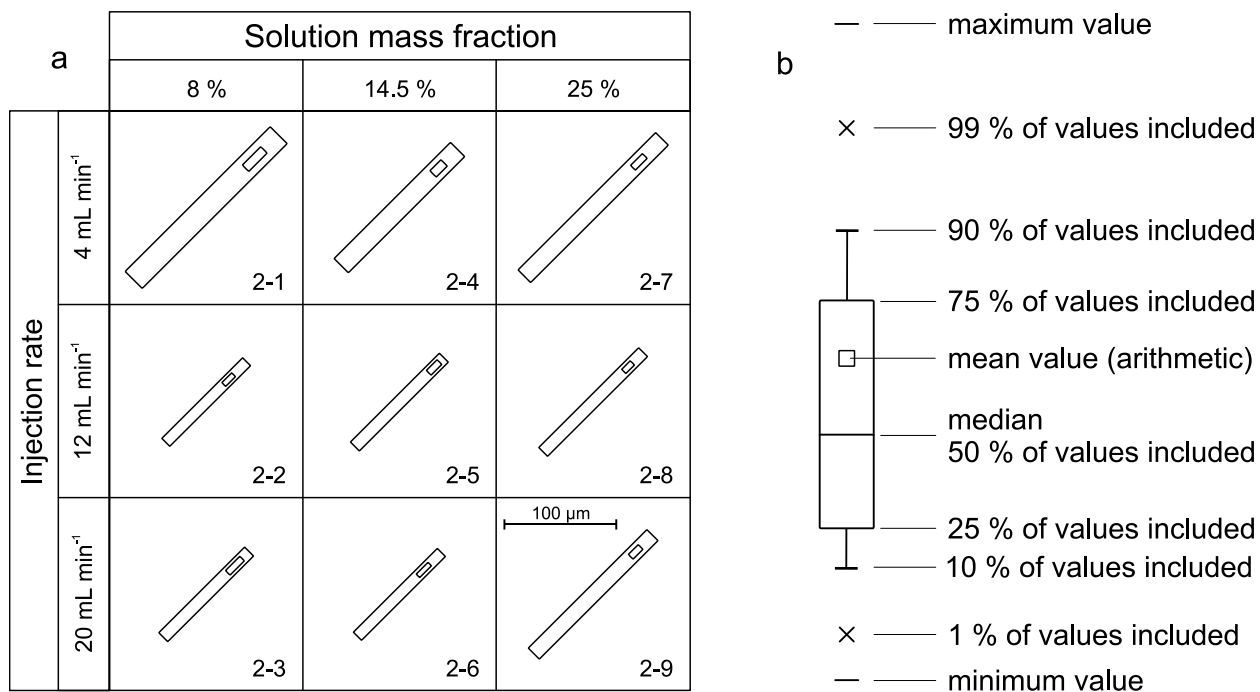


Fig. 5.21: a) For each sample of this second step the applied w and IR are summarized. The schematically illustrated crystals are based on the median values for crystal and inclusion sizes. The illustration allows comparing inclusion and crystal ratios between samples. b) Schematic legend of boxplots as used to describe the results.

As can be seen in Fig. 5.21a the crystals prepared by the antisolvent method under varying w and IR show some fluctuations in the median crystal dimensions. Particularly noticeable are the increased crystal sizes that were received at low IR (4 mL min⁻¹) compared to those at medium (12 mL min⁻¹) or high (20 mL min⁻¹) IR.

More detailed results according to crystal length and volume as well as relative inclusion amount (RIA) and absolute inclusion volume (AIV) per crystal are depicted in Figs. 5.23 and 5.24. To illustrate the results box-whisker diagrams (boxplot) were chosen. Symbol definitions can be found in Fig. 5.21b.

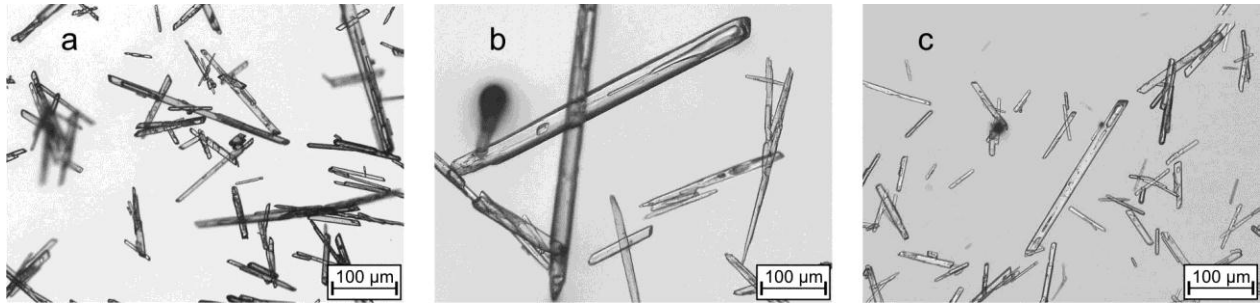


Fig. 5.22: Prepared crystals show low agglomeration degree and a high particle size distribution; a) Sample 2-6; b) Sample 2-9; c) Sample 3-2.

As can be seen in Fig. 5.23 there are variations in the crystal dimensions in both length and volume. These variations are based on the very inhomogeneous samples (Fig. 5.22) and makes the data evaluation more complicated. However, as already mentioned above crystals prepared at low IR (Samples 2-1, 2-4 and 2-7) are distinctly larger compared to crystals prepared at medium and high IR.

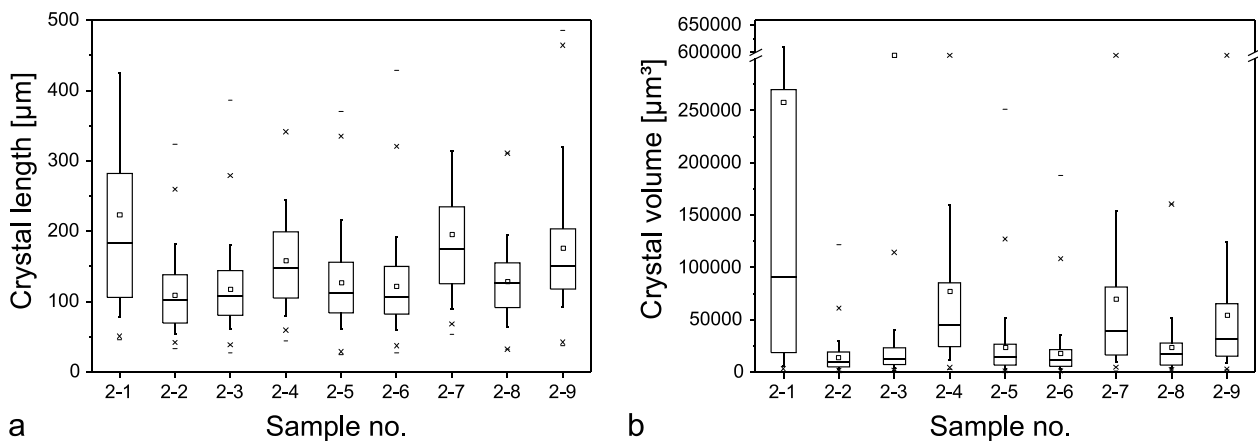


Fig. 5.23: Measured data for a) Crystal length [µm] and b) Crystal volume [µm³] in dependence on w and IR (second step).

In Fig. 5.24 the inclusion sizes are depicted as RIA per crystal (Fig. 5.24a) and AIV per crystal (Fig. 5.24b). These two diagrams offer the possibility to get general conclusions about the crystal-inclusion ratios. Considering the RIA (Fig. 5.24a) it can be seen that the parameters that were investigated in this enquiry (V_s , w and IR) hardly affected the crystal-inclusion ratio in a considerable way.

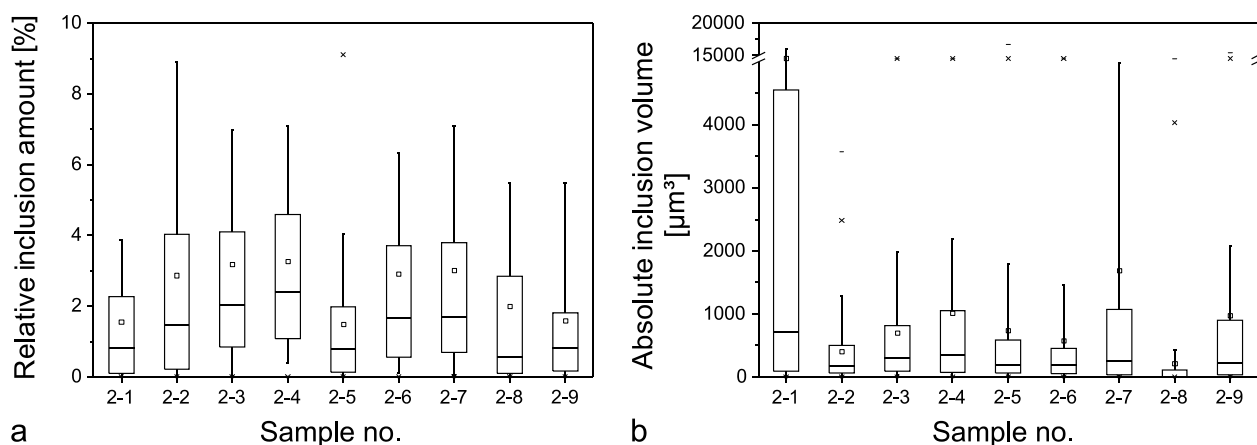


Fig. 5.24: Illustration of a) Relative inclusion amount (RIA) [%] and b) Absolute inclusion volume (AIV) [μm^3] in dependence on w and IR (second step).

It might be expected that larger crystals contain larger inclusions. Exemplarily, Sample 2-1 which owns the largest crystal volumes and Sample 2-2 with the smallest crystal dimensions (Fig. 5.23b) will be considered according to its RIA (Fig. 5.24a) and AIV (Fig. 5.24b). As can easily be seen in Fig. 5.24b, the large crystals of sample 2-1 contain large AIV and the small crystals of Sample 2-2 contain quite small AIV. However, as illustrated in Fig. 5.24a the RIA of Sample 2-1 are smaller than the RIA of Sample 2-2 which had smaller crystals and smaller absolute inclusion volumes. Considering these two examples it can be concluded that the RIA of crystals does not depend on the crystal dimensions.

To sum up the results of this second step on the effects of V_s , w and IR on the crystal and inclusion sizes it can be said that on the one hand low IR (4 mL min^{-1}) result in the growth of larger crystals than at medium (12 mL min^{-1}) or high (20 mL min^{-1}) IR. Based on the results it can, further, be concluded that there is no direct effect of crystal size on RIA.

5.3.3.3 3. Step: Influence of temperature, gas content and stirring rate

In the third step of the first enquiry the effects of solution temperature (T_s), gas content in both solution and antisolvent as well as the stirring rate (SR) were investigated. The results are illustrated as schematic crystal needles (Fig. 5.25) representing the median dimensions of the measured crystals of the samples. The orientation of the schematic crystals symbolizes the stirring rate as defined in Fig. 5.25a for samples 3-4 and 3-2.

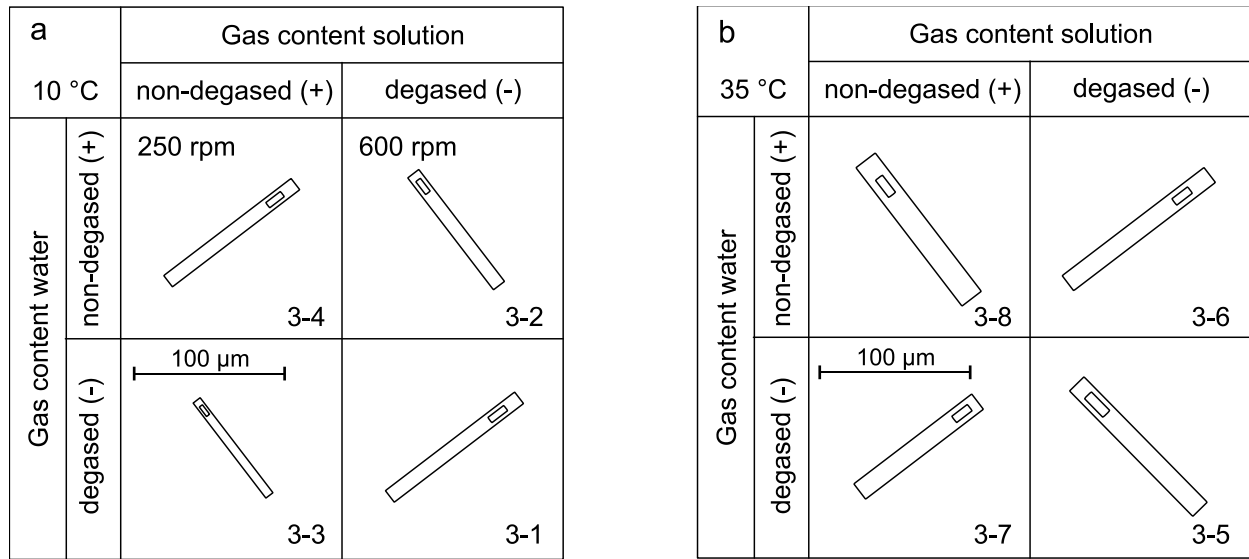


Fig. 5.25: Experimental conditions and median crystal and inclusion sizes of the third step for a) 10 °C and b) 35 °C solution temperature (T_S). The orientation of depicted crystals represents the stirring rate (SR) which is defined exemplarily for Samples 3-4 (250 rpm: \nearrow) and 3-2 (600 rpm: \nwarrow).

On the first view it can be seen that crystals grown at $T_S = 35$ °C are in general thicker than the ones grown at 10 °C while the crystal lengths remain almost constant. These observations can be seen in Fig. 5.26 as well.

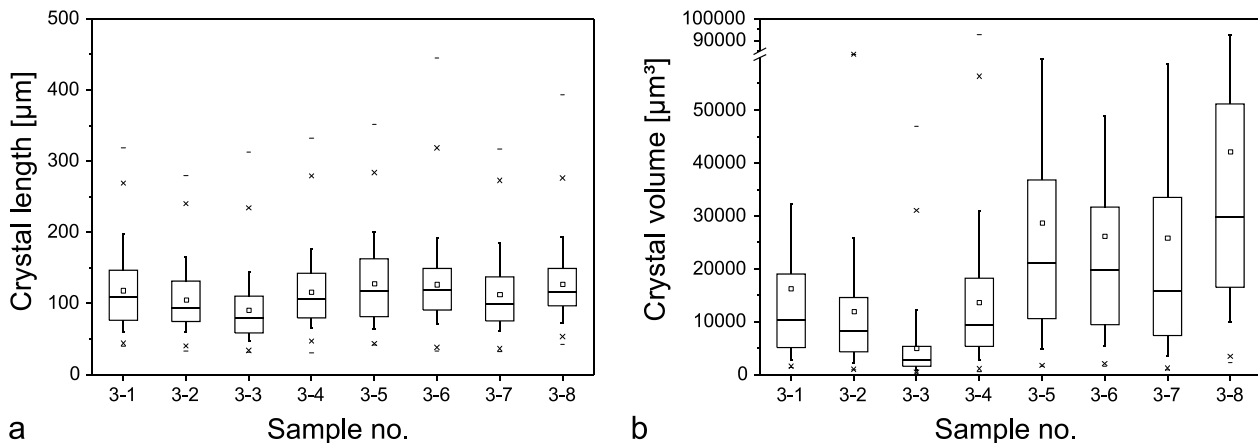


Fig. 5.26: Measured data for a) Crystal length [μm] and b) Crystal volume [μm^3] in dependence on solution temperature, degassing and stirring rate (step 3). The experimental conditions for each samples are given in Fig. 5.25.

Further, it can be seen in Fig. 5.26b that Samples 3-5 and 3-8 which were prepared at 35 °C under SR of 600 rpm had larger crystal volumes than those of samples 3-6 and 3-7 (250 rpm). At 10 °C (Samples 3-1 to 3-4) no effect of SR on the crystal size could be found.

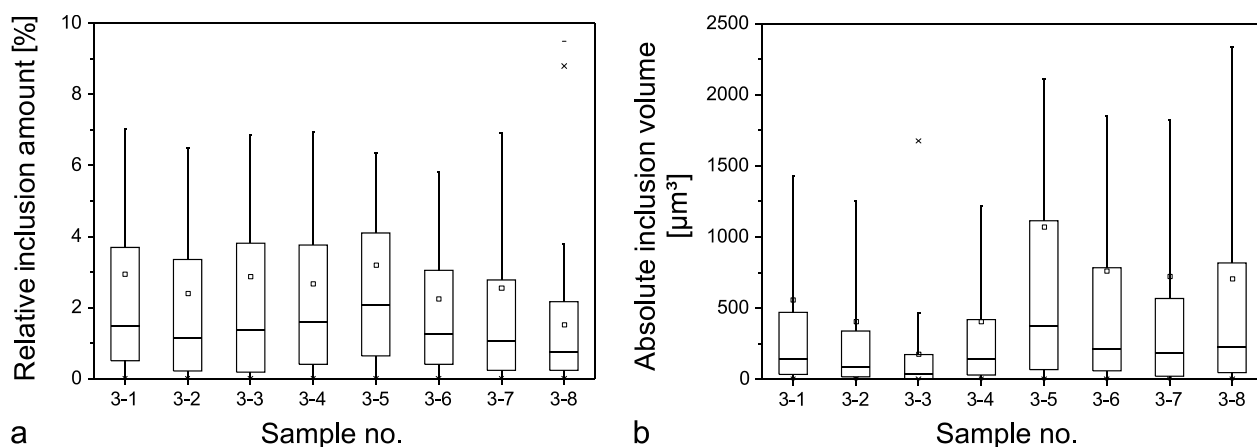


Fig. 5.27: Illustration of a) Relative inclusion amount (RIA) [%] and b) Absolute inclusion volume (AIV) [μm^3] in dependence on temperature (T_S), degassing and stirring rate (third step).

Fig. 5.27a shows that at $T_S=10^\circ\text{C}$ (Samples 3-1 to 3-4) the RIA were unaffected by SR or degassing. The highest RIA of this step can be found at Sample 3-5 which was prepared at $T_S=35^\circ\text{C}$ and SR=600 rpm using degassed solution and antisolvent. Sample 3-6 where a SR=250 rpm and degassed solution were applied the RIA was slightly smaller. Due to the experimental design it cannot be ensured if degassing or SR is the significant parameter to affect the RIA.

5.3.3.4 General results of the first enquiry

In this first enquiry it was possible to improve the quality of the generated crystals according to shape and agglomeration degree. Moreover, the IR could be identified as important parameter to manipulate the crystal lengths. Above an IR of 12 mL min^{-1} median crystal sizes of about $100\ \mu\text{m}$ are reached. The widths of the crystals were shown to be affected by T_S .

The RIA were found to be hardly affected by the experimental parameters investigated in this enquiry and the median RIA ranged for all samples between 1 and 2%. Due to the pursued application of such inclusion containing crystals for agent encapsulation the inclusion amount of crystals should be further increased.

5.3.4 Second enquiry on the effects of experimental parameters on crystal and inclusion sizes

In the second enquiry the solvent was changed from MeOH to EtOH which is not toxic and, thus, more suitable to be used in the production of compounds for skincare products. Moreover, the multivariate experimental design was replaced by the

investigations of the single parameters stirring rate (SR) and the application of seeding which were performed at different w of SA in ethanolic solution. As third parameter of this second enquiry it was investigated which effect the direction of solution/antisolvent-injection has on the generation of crystalline container systems regarding crystal and inclusion sizes.

5.3.4.1 Effect of stirring rate in dependence on mass fraction

The effect of SR was already investigated in Chapter 5.3.3.3. Since the results of that investigation were inconsistent with the observations described in literature, e.g. [Den66, Zha05, Kim09], it might be possible that the other parameters that were investigated in the same designed experimental step could overlay the effect of the SR on the crystal

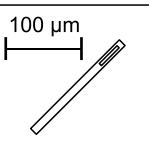
		Stirring rate	
		100 rpm	350 rpm
SA mass fraction of solution	4 %		
	8 %		
	15 %		

Fig. 5.28: Schematic illustration of inclusion containing crystals reflect the median dimensions of all crystals measured in each sample show the effects of stirring rate (SR) at different mass fractions (w) of SA in EtOH.

and inclusion sizes. In order to clarify this issue the effect of the SR was investigated for different w . The results are schematically illustrated in Fig. 5.28 and depicted in more detail in Figs. 5.29 and 5.30. Additionally to the samples run at 100 and 350 rpm crystals were generated under unstirred conditions, too. Those crystals from static conditions grew to long needles and reached lengths of more than 3 cm. However, it was not possible to handle these crystals in order to get representative and evaluable results since they broke in each step they were moved, e.g. transfer from beaker to frit or from frit to petri dish.

Furthermore, if some crystals could be positioned under the microscope without breaking those crystals were too long to measure within one operational window which was limited at lowest magnification (100x) to be 3500 μm .

As can be clearly seen in Figs. 5.28 and 5.29 the crystals that were generated at a SR=100 rpm were, depending on w , larger than the crystals prepared at SR=350 rpm. Considering w it can be noted that if the used solution contained 4 or 8% SA the effect of SR was more distinct than at $w=15\%$. Furthermore, it can be seen that the crystal sizes are for both 100 rpm and 350 rpm increasing with increasing w . This observation is in good agreement with the results described in Chapter 5.3.3.2.

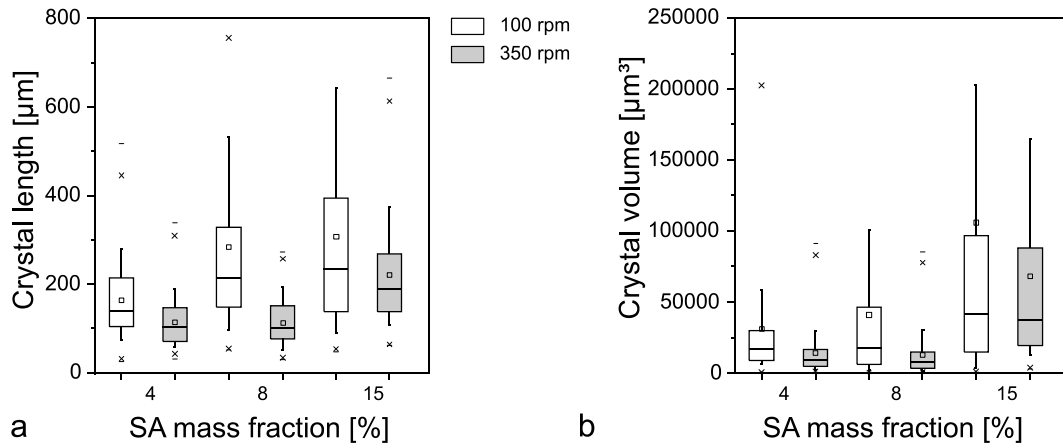


Fig. 5.29: Measured values for crystal sizes in a) Length and b) Volume plotted against the mass fraction (w) of the SA solution for stirring rates (SR) of 100 rpm (white boxes) and 350 rpm (gray boxes).

In Fig. 5.30 it can be seen that the AIV (Fig. 5.30b) of samples stirred at 350 rpm are smaller than those of crystals prepared at 100 rpm. Considering the RIA (Fig. 5.30a) hardly any significant effect of SR can be identified.

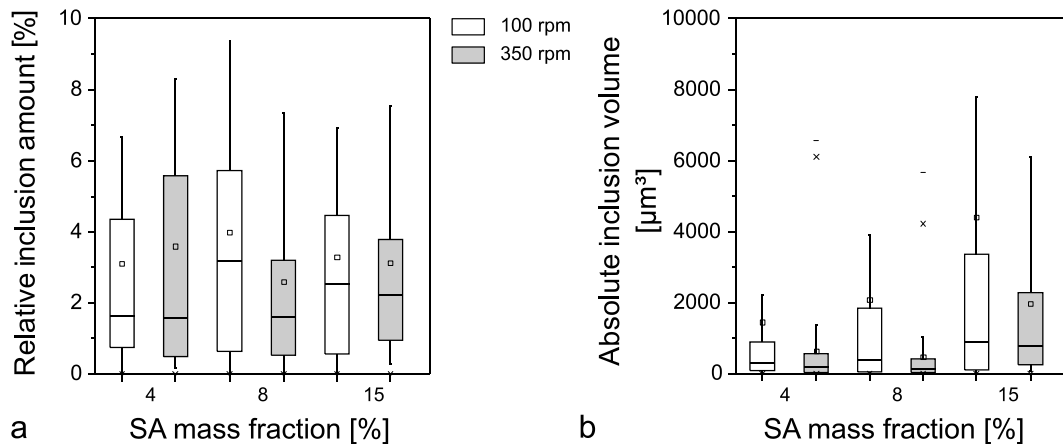
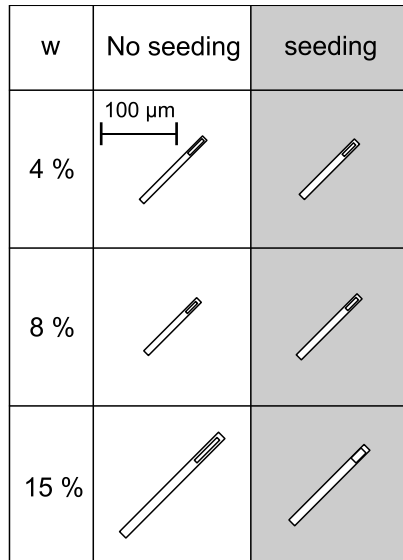


Fig. 5.30: a) Relative (RIA) and b) Absolute (AIV) inclusion amounts of crystals in dependence on mass fraction (w) of the used SA solution (x-axis) and the stirring rate (SR; white boxes: 100 rpm; gray boxes: 350 rpm).

The observed effects of SR on crystal and inclusion dimensions at the applied antisolvent crystallization can be summarized as follows: On the one hand, an increase in SR resulted in the generation of smaller crystals (Fig. 5.29a). On the other hand, the RIA remained quite unaffected by the variation of SR at $w=4\%$ and 15% (Fig. 5.30a). However, at $w=8\%$ a lower SR (100 rpm) rate resulted in enlarged RIA compared to higher SR (350 rpm).

5.3.4.2 Effect of seeding



As another important and widely used practice in crystallization the effect of seeding on the present issue was investigated. Three different w were applied.

At $w=4\%$ and $w=8\%$ the addition of seed crystals had only a negligible effect on the crystal sizes as can be seen in Figs. 5.31 and 5.32. Considering crystals prepared at $w=15\%$ a general increase in crystal dimensions compared to crystals prepared with SA solutions of lower w can be observed. Furthermore, when $w=15\%$ was used seeding revealed in a reduction of crystal dimensions.

Fig. 5.31: Schematic illustration of median crystal and inclusion dimensions in dependence on the performance of seeding for different SA mass fractions (w) of the ethanolic solution.

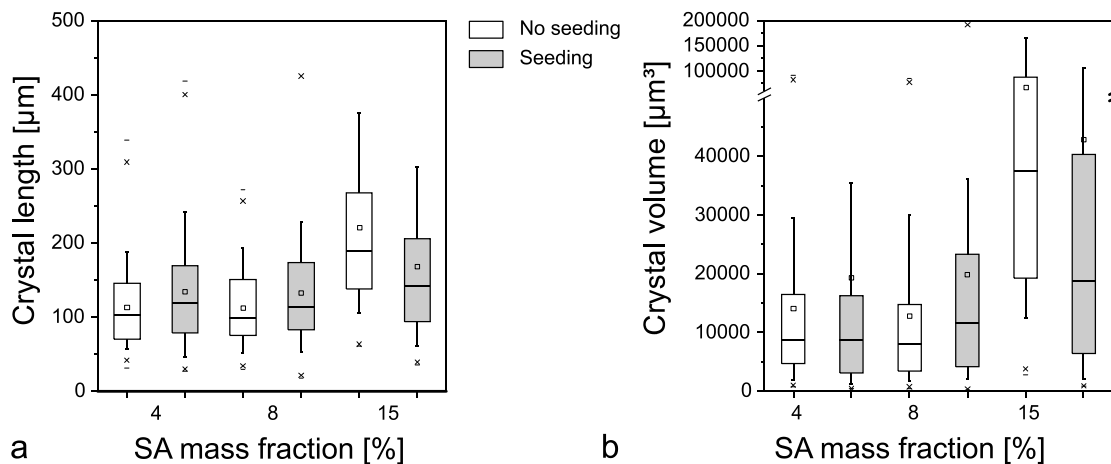


Fig. 5.32: Crystal dimensions expressed in a) Length and b) Volume in dependence on the performance of seeding (white boxes: No seeding; gray boxes: Seeding) plotted against SA mass fraction (w) of the solution.

If the effect of seeding on the inclusion amounts is taken into account it can be observed that, at $w=4$ and 8% seeding did not result the reduction of RIA (Fig. 5.33). However, the application of seeding even led to a slight enlargement of RIA. When the antisolvent was added to a solution of $w=15\%$ the inclusion dimensions were decreased by the addition of seed crystals.

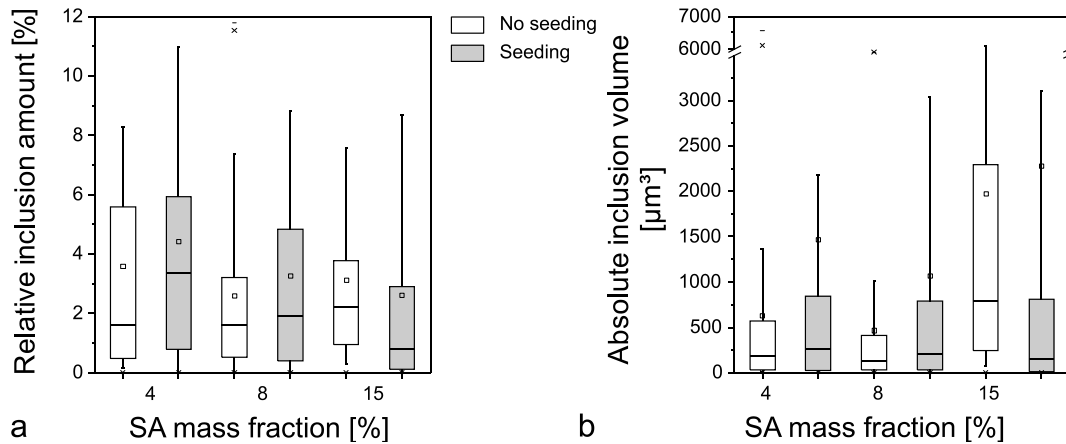


Fig. 5.33: Measured values for a) Relative and b) Absolute inclusion amounts depending the performance of seeding (white boxes: No seeding; gray boxes: Seeding) plotted against SA mass fraction of the solution.

To sum up the effect of the performance of seeding in this antisolvent process it can be noted that at $w=4$ and 8% of SA in ethanolic solution seeding had only low influence on crystal sizes. The inclusion sizes were slightly enlarged by the application of seed crystals. In case of $w=15\%$ both the crystal and inclusion dimensions were reduced by the addition of seeds compared to unseeded samples.

5.3.4.3 Effect of injection direction

T	w=8 %		w=15 %	
	Water into solution	Solution into water	Water into solution	Solution into water
10 °C				
20 °C				
35 °C				

Fig. 5.34: Illustration of median crystal and inclusion dimensions depending on the direction of injection (water injected into SA solution 'AS>S': White boxes; SA solution injected into water 'S>AS': Gray boxes) at different temperatures and for solution mass fractions (w) of 8 and 15% SA in EtOH.

As final experimental parameter that was investigated according to its influence on the generation of container crystals the direction of the solution/antisolvent-injection was investigated. Since all previous experiments were run by injecting the antisolvent water into the SA solution (AS>S) in this experimental step the solution was injected into the water (S>AS). The effect of the injection direction was investigated at 10, 20 and 35 °C each for $w=8\%$ and $w=15\%$. The median crystal and inclusion sizes of the samples are

illustrated schematically in Fig 5.34. Detailed results for the experiments using $w=8\%$

are shown in Figs. 5.35 and 5.36. Results for $w=15\%$ can be found in details in Figs. 5.37 and 5.38.

The presentation of the results of these experiments will be structured by the solution mass fraction. First, the results using $w=8\%$ and secondly those of $w=15\%$ will be presented.

Solution mass fraction of 8%

First the effects of the injection direction on the crystal and inclusion sizes at $w=8\%$ will be focused on. As can be seen in Figs. 5.34 and 5.35a the crystal lengths are quite uniform for all six samples of this group. However, the crystal widths are varying with temperature and depending on the injection direction (Fig. 5.35b). When water was injected into the solution (AS>S) the crystal volumes and, thus, the widths are increasing with temperature. Contrary to that, the change of the injection direction (S>AS) results in a reversed effect on crystal volumes. At 10 °C the largest crystal volumes can be observed and with increasing the temperature to 20 °C the crystals get smaller. A further temperature increase to 35 °C, however, has no significant effect.

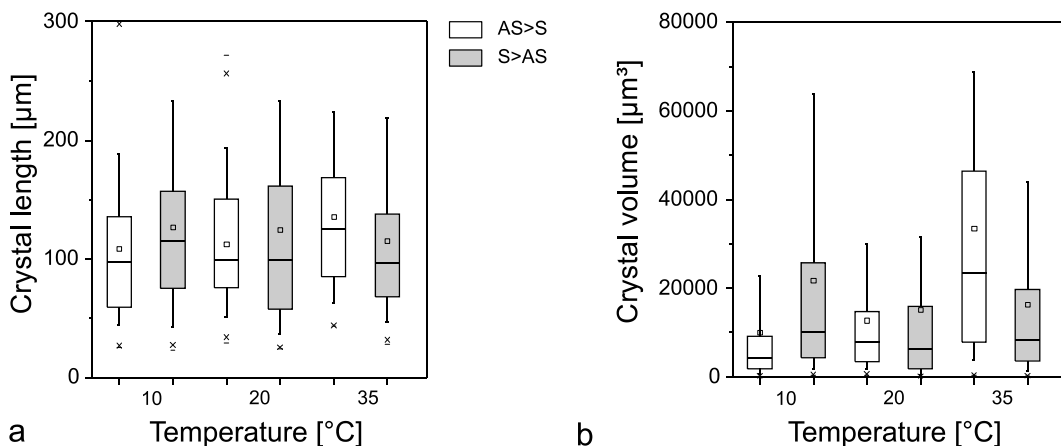


Fig. 5.35: Crystal dimensions in a) Length and b) Volume depending on the direction of injection (white boxes: Water injected into solution 'AS>S'; gray boxes: Solution injected into water 'S>AS') plotted against the temperature of antisolvent crystallization using solution mass fraction $w=8\%$.

The effect of injection direction on RIA (Fig. 5.36a) and AIV (Fig. 5.36b) are depicted below. If the water is added to the solution (AS>S) the RIA is decreasing with increasing temperature. If the solution is injected into the water (S>AS) RIA are increasing with a temperature increase from 10 °C to 20 °C. At both temperatures RIA are distinctly larger than in case of reversed injection direction (AS>S). At 35 °C no effect of the injection direction on the RIAs can be observed.

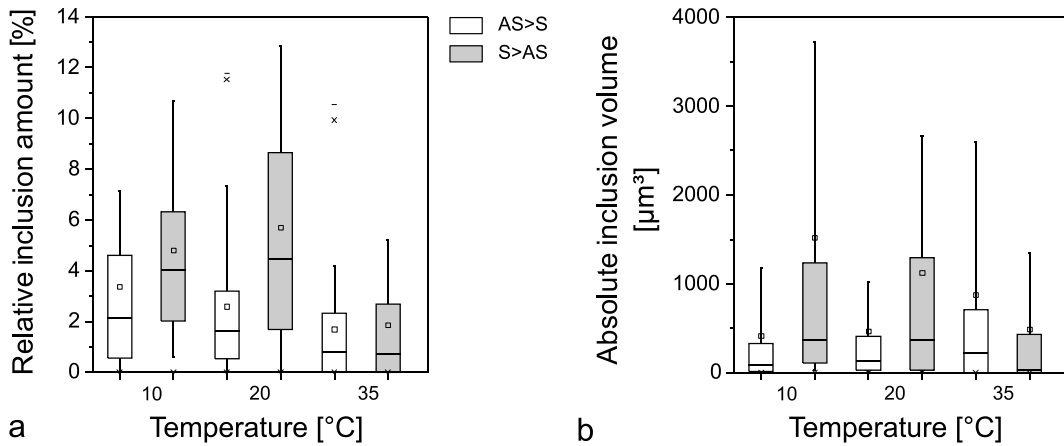


Fig. 5.36: a) Relative and b) Absolute inclusion amounts of crystal prepared by injecting water into the solution (white boxes) or solution into the water (gray boxes) plotted against the crystallization temperature of the antisolvent crystallization using a solution mass fraction of 8%.

In summary, the results show that in case of $w=8\%$ the injection of the solution into the antisolvent water (S>AS) at 10 and 20 °C RIA could be increased from 2% to about 4% while crystal dimension remained almost constant compared to the previously used injection direction (AS>S).

Solution mass fraction of 15%

Figs. 5.34 and 5.37 show that in case of $w=15\%$ crystals prepared by injecting the SA solution into water (S>AS) are in general smaller and their sizes are less affected by the temperature than crystals prepared using the reverse injection direction (AS>S).

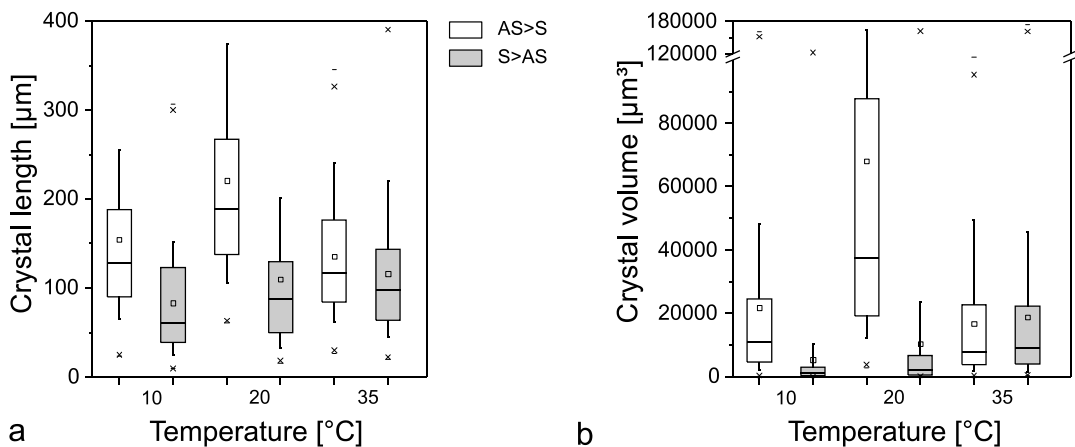


Fig. 5.37: Crystal dimensions in a) Length and b) Volume in dependence on the injection direction of the antisolvent crystallization (white boxes: Water injected into the solution 'AS>S'; gray boxes: Solution injected into water 'S>AS') plotted against the temperature, SA mass fractions of $w=15\%$ were used.

If the effect of the injection direction on the RIA is considered at $w=15\%$ (Fig. 5.38a) it can be seen that at 10 °C RIA are negligible affected by changing the injection direction. At 20 and 30 °C contradictory effect of injection direction on RIA can be observed.

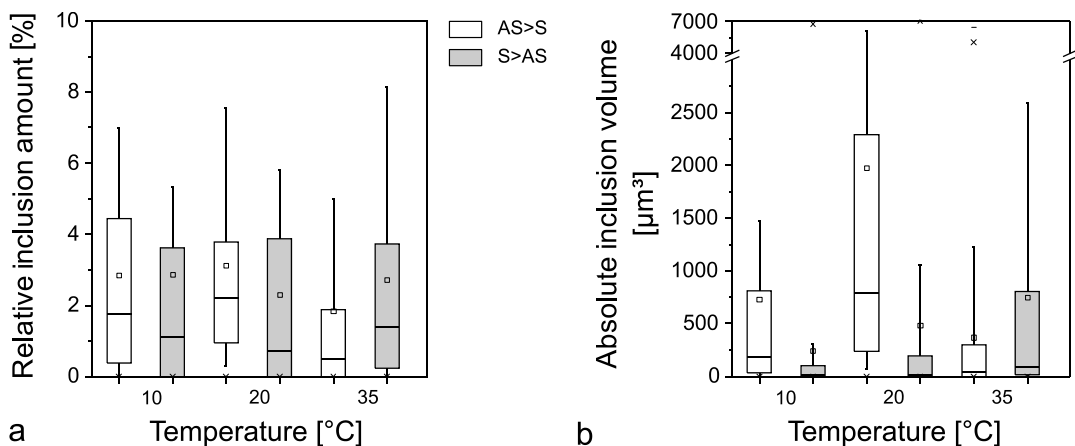


Fig. 5.38: a) Relative and b) Absolute inclusion amount in crystal depending on the injection direction (water injected into solution 'AS>S': White boxes; solution injected into water 'S>AS': Gray boxes) plotted against crystallization temperature, $w=15\%$.

The observed effects of the injection direction on crystal and inclusion dimensions are at $w=15\%$ quite different to those revealed at $w=8\%$. While at $w=15\%$ the crystal sizes depend distinctly on the injection direction RIA are hardly affected by this experimental parameter.

5.3.4.4 General results of the second enquiry

As important results of this second enquiry on the effects of experimental parameters on crystal and inclusion sizes it can be pointed out that lower SR result in larger crystals. Depending on w lower SR can, further, result in larger RIA than as observed at higher SR. This effect can be observed especially in case of $w=8\%$.

The performance of seeding revealed only at $w=15\%$ to a reductive effect on the crystal sizes. As unexpected effect it could be observed that at $w=4\%$ the RIA was increased by the application of seed crystals.

To assess the general results of the investigations regarding the injection direction it can be summarized that the effects of this experimental parameter on crystal and inclusion sizes offers the best possibility to manipulate the inclusion amounts. This parameter depend mainly on w and secondly on the temperature. In case of $w=8\%$ and at 10 or 20 °C the procedure of injecting the solution into the antisolvent revealed in a distinct enlargement of inclusion sizes compared to the reverse injection direction.

5.4. Encapsulation of foreign substances inside container crystals

The aim of this study is to investigate whether crystalline container systems can be applied for agent encapsulation or not. After intense enquiries on the experimental parameters in order to manipulate the amount of inclusions the approach of using SA crystals for agent encapsulation was considered by filling container crystals with foreign substances. Copper sulfate and ascorbic acid were chosen as test substances.

5.4.1 Copper sulfate

Aqueous copper sulfate solutions are of a typical blue color. During the rinsing step this visual effect allowed observing the removal of the blue mother liquor from the prepared crystals which finally appeared as white crystalline powder. The analysis of the dried and dissolved crystals led to a clear positive result. This qualitative proof of copper ions in the dissolved container crystals leads to the assumption that copper could be successfully encapsulated inside the SA crystals [Sei16].

5.4.2 Ascorbic acid

As second test substance for encapsulation experiments ascorbic acid (AA) was chosen because it could be detected in presence of high amounts of SA. The quantification of AA in dissolved SA container crystals revealed in amounts of 0.4 ± 0.3 mg AA per g crystals. Since the rinsing water contained only 0.08 ± 0.23 mg AA per g crystals, despite the high uncertainty of the method, it can clearly be proven that AA was encapsulated inside the container crystals [Sei16].

6. Discussion

6.1. Finding a model substance

According to Eddleston and Jones [Edd10] it should be possible to crystallize any substance in a tubular shape if the appropriate conditions can be fulfilled. Since the focus of this study is on the investigation of the applicability of crystalline container systems a model substance that can easily be crystallized in tubular, inclusion containing crystals is aimed.

As described earlier (Chapter 2.2) there are a few substances already reported on in literature that were approved to offer the potential to form container systems. The properties of these, already described substances were investigated according to their properties and applicability for potential product uses by means of literature research and will be discussed according to their suitability as model substances.

The model substances from previous studies on crystalline container systems were sodium-2-ketogulonate monohydrate (SKGM), glucose anhydrate, sodium acetate trihydrate and the APIs theophylline and carbamazepine [Sch10, Sch11b, Ulr13]. In case of pharmaceutical products very high purities of compounds are necessary and if substance compositions are used the amounts of the single compounds have to be very exact and reproducible. If crystalline container systems are used for agent encapsulation the required accuracy due to product purification and composition cannot be fulfilled. For that reason the APIs theophylline and carbamazepine, even though these substances led to promising results in previous studies, had to be excluded for the current issue.

One substance that is very well investigated due to its formation of hollow crystal needles is SKGM. This substance is technically used as precursor structure in ascorbic acid production. Since SKGM is neither applied in foods nor in cosmetics this well investigated model system had to be excluded as model substance.

Sodium acetate is described as another model substance which led to promising results in a previous study [Sch11b]. This substance is authorized in the EU as food additive (E262) [Eur11]. It can be used as acidity regulator and preservative in canned fruits and vegetables, defined sorts of bread, meat preparations and processed cereal-based

foods for infants and young children [Eur11]. For all these uses no maximum amount is provided. In order to get stable container crystals of sodium acetate trihydrate the surrounding medium has to be saturated with this substance. However, due to its high water solubility (anhydrate: 365 g L^{-1}), hygroscopic behavior and intense acid taste [Man72, IFA16b] potential applications are assessed to be unlikely.

As last substance that was described in literature to be successfully filled was glucose anhydrate [Sch10]. Glucose is a widely used ingredient in many foods. It owns a high solubility in water (470 g L^{-1} [IFA16a]) and, therefore, it might be hard to find a product where potential glucose needles could be stable against dissolution. However, for glucose it could be considered to use its crystals as dry material, e.g. sprinkles for cakes or ice cream. The encapsulation of alcoholic solution [Sch10] could allow to fill these crystals with flavor agents. However, due to the use of the anhydrate form its stability against re-hydration has to be taken into account. Mathlouthi et al. [Mat12] investigated the monohydrate-anhydrate transition of glucose depending on time, temperature and ambient humidity. The transition temperature of glucose monohydrate to the anhydrate form was determined to occur at temperatures above $50 \text{ }^\circ\text{C}$. Furthermore, it could be proven by Mathlouthi et al. [Mat12] that the re-hydration of the glucose anhydrate happens at $20 \text{ }^\circ\text{C}$ and is completed after 105 min at 97% relative humidity. Schuster et al. [Sch10] could handle this problem by drying crystals in an oven at a temperature of $60 \text{ }^\circ\text{C}$ until investigation by optical microscope. No information about the stability of dried crystals at ambient conditions is given. Considering the re-hydration of glucose anhydrate at $20 \text{ }^\circ\text{C}$ as described by Mathlouthi et al. [Mat12] it is assumed that the storage stability of glucose anhydrate crystals is too short to use them as container materials. According to these complications in product handling glucose monohydrate had to be excluded as model substance for this study.

The consideration of glucose anhydrate crystals gave a meaningful example which difficulties could occur in case of metastable polymorphs or solvates according to long term and storage stability. Due to those findings the decision of excluding metastable solvates and polymorphs as model substances was made in order to provide general information on the opportunities of applying crystalline containers.

According to the wide range of specific claims that had to be fulfilled salicylic acid (SA) was found to be the optimal model substance. As described detailed in Chapter 4.1.1 it is authorized and applied as (active) compound for cosmetic uses (2-3%), owns low water solubility and no solvate forms are known [Nor06]. There are some polymorphic SA crystals described that were generated by means of organic modifiers [Xu06], however, those polymorphs were prepared elaborately and, thus, a spontaneous transition is not to be expected.

6.2. Crystallization behavior of SA depending on the presence of dissolved gases

6.2.1 Saturation curve, solubility, MZW and crystal growth rate

Due to the perfect fit of the saturation curves of degassed and non-degassed samples as well as the negligible differences in the solubility curves that were measured by means of US technique it can be concluded that in the present case study no effect of dissolved gases on the thermodynamics of the system can be found.

The difference between measured and literature solubility data (Fig. 5.1b) can be explained by the different methods used to determine the SA amounts in the solution. In the present study the SA mass fraction was determined by means of refractometer measurements against external calibration. Nordström and Rasmuson [Nor06] determined the SA mass fraction gravimetrically and presented the values as mole fraction solubility. As further source to explain the variation of solubility data from both measurement techniques and literature data some inaccuracies in temperature measurements can be mentioned.

Considering the MZW it was expected that degassing might lead to a distinct increase in MZW since Wohlgemuth et al. [Woh09, Woh10] described the promotion of nucleation by gas bubbles. However, the results of the MZW measurements by means of US (Fig. 5.2) showed that the MZW is hardly influenced by the reduction of the amount of dissolved gases [Sei17].

As described in Chapter 2.4 in other studies it could be observed that dissolved gases affected growth rates [Wal11a, Hua16] and even solubility and, thus, thermodynamics of

the model substances [Hua16]. Since these effects were not proven in this study it can be assumed that the influences of dissolved gases depend strongly on the used model system.

6.2.2 Effects of solution degassing on dissolution rate

The results of kinetic experiments showed that the growth rate of SA was not affected by degassing but the dissolution rate was. Moreover, it was observed that the dissolution rate seems to be inhibited by the presence of dissolved gases, especially at 10 °C.

An approach to explain this observation can be found in the solubility of dissolved gases (oxygen and nitrogen) in dependence on the SA amount which is depicted in Fig. 5.7. There, it can be seen that with increasing SA mole fraction the solubility of both oxygen and nitrogen decrease. Referring this to the dissolution mechanism this means that the increase of SA concentration caused by the crystal dissolution leads to a decrease of gas solubility, especially close to the crystal surfaces, and the gases are displaced from the solution, e.g. by the formation of tiny bubbles. These bubbles can hinder the mass transport mechanism between crystal surface and solution and, thus, the dissolution step is inhibited, especially, if the substance dissolves overridingly diffusion controlled as in case of SA [Per13]. If the gas amount of the solution was reduced by the degassing step the solution can be seen as undersaturated with gas. Thus, the gas amount that is left in the solution is expected to be too small to be displaced from the solution even if the gas solubility decreases. However, if the decrease of oxygen solubility close to the crystal surfaces would be intense enough to initiate bubble nucleation, gas bubbles could dissolve very fast in the well stirred and gas undersaturated surrounding liquid [Sei17]. Consequently, hardly any dissolution inhibiting effect would be observed in case of degassed solutions.

Moreover, it was observed that the difference in dissolution rates is more obvious at 10 °C than at 30 °C. A possible explanation approach can be found by Najafi et al. [Naj08]. In their study the sliding velocity of single micro-bubbles along an oblique glass plate under different conditions was investigated. It was found that at lower temperature the bubbles moved slower along the plate and stuck longer to it than at higher temperature. This effect was explained by the decrease in viscosity with increasing

temperature. Other effects, e.g. on density or interfacial tension, which might complete the explanation of the temperature effect as well, were not considered. For the present case, this means that at lower temperature the affinity of the bubble to stick to the surface is higher than at higher temperature. For the observations of dissolution rates that were made in this study this means that appearing gas bubbles stick longer to the crystal surfaces at 10 °C than at 30 °C and, thus, the inhibiting effect of displaced gases, e.g. gas bubbles, on crystal dissolution decreases with increasing temperature.

6.3. Stability of SA crystals in dependence on solvent compositions

One important factor that has to be considered regarding a potential application of crystalline container systems is their stability in a potential product. With the intention to clarify this issue the SA solubility was investigated exemplarily for ethanol-water-mixtures. Since a high number of organic solvents are typically used in cosmetics, e.g. i-propanol or glycerol, a model to predict the SA solubility and, thus, estimate the composition of potential products to ensure the stability of the container crystals was developed.

6.3.1 SA solubility in EtOH-water-mixtures

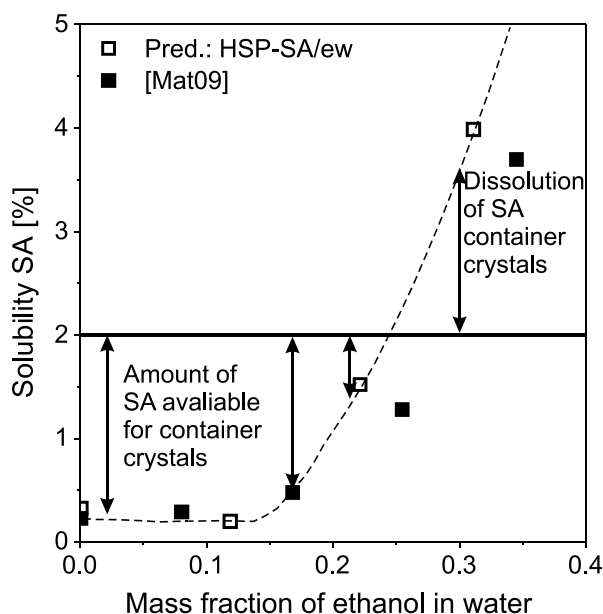


Fig. 6.1: SA amounts that are available for container crystals (at 25 °C) depend on solubility of SA in ambient medium and, thus, on solvent composition, exemplarily illustrated for EtOH-water-mixtures containing 2% SA.

It has to be pointed out that in case of crystalline container systems the ambient medium has to be saturated with the container substance to ensure the containers' stability. Only the amount of container substance that is additionally added to the medium will not dissolve and, thus, will be available as container crystals. The determined ternary diagram (Fig. 5.8) allows defining the EtOH-water-composition where SA will not dissolve.

As can be seen well in the diagram (Fig. 5.8) water is a good antisolvent for SA and the solubility of SA in this ternary system

depends almost exclusively on the EtOH amount. This is illustrated in Fig. 6.1 for EtOH-water-mixtures that contain 2% SA. It can be seen that for EtOH-water-mixtures the solvent phase can contain up to an EtOH mass fraction of 0.17 (17%) without increasing the solubility of SA significantly. Thus, in this composition range SA amounts of more than 1.5% of the aimed amount of 2% can be applied as container crystals.

It can be summarized that the amount of SA container crystals depend on the solubility of SA in the ambient medium. The lower the solubility of SA the more container crystals can be available as encapsulation material in a product.

6.3.2 Development of a solubility prediction model for SA in EtOH-water-mixtures

The use of crystalline container materials requires special demands on the solvent composition since the medium has to be saturated with the container material in order to avoid the containers' dissolution. For that reason a model to predict the solubility in solvent-water-mixtures was developed in order to estimate the amount of container material that is available for encapsulation (Fig. 6.1) and to ensure the containers' stability against dissolution.

As proven in Chapter 5.2.4 the solubility predictions based on HSP-SA/ew led to satisfactory results. The model was applied exemplarily for i-propanol- and glycerol-water-mixtures. The revealed solubility results showed that both solvents can be used in moderate amounts (up to 20% i-propanol and 10% glycerol) without a considerable effect on the SA solubility. Thus, in general it seems to be possible to use SA container crystals in products that contain moderate amounts of organic solvents. However, it should be considered that the solubility predictions refer to simplified three-component-mixtures. Due to the high complexity of formulations of skincare products, e.g. solvents (water, organic solvents, oils), agents (moisturizers, UV filters), additives (emulsifiers, preservatives) [Fin05], it is hardly possible to consider all the different kinds of substances that might influence the SA solubility in one model. In case of investigating the stability of SA containers in a real potential skincare product with known formulation the solubility of SA container crystals should be verified experimentally.

6.3.3 Valuation of the used HSP model

The HSP-model is based on the assumption that for each substance three parameters can be defined to describe all properties that are relevant for the solubility behavior. These properties namely are non-polar or dispersion energy (δ_D), permanent dipole-permanent dipole or polar cohesive energy (δ_P) and hydrogen bonding energy (δ_H). The first two parameters (δ_D , δ_P) represent molecular properties. However, the term of hydrogen bonding energy (δ_H) is assessed to be oversimplified because it represents all kinds of interactions that are not expressed by the other ones, e.g. induced dipoles [Han00]. The calculated HSP as presented in the user's handbooks [Han00, Han07] are based on the boiling point (δ_D), estimated dipole moments (δ_P), group contribution models (δ_P , δ_H) and similarities to related compounds (δ_H). Thus, none of the calculated HSP can be seen as precise or absolute values and differences to experimental data will certainly occur [Han00, Han07]. For that reason the determination of HSP as performed in this thesis is not contradictory to the HSP model but an extension and specification by the use of experimental data regarding the application on a defined aim.

For the used method to determine the HSP for SA (and nitrogen) an equation system was generated based on solubility data and solved in order to reach maximum correlation between solubility values from literature and the modeled values similarly as described by Sato et al. [Sat14]. This method is very appropriate in order to get both the HSP and the associated quantification equation. This equation which describes the relation between the mole fraction solubility and R_a is essential to predict the solubility of a substance quantitatively. If the HSP are calculated by means of an equation system based on solubility data the results can only reflect the type of interactions they are based on. Depending on the aim the HSP are used for, the appropriate solubility data for HSP determination can be varied. In case of the determination of HSP-SA/ps (or HSP-Ni) a wide range of solvents with different properties was used, e.g. alcohols, acetonitrile, acetone, ethyl acetate and dioxane. This allows some general estimation for solubility predictions which are able to deliver results of correct magnitude and tendency as shown in Fig. 5.10 (or Fig. 5.7). In a second case the pursued aim was the prediction of SA solubility in water containing solvent mixtures. Therefore, the HSP determination was based on specific solubility data of SA in EtOH-water-mixtures. As can be seen in

Fig. 5.12 the specified HSP-SA/ew resulted in better fitting solubility predictions than those based on HSP-SA/ps.

The used HSP-model was easy to apply and the received results are rated as reliable according to magnitude and tendency. Since HSP for a wide range of solvents are provided in literature [Han00, Han07] the R_a values of any SA-solvent composition can be determined. Due to the defined x_{SA} - R_a -relation the SA solubility in any solvents or solvent compositions can be estimated without the need of solubility data from literature. In case of predicting SA solubility in solvent-water-mixtures the received results are rated to be, depending on the solvent's similarity to EtOH, more or less solid estimations. Especially in case of more components, the solubility of SA should be ensured experimentally. Overall, the presented model delivers a great possibility to estimate the SA solubility in solvent-water-mixtures and, thus, a base to decide if SA container crystals might be applied in a product.

6.4. Investigations on inclusion containing crystals

The idea of container crystals is based on encapsulating a foreign substance inside the inclusions of crystals. In order to attain maximum encapsulation potential the inclusions inside the crystals need to be as large as possible. For that reason the effects of growth rates and different experimental parameters on the formation of liquid inclusions were investigated.

6.4.1 Effect of growth rates on inclusion formation

The dependency of the formation of liquid inclusions on the growth rate of a crystal face is reported on in literature several times, e.g. [Bro68, Sai99, Edd10, Wal11a, Per13, Bob15, Bob16b]. In general it can be observed that an increase in growth rates enhances the formation of liquid inclusions which could also be observed in the present study (Chapter 5.3.1). Basically, there are two approaches that can be used to explain the formation of inclusions. On the one hand, tubular structures occur if due to the fast crystal face growth the diffusion of the material to the center of the crystal face is limited, thus, only the edges can grow (Fig. 2.9). This mechanism, which leads to a funnel-shaped inclusion, was investigated by Perry et al. [Per13] in a case study using SA and is depicted in Fig. 6.2a. This diffusion-limited mechanism is discussed to be enhanced

by the adsorption of foreign particles or gas bubbles on the crystal surfaces [Wal11a]. On the other hand, it could be observed that a sudden increase in growth rate, e.g. by mechanical contact to the growing surface, results in the formation of macro steps which can initiate inclusion formation (Fig. 6.2, b) [Sai99]. Even if no contacts were performed and the growth rates of single faces fluctuate spontaneously the formation of liquid inclusions can be observed (Fig. 6.2, c) [Bob15, Bob16b].

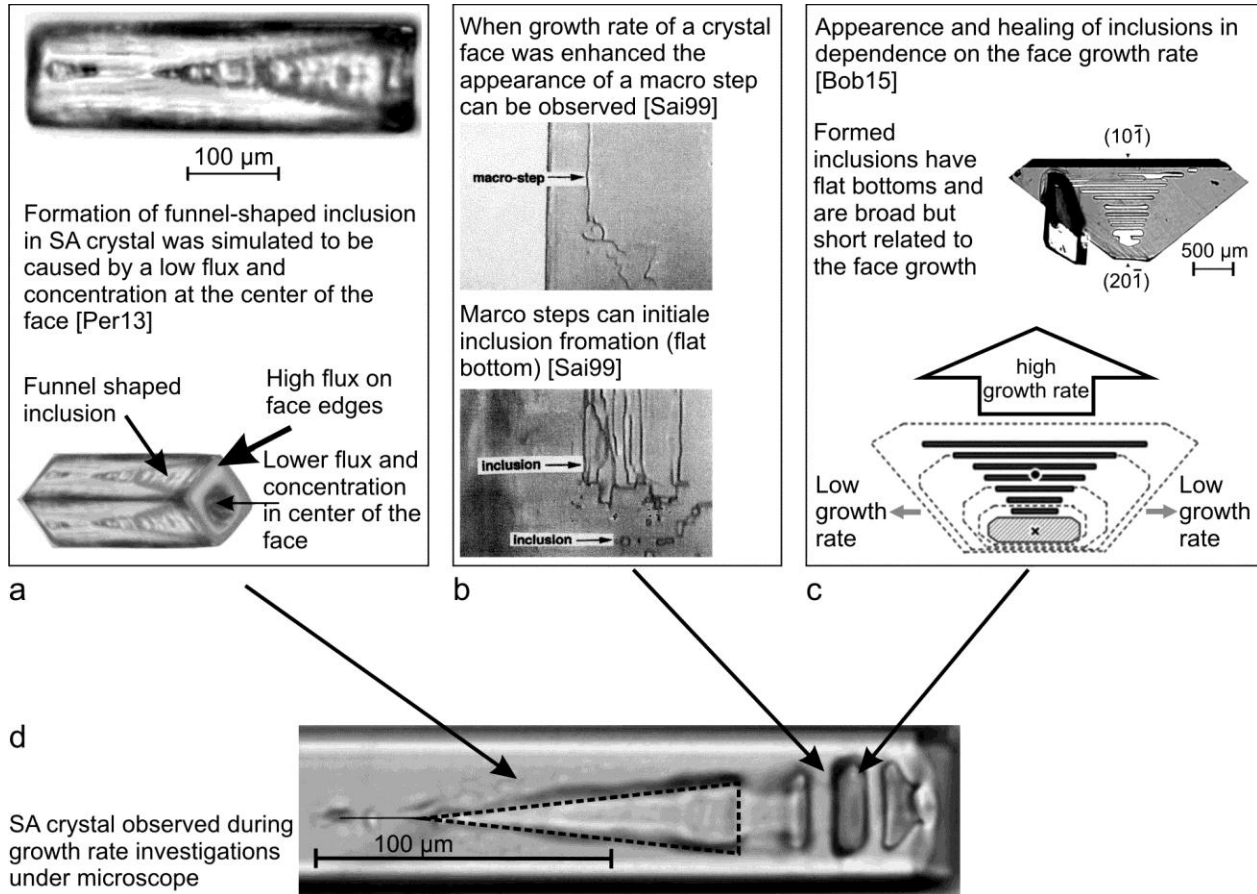


Fig. 6.2: Mechanisms to describe the formation of liquid inclusions; a) Diffusion-limited formation of funnel-shaped inclusions of SA [Per13]; b) Observation of macro steps on crystalline surface after induced growth rate enhancement [Sai99]; c) Formation of liquid inclusions depending on the face growth rate [Bob15]; d) Crystal from microscopic growth rate measurements which contains different inclusions.

In Fig. 6.2d a crystal that was observed during microscopic observation on single crystals growth during static antisolvent crystallization is depicted. This crystal contains different types of inclusions which are on the left a funnel-shaped inclusion which seems to be enclosed and on the right two inclusions with flat bottoms. If the inclusions inside this crystal are compared to images of inclusion containing crystals from literature [Sai99, Per13, Bob15] similar inclusion shapes can be found. The shape of the funnel-like inclusion fits perfect to an inclusion observed by Perry et al. [Per13] in SA crystals

(Fig. 6.2a). In their study the formation of such inclusions was determined to be caused by a diffusion-limited mechanism.

On the right of the depicted crystal (Fig. 6.2d) the inclusions with flat bottoms as inclusion bases remind on the images published by Bobo et al. [Bob15] and Bobo [Bob16b]. In their study on the inclusion formation in single ammonium perchlorate crystals in dependency on the growth rate of single crystal faces similar inclusion shapes were observed. Those are discussed to be caused by fluctuations in growth rates. If the growth rate of a phase suddenly increased the occurrence of an inclusion could be observed. When the growth rate dropped the inclusion sealed. It is discussed that the solid section between two of these inclusions might be formed by a transient crystal face [Bob16b, Bro68].

The different observed shapes of inclusions lead to the assumption that in case of SA different mechanisms of inclusion formation can occur within the same crystal. Based on inclusion formation theories from literature it might be concluded that, on the one hand, the funnel-shaped inclusions are formed if the growth rate is constantly faster than the diffusion. On the other hand, fluctuations in growth rate, which might be caused by fluctuations in local supersaturation, can result in flat inclusions. However, it should be pointed out that even if the conditions which are necessary for inclusion formation are fulfilled the appearance of inclusions cannot be ensured.

6.4.2 Investigations on the effects of experimental parameters on the crystal and inclusion sizes

The investigations on the effects of experimental parameters on crystal and inclusion sizes were performed in the context of preparing crystalline container systems of SA. For this application possibly high inclusion amounts and, thus, a high potential for agent encapsulation is aimed. In order to develop a stable crystallization process for container production the relevant experimental parameters have to be considered according to their effects on the crystal sizes and inclusion amounts.

The importance of the performed investigations can be seen well in Fig. 5.20. There, the effect of an unfavorable combination of the experimental parameters (Fig. 5.20a and b) resulted in very thin crystals with high agglomeration degree and low inclusion amounts.

This is contrasted by the appearance of the crystals in Fig. 5.20c where by adjusting a few experimental parameters inclusion containing crystals with low agglomeration could be prepared.

6.4.2.1 Effects of experimental parameters on particle sizes

Antisolvent crystallization is widely used in the preparation of nano- and micro-scaled particles of APIs. There are several studies, e.g. [Wan07, Li11, Hat12, Kak12a, Kak12b, Par12, Kak13, Lon13], where the effect of experimental parameters on the particle size was investigated. An overview is given in Tab. 6.1.

It should be pointed out that in the studies presented in Tab. 6.1 experimental setups where the solution was injected into the antisolvent were chosen. For that reason, these literature data are only limited directly comparable to the results of this study. However, if the explanations given by the authors are considered the literature results can be transferred to the measured data of this study. [Wan07, Li11, Hat12, Kak12a, Kak12b, Par12, Kak13, Lon13]. The basic approach to discuss the effects of experimental parameters on particle sizes is based on the nucleation theory which describes that the higher the supersaturation level the more nuclei appear and the smaller are the final crystals. This single approach can be used to explain the effects of all parameters that manipulate the supersaturation, e.g. concentration or w , injection rate and solvent/antisolvent ratio.

Tab. 6.1: Overview of the effects of experimental parameters on particle sizes of different APIs as described in literature; Increase: ↗, Decrease: ↘. The effects shown in the table are quite generalized, thus, it should be pointed out that all effects occur within limited ranges.

Parameter	Substance	Effects		Ref	Observations in this study	
Concentration	Carbamazepine	c↗	ps↘	[Par12]		
	Curcumin	c↗	ps↘	[Kak12a]		
	Beclomethasone dipropionate	c↗	ps↘	[Wan07]		
	Quercetin	c↗	ps↗	[Kak12b]		
	Artemisinin	c↗	ps↘	[Kak13]		
	Salicylic acid	c↗	ps↘	[Hat12]		
	Poorly water soluble drugs (review)	c↗	ps↘	[Lon13]		
	Temperature	Carbamazepine	T↗	ps↗	[Par12]	T↗
Curcumin		T↗	ps↗	[Kak12a]		
Bicalutamide		T↗	ps↗	[Li11]		
Beclomethasone dipropionate		T↗	ps↗	[Wan07]		
Artemisinin		T↗	ps↗	[Kak13]		
Salicylic acid		No effect		[Hat12]		
Poorly water soluble drugs (review)		T↗	ps↗	[Lon13]		
Solution injection rate (SIR)	Carbamazepine	SIR↗	ps↘	[Par12]		
	Curcumin	SIR↗	ps↘	[Kak12a]		
	Quercetin	SIR↗	ps↘	[Kak12b]		
	Artemisinin	SIR↗	ps↘	[Kak13]		
	Salicylic acid	SIR↗	ps↗	[Hat12]		
	Poorly water soluble drugs (review)	SIR↗	ps↘	[Lon13]		
	Solvent-Antisolvent volume ratio (S/AS)	Curcumin	S/AS↗	ps↘	[Kak12a]	
Beclomethasone dipropionate		S/AS↗	ps↘	[Wan07]		
Quercetin		S/AS↗	ps↘	[Kak12b]		
Artemisinin		S/AS↗	ps↘	[Kak13]		
Salicylic acid		S/AS↗	ps↘	[Hat12]		
Poorly water soluble drugs (review)		S/AS↗	ps↘	[Lon13]		
Stirring rate (SR)		Curcumin	SR↗	ps↘	[Kak12a]	SR↗
	Bicalutamide	SR↗	ps↘	[Li11]		
	Beclomethasone dipropionate	SR↗	ps↘	[Wan07]		
	Quercetin	SR↗	ps↘	[Kak12b]		
	Artemisinin	SR↗	ps↘	[Kak13]		
	Salicylic acid	SR↗	ps↘	[Hat12]		
	Poorly water soluble drugs (review)	SR↗	ps↘	[Lon13]		
	Stirring time (ST)	Beclomethasone dipropionate	ST↗	ps↘	[Wan07]	
Salicylic acid		No effect		[Hat12]		

In case of stirring rate and stirring time the explanation based on the supersaturation levels is only of partial interest. On the one hand, a high stirring rate leads to a fast homogenization of solution and antisolvent and, thus, a high, homogeneous

supersaturation level can be achieved which results in a high number of nuclei [Lon13, Kak12]. On the other hand, stirring causes abrasions on the crystals or breakage. The faster and longer the batch is stirred the smaller are the received crystals [Wan07].

In context of temperature effects on particle sizes three effects have to be considered. The first one is again the effect of supersaturation as described above. At a lower temperature a higher supersaturation can be reached which results in a higher number of nuclei. As a second effect, it should be considered that the critical nucleus size decreases with temperature [Mul01]. As a third effect of temperature an increase in the viscosity with decreasing temperature should be mentioned. This effect, which can occur with an increase in concentration as well, can inhibit the nucleation rate and result in the formation of less nuclei and larger crystals as can be seen in case of Quercetin presented in Tab. 6.1 [Kak12b]. In the present study using short-chained alcohols (MeOH or EtOH), SA and water the increase of viscosity from both temperature and concentration effects are of negligible meaning.

Besides the general consideration of temperature on crystal sizes it was observed that with increasing temperature the widths of the crystals increased while their lengths were quite unaffected. This phenomenon can be explained by the intensity of the temperature dependence on growth rate for diffusion- and surface integration-controlled growth. The temperature dependence of the mass transfer coefficients k for surface integration (k_r) and volume diffusion step (k_d) as well as the corresponding activation energies E are described in Tab. 6.2.

Tab. 6.2: Definitions of mass transfer coefficients k from temperature for surface integration and volume diffusion step as well as the corresponding Arrhenius activation energies E [Lew15].

Surface integration	Diffusion
$k_r = k_{r0} e^{-E_r/RT} \quad (6.1)$ $E_r \approx 40-60 \text{ kJ mol}^{-1}$	$k_d = k_{d0} e^{-E_d/RT} \quad (6.2)$ $E_d \approx 10-20 \text{ kJ mol}^{-1}$

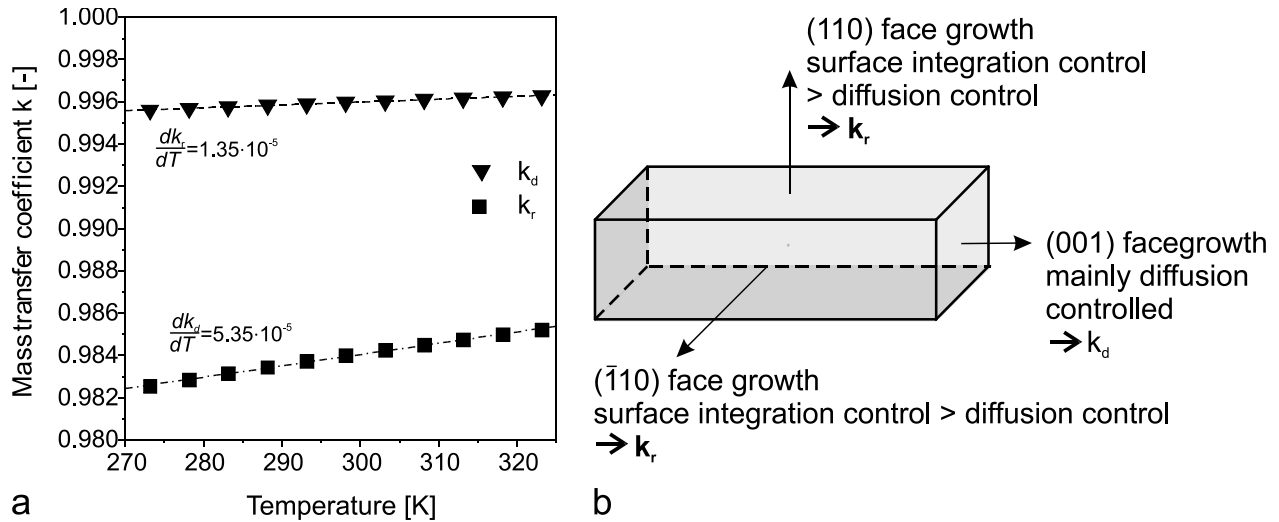


Fig. 6.3: a) Mass transfer coefficients for surface integration (k_r , ■) and volume diffusion step (k_d , ▼) plotted against temperature; b) Dominating mechanisms for growth of SA crystal faces [Per13].

In Fig. 6.3a k_r and k_d are calculated assuming that the initial transfer coefficients k_{r0} and k_{d0} that are not of interest in this case and can be neglected ($k_{r0}=k_{d0}=1$). Further, in each case the lowest activation energy E was used ($E_r=40 \text{ kJ mol}^{-1}$; $E_d=10 \text{ kJ mol}^{-1}$). As can be seen in the diagram both k_r and k_d and, thus, the growth rates are increasing with increasing temperature. However, the slope of k_r is 4-times the slope of k_d . If these findings are connected to the growth behavior of single faces of SA crystals as described by Perry et al. [Per13] the observed increase of growth in width at higher temperatures can be explained. The growth of the (110) and $(\bar{1}10)$ faces which define the growth in width are limited considerably by surface integration while the (001) face growth is dominated by a diffusion controlled mechanism (Fig. 6.3b). If the temperature increases the growth rates of (110) and $(\bar{1}10)$ faces increase more intense than the growth rates of (001) faces. As a result the growth in width is enhanced more intensely with increasing temperature than the growth in length.

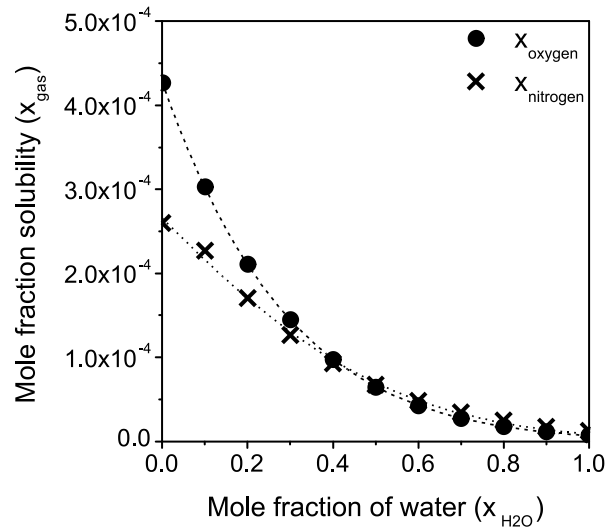


Fig. 6.4: Solubility of oxygen and nitrogen in ethanol in dependence on the water amount predicted by means of the HSP model. The gas solubility is decreasing with increasing water content.

One parameter that was not investigated in context of antisolvent crystallization, yet, is the effect of degassing on the particle sizes. If water and EtOH are mixed the solubility of gases, e.g. oxygen and nitrogen, decrease (Fig. 6.4). The solubility curves of both gases in dependence on the solvent mixture can be calculated by means of the HSP-model. The depicted decrease in gas solubility leads to the nucleation of gas bubbles in the liquid. As shown by Wohlgemuth et al. [Woh09, Woh10] the surfaces of gas bubbles can act as nucleation centers and, thus, nucleation is initiated at lower supersaturation. As a result it can be expected that less nuclei are formed and the crystal size is increased. If the liquids are degassed the appearance of bubbles can be reduced and nucleation is expected to happen at higher supersaturation. For that reason, larger crystals were expected if solution and antisolvent were degassed. However, no clear effect of solution and antisolvent degassing on the crystal sizes could be identified.

6.4.2.2 Effects of experimental parameters on inclusion sizes

In case of experimental effects on the inclusion sizes in crystals only little information can be found in literature as presented in Tab. 6.3. It should be noted that the information described below refer to experiments from cooling crystallization and that the inclusion sizes (IS) were either estimated according to microscopic observations [Den66] or referred to the amount of enclosed solvent [Zha05, Kim09].

Tab. 6.3: Literature data on the effects of experimental parameters on the inclusion sizes; Increase: ↗, Decrease: ↘.

Parameter	Substance	Effects	Ref
Temperature	Adipic acid	T ↗ IS ↗	[Zha05]
	Cyclotrimethylene trinitramine	T ↗ IS ↗	[Kim09]
	Hexamethylene tetramine	Depending on SR	[Den66]
Stirring rate	Adipic acid	No effect	[Zha05]
	Hexamethylene tetramine	SR ↗ IS ↘	[Den66]
Seeding Density	Adipic acid	SD ↗ IS ↘	[Zha05]

In general the inclusion formation is described in context with high growth rates and growth rate fluctuations, e.g. [Den66, Sai99, Zha05, Kim09, Edd10, Wal11a, Per13, Bob15, Bob16b]. In the present study the effects of experimental parameters on the relative inclusion amounts (RIA) were investigated considering the interactions between different parameters, e.g. effect of stirring rate at three different mass fraction levels (Chapter 5.3.4.1). This experimental procedure gives comprehensive results of the inclusion formation under different conditions. However, the results are difficult to

interpret in order to present some general statements. Another reason that prevents summarizing the results is that there are high variations in the data which are based on the inhomogeneous samples. The most distinct possibility to manipulate the RIA is to adjust the direction of injection. However, this parameter in turn depends on solution mass fraction w and temperature.

Waldschmidt et al. [Wal11a] described that solution degassing resulted in a distinct decrease of liquid inclusions in ciclopirox crystals. It is discussed that the inclusion formation and sizes depend on the growth rates which in turn depend in their case study on the type of gas dissolved in the solution. If the solution was degassed a distinct decrease of growth rate could be observed and the inclusion formation was reduced. In Chapter 5.1.3 the results of the effects of solution degassing on growth rate of SA crystals from cooling crystallization are presented. It was found that the growth rates of SA were unaffected by the reduction of the solutions' gas amounts. For that reason, no effect of degassing on the RIA was expected in case of antisolvent crystallization. Another possible effect of dissolved gases on the inclusion formation is the adsorption of gas bubbles on the growing crystal faces [Wal11a]. The reduction of the gas amount dissolved in solution and antisolvent could, therefore, be another approach of manipulating the formation on liquid inclusions. However, a clear RIA decrease which might have been expected if liquids were degassed could not be observed. In summary, no effects of degassing the solution and/or antisolvent were found.

In literature [Sai99] there are some examples described where crystal growth could be manipulated in order to induce the formation of inclusions, e.g. by mechanical contacts of the growing crystal surface. However, even if the experimental parameters are adjusted in order to reach high growth rates, e.g. by increasing the temperature or the injection rate, as necessary condition for inclusion formation there is no guarantee to receive crystals with large RIA. This confirms the findings described, e.g. by Waldschmidt et al. [Wal11a].

6.5. Preparation of filled container crystals of SA

As could be shown in Chapter 5.4 two cases could be presented where a foreign substance could successfully be encapsulated inside SA container crystals. Firstly, a

qualitative prove of copper ions that were enclosed in SA crystals could be presented. Since copper sulfate is an inappropriate substance to be applied in skin care products ascorbic acid (AA) which is more suitable was chosen as second test foreign substance.

6.5.1 Model system SA-AA

As described in Chapter 4.1.1 SA is used as keratolytic agent in skin care products in context of, e.g. acne and dandruff treatment as well as for skin- and hair-conditioning. In order to develop a suitable model system for this case study a substance that matches to SA according to a potential application as well as chemical and crystallization properties. AA was found to fulfill all these claims and, thus, it was chosen to be encapsulated inside SA container crystals.

AA (vitamin C) is of growing interest for skin care products because of its antioxidant properties which offer the benefits of neutralizing free radicals which are one important reason for photo aging of the skin. Topical ascorbic acid treatment protects the skin from oxidative stress which is one of its functions to suppress photo aging. Further, vitamin C functions in the skin as cofactor in collagen synthesis and it has potent anti-inflammatory effects. Thus, AA is used, e.g. in anti-aging and anti-acne products [Kel98, Sta01, Far05, Man09]. From a dermatologic point of view, AA is a beneficial agent to be combined with SA. While SA functions keratolytically (removal of dead skin particles), AA promotes the renewal of the skin by supporting collagen synthesis. It is discussed in literature [Man09] that AA delivery into the skin can be improved by lowering the pH below 3.5. This pH can be provided by the use of SA whose pH is 2.4 in aqueous solution [IFA16c, Ras92]. In order to deliver AA in pharmacological levels to the skin concentrations of 10% should be achieved [Kel98].

In general AA is quite sensitive against environmental influences, e.g. UV irradiation or air oxygen. For that reason it needs to be protected in order to preserve its beneficial effects on skin metabolism. Its encapsulation inside container crystals offers the possibility of a physical protection from outer influences. Moreover, due to its oxidative properties SA has the potential to prevent reduction of AA and, thus, stabilizes it in its active form.

6.5.2 Experimental parameters chosen for preparation of container crystals

The choice of the experimental parameters for the preparation of SA container crystals was based on the results from investigations of experimental parameters on the crystal and inclusion sizes (Chapter 4.2.8). As most important parameter to reach crystals with possibly high inclusion amounts the injection direction was identified. It was figured out that if an 8% SA solution was injected into the antisolvent at 10 or 20 °C the relative inclusion amount (RIA) could be increased to about 4% which is twice the RIA that was reached if the antisolvent was injected into the solution (Chapter 5.3.4.3). These results were taken as basis for defining injection direction and solution mass fraction w . Considering the working temperature, it could be seen in the appropriate experiments performed at 10 °C that the revealed crystals showed smaller variations than those prepared at higher temperatures (Chapter 5.3.3.3). In order to reduce the particle size distribution and, thus, get more uniform samples 10 °C was chosen as working temperature for crystallization. Another parameter that needed to be defined was the injection rate (IR). Since no differences between samples prepared at $IR \geq 12 \text{ mL min}^{-1}$ using $w=8\%$ solutions (Chapter 5.3.3.2) an $IR=20 \text{ mL min}^{-1}$ was chosen in order to reduce the duration of experiments. The stirring rate (SR) was set to 100 rpm which resulted at $w=8\%$ in larger crystals and larger inclusions than when $SR=350 \text{ rpm}$ were applied (Chapter 5.3.4.1). As final parameter whose effects on the crystal and inclusion sizes were investigated the gas content of the liquids was not manipulated. The effect of solution and/or antisolvent degassing was irrelevant regarding crystal or inclusion sizes. Thus, this time consuming step was not performed during crystallization of SA containers. According to the chosen experimental parameters RIA of 2-4% can be expected.

6.5.3 Potential of inclusion containing SA crystals for application as container crystals

The amount of AA that was encapsulated inside SA container crystals could be quantified to be $0.4 \pm 0.3 \text{ mg per g crystals}$. Assuming that the surrounding liquid is enclosed inside the inclusions during crystal growth the determined AA amount can be used to estimate the inclusion amount of the container crystals. Since the amount of AA in the antisolvent is known to be 5% the inclusion amount can be estimated in

dependency on the solvent composition which changes during the process. The first crystals appeared when less than 5 mL of SA solution were injected into the AA containing antisolvent. Thus, it can be assumed that there are some crystals containing almost 100% on the AA containing antisolvent. Assuming that this liquid contained 5% AA the inclusion amount can be estimated to be about 0.8%. The final SA solution-antisolvent ratio is about 30:70 (v:v) which results in estimated inclusion amounts of about 1.1%. Based on these estimations it can be concluded that the prepared container crystals contain approximately 1% inclusions [Sei16].

This result is lower than expected based on the enquiries on the effects of the experimental parameters on crystal and inclusion sizes. However, it should be pointed out that in the microscopic investigations only intact crystals were considered while broken crystals and crystal fragments were neglected. This might explain the difference between the expected RIA of 2-4% and the results received from the determination of AA content of approximately 1%.

Schuster et al. [Sch10] presented in their study on glucose anhydrate needles which were filled with ibuprofen by inducing a phase transition from glucose monohydrate into anhydrate needles in dried methanol containing 60% ibuprofen. The quantification of ibuprofen in 100 mg crystals that were dissolved in 1 mL methanol was determined to be $0.361 \text{ mmol L}^{-1}$. Based on this information the inclusion amount can be calculated as described above to be about 0.12%.

Conclusively, the results of this study showed that the inclusion amounts could be increased by about 10 times compared to previous approaches of investigating the potential of crystalline container systems. However, inclusion amounts of about 1% are still quite small and it has to be considered that the inclusions cannot be filled completely with a pure solid substance but a solution. In case of antisolvent crystallization the included liquor consists of the solution's solvent, in this case EtOH, the antisolvent, water, and the foreign material that is aimed to be encapsulated, here AA. One approach to increase the amount of the foreign substance could be to increase its concentration in the antisolvent. This procedure might work within limited ranges which are defined by the solubility of the foreign substance in both solvents used for the crystallization process. Moreover, it has to be excluded that the foreign substance

affects the crystallization of the container material, e.g. according to morphology or solubility. If the inclusion amounts are aimed to be further increased it should be considered that increasing the relative inclusion size leads to the reduction of the wall thickness which might in turn affect the physical stability of the containers.

As discussed above AA states in both dermatological and chemical context a good combination with SA. However, the amounts of AA that could be encapsulated inside SA container crystals (0.4 ± 0.3 mg per g crystals) are too low to provide concentrations of roughly 10% in a final product which are necessary to achieve pharmacological level.

7. Conclusions

The aim of this study was to investigate the applicability of crystalline container systems, exemplarily for skincare products. Based on a model system the preparation conditions and required properties of the potential product were investigated.

1. Model substance

As model substance the cosmetic and dermatological agent salicylic acid (SA) was chosen. This low water soluble agent is authorized to be applied as active agent in amounts of up to 2% in cosmetic products and owns a high tendency to form liquid inclusions.

2. Determine product conditions for application of container crystals

In order to verify whether SA container crystals can be applied in a cosmetic product without their dissolution the solubility of SA in ethanol-water mixtures was determined. This allowed estimating the solvent composition which offers the necessary conditions for the container crystals to be stable against dissolution. Moreover, a model to predict the solubility of SA in solvent-water mixtures without the need of solubility data from literature was developed.

3. Investigate the experimental parameters for container generation

In two systematic enquiries the effects of experimental parameters on crystal and inclusion sizes were investigated by means of optical microscopy. Based on the results the experimental parameters that offer the possibility to prepare crystals that contain relative inclusion amounts of 2-4% were identified.

4. Filling of the container crystals

As exemplary filling substance, ascorbic acid (AA) was chosen. The application of this vitamin offers great benefits for skin care, especially, in combination with SA. The amount of encapsulated AA could be quantified to be 0.4 ± 0.3 mg per g crystals. Based on these results the inclusion amount could be estimated to be about 1% of the crystals.

5. Verify the applicability of container crystals

The investigations of the SA solubility in ethanol-water-mixtures showed that the solvent conditions to ensure the stability of the container crystals against dissolution can be easily applied for cosmetic products. Thus, as one final conclusion of this thesis container crystals can be added to a product without their dissolution.

Regarding the inclusion amounts, it can be summarized that from the theoretically expected 2-4% relative inclusion amounts only 1% could be proven based on the amount of encapsulated material. It should be considered that the inclusions can only be filled with a solution consisting of both solvents used during the antisolvent crystallization, the container material and the foreign substance that is aimed to be encapsulated. For that reason, only small amounts of a foreign substance ($\ll 1\%$) can be encapsulated inside crystalline containers. In case of AA the amounts that can be encapsulated are too small to induce a physiological function. However, the system might be applied for, e.g. flavor agents, which are potent even in trace amounts.

8. Summary

The idea of using crystalline materials for agent encapsulation is discussed in literature for several years and a few exemplary model systems are already presented. However, up to now only the possibility of preparing such container crystals of metastable polymorphs was in the focus of the studies.

For that reason the aim of this study was to investigate inclusion containing crystals as encapsulation material due to their applicability in potential products, exemplarily skincare products. As model substance salicylic acid was chosen because of its stable crystal habit and high tendency to form liquid inclusions. Further, it is used as active agent in cosmetics and has low water solubility. In this study the general crystallization behavior of this model substance was investigated.

Since dissolved gases are described in literature to affect the formation of liquid inclusions this parameter was focused on when solubility, metastable zone width as well as growth and dissolution rates of salicylic acid in methanol were determined. In order to estimate the stability of the container crystals in a potential product the solubility of salicylic acid was investigated exemplarily in case of ethanol-water mixtures. The development of a solubility prediction model based on the Hansen Solubility Parameters, further, allowed estimating the solubility of the container crystals in other solvent-water mixtures without the need of solubility data from literature.

After the conditions to ensure the stability of container crystals in a potential product were defined the preparation of container crystals with possibly high inclusion amounts were focused on. In systematic enquiries the effects of experimental parameters on crystal and inclusion sizes, including interactions between different parameters, were investigated. By adjusting the experimental conditions theoretical inclusion amounts of 2-4% could be expected. By means of filling the container crystals with ascorbic acid the concept of agent encapsulation using inclusion containing crystals was proven. Due to the quantification of the enclosed ascorbic acid amount of 0.4 ± 0.3 mg per g crystals the inclusion amount could be determined to be approximately 1%. Moreover, the amount of encapsulated ascorbic acid gives a general idea of the potential application of container crystals as encapsulation material. Concerning the encapsulation potential of $\gg 1\%$

which is too low for carrying active agents in appropriate amounts a possible application could be the encapsulation of flavor agents.

9. Zusammenfassung

Der Gedanke kristalline Materialien zur Wirkstoffverkapselung einzusetzen wird in der Literatur seit einigen Jahren diskutiert und ein paar beispielhafte Modellsysteme wurden bereits vorgestellt. Bisher wurde in diesen Studien jedoch nur die Möglichkeit solche kristallinen Container aus metastabilen Polymorphen herzustellen untersucht.

Aus diesem Grund lag die Zielsetzung dieser Arbeit darauf, Kristalle mit flüssigen Einschlüssen auf ihre Eignung als Verkapselungssysteme im Hinblick auf mögliche Anwendungen, zum Beispiel in Kosmetikprodukten, zu untersuchen. Als Modellschubstanz wurde Salizylsäure wegen ihrer stabilen kristallinen Beschaffenheit und ihrer hohen Tendenz flüssige Einschlüsse zu bilden ausgewählt. Zudem wird es als Wirkstoff in Kosmetikprodukten eingesetzt und besitzt eine geringe Wasserlöslichkeit. Als Teil dieser Arbeit wurde allgemein das Kristallisationsverhalten dieser Modellschubstanz untersucht.

Da in der Literatur gelöste Gase mit der Entstehung flüssiger Kristalleinschlüsse in Verbindung gebracht werden, wurden Löslichkeit, metastabiler Bereich sowie Wachstums- und Auflöseraten von Salizylsäure in Methanol im Hinblick auf den Einfluss gelöster Gase bestimmt. Um die Stabilität der kristallinen Containersysteme in einem potentiellen Produkt einzuschätzen wurde die Löslichkeit von Salizylsäure beispielhaft für Ethanol-Wasser-Gemische untersucht. Die Entwicklung eines Modells zur Vorhersage der Löslichkeit auf Grundlage der „Hansen Solubility Parameter“ erlaubte es zudem die Löslichkeit der Containerkristalle in weiteren Lösungsmittel-Wasser-Gemischen ohne die Notwendigkeit entsprechender Literaturdaten abzuschätzen.

Nachdem die notwendigen Bedingungen zur Gewährleistung der Stabilität der Containerkristalle in einem möglichen Produkt definiert wurden, konnte die Herstellung solcher Containerkristalle, welche möglichst große Anteile flüssiger Einschlüsse aufweisen sollen, verfolgt werden. Mittels systematischer Untersuchungen wurden die Einflüsse experimenteller Parameter, einschließlich möglicher Wechselwirkungen zwischen verschiedenen Parametern, auf Kristall- und Einschlussgrößen untersucht. Durch das Anpassen der experimentellen Bedingungen konnten theoretische Einschlussgehalte von 2-4% erwarten werden. Durch das Befüllen der Containerkristalle mit Ascorbinsäure konnte die Machbarkeit der Wirkstoffverkapselung mittels flüssiger

Kristalleinschlüsse bestätigt werden. Basierend auf der Quantifizierung des eingeschlossenen Ascorbinsäuregehaltes von $0,4 \pm 0,3$ mg pro g Kristalle konnte der Gehalt flüssiger Einschlüsse auf ungefähr 1% geschätzt werden. Dieser Gehalt an verkapselter Ascorbinsäure gibt eine allgemeine Vorstellung der möglichen Anwendung solcher Containerkristalle als Verkapselungsmaterial. Hinsichtlich des Verkapselungspotentials von $\gg 1\%$, welches zu gering ist, um Wirkstoffe in entsprechenden Dosen bereitzustellen, wäre jedoch als mögliche Anwendung die Verkapselung von Aromen denkbar.

10. Abbreviations and symbols

10.1.1 Abbreviations

3D	three-dimensional
AA	ascorbic acid
AIV	absolute inclusion volume
API	active pharmaceutical ingredient
approx.	approximately
AS	antisolvent
BC	before Christ
col	colorant
DMA	dexamethasone acetate
DMF	dimethylformamide
DMSO	dimethyl sulfoxide
e.g.	for example
Eq.	equation
et al.	et alii (and others)
EtOH	ethanol
EU	European Union
ew	ethanol-water-mixtures
Fig.	Figure
FT-IR	Fourier Transform Infrared
HPLC	high performance liquid chromatography
HSP	Hansen Solubility Parameters
i-propanol	iso-propanol
IR	injection rate
IS	inclusion size
IUPAC	International Union of Pure and Applied Chemistry
log	common logarithm (decadic)
MeOH	methanol
MS	Microsoft
MZW	metastable zone width
Ni	nitrogen
No.	number
non-deg.	non-degassed
OM	optical microscopy
ORM	optical reflectance measurement
Ox	oxygen
ppm	part per billion
ps	pure solvents
Ref.	Reference
RESS	rapid expansion of supercritical solutions

RIA	relative inclusion amount
rpm	rotation per minute
S	solution
S/AS	solution-antisolvent-ratio
SA	salicylic acid
sat. curve	saturation curve
SEM	scanning electron microscopy
SKGA	sodium-2-ketogulonate anhydrate
SKGM	sodium-2-ketogulonate monohydrate
SR	stirring rate
Tab.	Table
US	ultrasound
UV	ultraviolet
v:v	volume ratio
XRPD	X-ray powder diffraction

10.1.2 Latin symbols

A	surface
C	concentration
d	differential operator
E	Energy
k	mass transfer coefficient
l	liquid
m	mass
n	number of data points
R	correlation coefficient
R	gas constant
R_a	distance of HSP of two compounds in a Cartesian coordinate system
S	supersaturation
s	solid
T	temperature
t	time
V	volume
w	mass fraction
x	mole fraction

10.1.3 Greek symbols

Δ	difference
δ	interactions
φ	volume fraction

10.1.4 Indices

0	initial state
1	compound 1
2	compound 2
*	final state
AS	antisolvent
D	dispersion
d	volume diffusion
EtOH	ethanol
gas	gas
H	hydrogen bonding
i	interaction type
j	summation index
m	molar
MeOH	Methanol
Ni	nitrogen
Ox	oxygen
P	dipole
r	surface integration
S	solution
SA	salicylic acid
seed	seed crystals
sol	solution
water	water

11. References

- [Bec01] Bechtloff, B., Nordhoff, S., Ulrich, J., Pseudopolymorphs in Industrial Use, *Cryst. Res. Technol.* 36 (2001) 1315–1328.
- [Ben06] Benita, S., *Microencapsulation, Methods and Industrial Applications*, second ed., CRC Press LCC, Boca Raton, 2006.
- [Ben99] Benceñzdi, D., Blake, A., Encapsulation and the controlled release of flavors, *Leatherhead Food RA Ind. J.* 2 (1999), 36–48.
- [Bla01] Blandin, A.F., Mangin, D., Nallet, V., Klein, J.P., Bossoutrot, J.M., Kinetics Identification of Salicylic Acid Precipitation through Experiments in a Batch Stirred Vessel and a T-Mixer, *Chem. Eng. J.* 81 (2001) 91–100.
- [Bob15] Bobo, E., Petit, S., Coquerel, G., Growth Rate Dispersion at the Single-Crystal Level, *Chem. Eng. Technol.* 38 (2015) 1011–1016. doi:10.1002/ceat.201400766.
- [Bob16a] Bobo, E., Lefez, B., Caumon, M.-C., Petit, S., Coquerel, G., Evidence of two types of fluid inclusions in single crystals, *CrystEngComm.* 18 (2016) 5287–5295. doi:10.1039/C6CE00956E.
- [Bob16b] Bobo, E., Contribution on the formation and the behaviors of fluid inclusions in crystals, PhD-thesis, University of Rouen, 2016.
- [Bro68] Brooks, R., Horton, A.T., Torgesen, J.L., Occlusion of mother liquor in solution-grown crystals, *J. Cryst. Growth.* 2 (1968) 5, 279–283. doi:10.1016/0022-0248(68)90015-8.
- [Cao13] Cao, Z., Yu, X., Yue, Y., Hu, Z., Synthesis and growth mechanism of tubular $\text{YAl}_3(\text{BO}_3)_4$ crystals in millimeter diameter, *J. Cryst. Growth.* 362 (2013) 111–115. doi:10.1016/j.jcrysgro.2011.09.060.
- [Car12] Cartigny, Y., Delage, S., Lanontaine, A., Study of the behaviour of Sodium 2 Keto-L-Gulonate Monohydrate (SKGM) in methanol by Dynamic Vapor Sorption measurements: Characterization of a new (transient) solvated phase, Presentation 23.10. 2012, Rouen.

- [Car85] Cardew, P.T., Davey, R. J., The kinetics of solvent-mediated phase transformations, *Proc. R. Soc. Lond. A*, 398 (1985) 1815, 415-428.
- [Che08] Cheng, S.Y., Yuen, C.W.M., Kan, C.W., Cheuk, K.K.L., Development of Cosmetic Textiles Using Microencapsulation Technology, *Res. J. Text. Appar.* 12 (2008) 41–51. doi:10.1108/RJTA-12-04-2008-B005.
- [CIR03] Cosmetic Ingredient Review (CIR) Panel, Safety Assesment of Salicylic Acid, Butyloctyl Salicylate, Calcium Salicylate, C12-15 Alkyl Salicylate, Caprylol Salicylic Acid, Hexyldodecyl Salicylate, Isocetyl Salicylate, Isodecyl Salicylate, Magnesium Salicylate, MEA-Salicylate, Ethylhexyl Salicylate, Potassium Salicylate, Methyl Salicylate, MyristylSalicylate, Sodium Salicylate, TEA-Salicylate and Tridecyl Salicylate, *Int. J. Toxicol.* 22 (2003) 1-108. doi:10.1080/10915810390239487.
- [Den66] Denbigh, K., White, E., Studies on Liquid Inclusions in Crystals, *Chem. Eng. Sci.* 21 (1966) 739–754.
- [Det07] Dette, S.S., Stelzer, T., Römbach, E., Jones, M.J., Ulrich, J., Controlling the Internal Diameter of Nanotubes by Changing the Concentration of the Antisolvent, *Cryst. Growth Des.* 7 (2007) 1615–1617. doi:10.1021/cg0700768.
- [Det09] Dette, S. S., Kristalline Röhren - Erzeugt durch die Dehydratation in organischen Lösungsmitteln, Dissertation, Martin Luther University Halle-Wittenberg, Shaker Verlag, 2009.
- [Det10a] Dette, S.S., Stelzer, T., Jones, M.J., Ulrich, J., Dehydration behaviour of hydrates, *Cryst. Res. Technol.* 45 (2010) 697–702. doi:10.1002/crat.201000188.
- [Det10b] Dette, S.S., Stelzer, T., Jones, M.J., Coquerel, G., Ulrich, J., Fascinating control of crystalline microstructures, *Chem. Eng. Res. Des.* 88 (2010) 1158–1162. doi:10.1016/j.cherd.2009.10.003.
- [Det12] Dette, S.S., Sanselme, M., Stelzer, T., Renou, L., Jones, M.J., Couvrat, N., Coquerel, G., Ulrich, J., Structural investigation on sodium-2-keto-L-

- gulonate-monohydrate, *J. Mol. Struct.* 1020 (2012) 121–126. doi:10.1016/j.molstruc.2012.03.062.
- [Edd10] Eddleston, M.D., Jones, W., Formation of Tubular Crystals of Pharmaceutical Compounds, *Cryst. Growth Des.* 10 (2010) 365–370. doi:10.1021/cg900969n.
- [Eur09] European Commission, Regulation (EC) No 1223/2009 of the European Parliament and of the Council of 30 November 2009 on cosmetic products, *Off. J. Eur. Union.* (2009) 342–359.
- [Eur11] European Parliament and Council, Commission Regulation (EU) No 1129/2011 of 11 November 2011 amending Annex II to Regulation (EC) No 1333/2008 of the European Parliament and of the Council by establishing a Union list of food additives, *Off. J. Eur. Union.* L295 (2011) 1–177. doi:10.3000/19770677.L_2011.295.eng.
- [Far05] Farris, P.K., Topical vitamin C: a useful agent for treating photoaging and other dermatologic conditions., *Dermatol. Surg.* 31 (2005) 814–817; discussion 818. doi:10.1111/j.1524-4725.2005.31725.
- [Fin05] Fink, E., *Kosmetik, Wirk- und Hilfsstoffliste, Beratungsleitfaden*, first ed., Wissenschaftliche Verlagsgesellschaft mbH Stuttgart, Stuttgart, 2005.
- [Fre15] Frenzel, M., Steffen-Heins, A., Impact of quercetin and fish oil encapsulation on bilayer membrane and oxidation stability of liposomes, *Food Chem.* 185 (2015) 48–57. doi:10.1016/j.foodchem.2015.03.121.
- [Ger01] Gerdes, E., *Qualitative Anorganische Analyse*, second ed., Springer-Verlag Berlin Heidelberg, Heidelberg, 2001.
- [GfD07] GD Gesellschaft für Dermopharmazie e.V.: *Wirkstoffdossiers für externe dermatologische Rezepturen*, GD Gesellschaft für Dermopharmazie, Köln 2007, Seite 18.
- [Gou04] Gouin, S., Microencapsulation: Industrial appraisal of existing technologies and trends, *Trends Food Sci. Technol.* 15 (2004) 330–347. doi:10.1016/j.tifs.2003.10.005.

- [Gra97] Grassmann, P. Widmer, F., Sinn, H., Einführung in die thermische Verfahrenstechnik, Walter de Gryter, Berlin, 1997.
- [Han00] Hansen, C. M., Hansen Solubility Parameter – A User’s Handbook, first ed., CRC Press LLC, Boca Raton, 2000.
- [Han07] Hansen, C. M., Hansen Solubility Parameter – A User’s Handbook, second ed., CRC Press LLC, Boca Raton, 2007.
- [Hat12] Hatkar, U.N., Gogate, P.R., Process intensification of anti-solvent crystallization of salicylic acid using ultrasonic irradiations, Chem. Eng. Process. Process Intensif. 57-58 (2012) 16–24. doi:10.1016/j.cep.2012.04.005.
- [Hel12] Helmdach, L., Feth, M.P., Ulrich, J., Online analytical investigations on solvent-, temperature- and water vapour-induced phase transformations of citric acid, Cryst. Res. Technol. 47 (2012) 967–984. doi:10.1002/crat.201200215.
- [Hen03] Henry, W., Experiments on the Quantity of Gases Absorbed by Water, at Different Temperatures, and under Different Pressures, Philos. Trans. R. Soc. London. 93 (1803) 29–274. doi:10.1098/rstl.1803.0004.
- [Hua16] Huang, J., Yin, Q., Ulrich, J., The Effect of Dissolved Gases as Impurities on Crystallization, Chem. Eng. Technol. 39 (2016) 1213–1218. doi:10.1002/ceat.201500674.
- [IFA16a] IFA Institut für Arbeitsschutz der Deutschen Gesetzlichen Unfallversicherung, GESTIS-Stoffdatenbank: D-Glucose [02.08.2016].
- [IFA16b] IFA Institut für Arbeitsschutz der Deutschen Gesetzlichen Unfallversicherung, GESTIS-Stoffdatenbank: Natriumacetat [10.08.2016].
- [IFA16c] IFA Institut für Arbeitsschutz der Deutschen Gesetzlichen Unfallversicherung, GESTIS-Stoffdatenbank: Salicylsäure [15.08.2016].

- [Jon06] Jones, M.J., Dette, S.S., Ulrich, J., Rapid crystal growth without inherent supersaturation induced by nanoscale fluid flows?, *Cryst. Res. Technol.* 41 (2006) 5–9. doi:10.1002/crat.200510521.
- [Jon60] Jones, A.H., Sublimation Pressure Data for Organic Compounds, *J. Chem. Eng. Data.* 5 (1960) 196–200. doi:10.1021/je60006a019.
- [Kak12a] Kakran, M., Sahoo, N.G., Tan, I.L., Li, L. Preparation of nanoparticles of poorly water-soluble antioxidant curcumin by antisolvent precipitation methods, *J. Nanoparticle Res.* 14 (2012). doi:10.1007/s11051-012-0757-0.
- [Kak12b] Kakran, M., Sahoo, N.G., Li, L., Judeh, Z. Judeh, Fabrication of quercetin nanoparticles by anti-solvent precipitation method for enhanced dissolution, *Powder Technol.* 223 (2012) 59–64. doi:10.1016/j.powtec.2011.08.021.
- [Kak13] Kakran, M., Sahoo, N.G., Li, L., Judeh, Z., Particle size reduction of poorly water soluble artemisinin via antisolvent precipitation with a syringe pump, *Powder Technol.* 237 (2013) 468–476. doi:10.1016/j.powtec.2012.12.029.
- [Kaw84] Kawashima, Y., Development of Spherical Crystallization Technique and Its Application to Pharmaceutical Systems, *Arch. Pharm. Res.* 7 (1984) 145–151. doi:10.1007/BF02856629.
- [Kel98] Keller, K.L., Fenske, N.A., Uses of vitamins A, C, and E and related compounds in dermatology: A review, *J. Am. Acad. Dermatol.* 39 (1998) 611–625. doi:10.1016/S0190-9622(98)70011-8.
- [Kim09] Kim, J.W., Kim, J.K., Kim, H.S., Koo, K.K., Characterization of liquid inclusion of rdx crystals with a cooling crystallization, *Cryst. Growth Des.* 9 (2009) 2700–2706. doi:10.1021/cg801343b.
- [Kir91] Kirby, C.J., White, C.J., Rigby, N., Covxon, D.T., Law, B.A., Stabilization of ascorbic acid by microencapsulation in liposomes, *International Journal of Food Science & Technology* 26 (1991), 437-449. doi: 10.1111/j.1365-2621.1991.tb01988.x.

- [Kre46] Kretschmer, C.B., Nowakowska, J., Wiebe, R., Solubility of Oxygen and Nitrogen in Organic Solvents from -25 ° to 50 °C ., *Ind. Eng. Chem.* 38 (1946) 506–509.
- [Leb99] Lebwahl, M., The role of salicylic acid in the treatment of psoriasis, *Int. J. Dermatol.* 38 (1999) 16–24. <http://www.ncbi.nlm.nih.gov/pubmed/10065604>.
- [Lew15] Lewis, A., Seckler, M., Kramer, H., v. Romalen, G., *Industrial Crystallization - Fundamentals and Applications*, first ed., Cambridge University Press, Cambridge, 2015.
- [Li11] Li, C., Li, C., Le, Y., Chen, J.F., Formation of bicalutamide nanodispersion for dissolution rate enhancement, *Int. J. Pharm.* 404 (2011) 257–263. doi:10.1016/j.ijpharm.2010.11.015.
- [Lim13] Lim, J., Jang, S., Cho, H.K., Shin, M.S., Kim, H., Solubility of salicylic acid in pure alcohols at different temperatures, *J. Chem. Thermodyn.* 57 (2013) 295–300. doi:10.1016/j.jct.2012.09.006.
- [Lon13] Lonare, A. A., Patel, S.R., Antisolvent Crystallization of Poorly Water Soluble Drugs, *Int. J. Chem. Eng. Appl.* 4 (2013) 337–341. doi:10.7763/IJCEA.2013.V4.321.
- [Lor98] Lorenzo-Lamosa, M.L., Remuñán-López, C., Vila-Jato, J.L., Alonso, M.J., Design of microencapsulated chitosan microspheres for colonic drug delivery, *J. Control. Release.* 52 (1998) 109–118. doi:10.1016/S0168-3659(97)00203-4.
- [Mal04] Mallet, F., Petit, S., Lafont, S., Billot, P., Lemarchand, D., Coquerel, G., Crystal Growth Mechanism in a Solution of Hollow Whiskers of Molecular Compounds, *Cryst. Growth Des.* 4 (2004) 965–969. <http://pubs.acs.org/doi/abs/10.1021/cg030046e>.
- [Man09] Manela-Azulay, M., Bagatin, E., Cosmeceuticals vitamins, *Clin. Dermatol.* 27 (2009) 469–474. doi:10.1016/j.clindermatol.2009.05.010.

- [Man72] Mannan, K.M., Rahaman, M.O., Crystallographic data for sodium acetate trihydrate, sodium acetate tetrahydrate, and 2,5-bis(benzylidene)cyclohexanone, *Acta Crystallogr. Sect. B Struct. Crystallogr. Cryst. Chem. B28* (1972) 320. doi:10.1107/S0567740872002262.
- [Mar11] Martins, D., Stelzer, T., Ulrich, J., Coquerel, G., Formation of Crystalline Hollow Whiskers as Relics of Organic Dissipative Structures, *Cryst. Growth Des.* 11 (2011) 3020–3026. doi:10.1021/cg2002892.
- [Mat09] Matsuda, H., Kaburagi, K., Matsumoto, S., Kurihara, K., Tochigi, K., Tomono, K. Solubilities of Salicylic Acid in Pure Solvents and Binary Mixtures Containing Cosolvent Solubilities of Salicylic Acid in Pure Solvents and Binary Mixtures Containing Cosolvent, *J. Chem. Eng. Data.* 54 (2009) 480–484. doi:10.1021/je800475d.
- [Mat12] Mathlouthi, M., Benmessaoud, G., Rogé, B., Role of water in the polymorphic transitions of small carbohydrates, *Food Chem.* 132 (2012) 1630–1637. doi:10.1016/j.foodchem.2011.11.103.
- [Mik05] Miki, H., Fukunaga, R., Asakuma, Y., Maeda, K., Fukui, K., Distribution of dye into KDP crystals in a continuous MSMR crystallizer, *Sep. Purif. Technol.* 43 (2005) 77–83. doi:10.1016/j.seppur.2004.10.006.
- [Mon06] Montes, I., Sanabria, D., García, M., Castro, J., Fajardo, J., A Greener Approach to Aspirin Synthesis Using Microwave Irradiation, *J. Chem. Educ.* 83 (2006) 628-631. doi:10.1021/ed083p628.
- [Mos14] Mostafavi, M., Petersen, S., Ulrich, J., Effect of Particle Shape on Inline Particle Size Measurement Techniques, *Chem. Eng. Technol.* 37 (2014) 1721–1728. doi:10.1002/ceat.201400212.
- [Mos15] Mostafavi, M., Ulrich, J., Monitoring phase transitions of crystals in-line, *Adv. Powder Technol.* 26 (2015) 657–664. doi:10.1016/j.apt.2015.01.018.
- [Mul01] Mullins, J. W., *Crystallization*, fourth ed., Reed Educational and Professional Publishing Ltd, Oxford, 2001.

- [Mye02] Myerson, A.S., Handbook of Industrial Crystallization, second ed., Butterworth-Heinemann, Woburn, 2002.
- [Naj08] Najafi, A.S., Xu, Z., Masliyah, J., Measurement of sliding velocity and induction time of a single micro-bubble under an inclined collector surface, *Can. J. Chem. Eng.* 86 (2008) 1001–1010. doi:10.1002/cjce.20116.
- [Nel02] Nelson, G., Application of microencapsulation in textiles, *Int. J. Pharm.* 242 (2002) 55–62. doi:10.1016/S0378-5173(02)00141-2.
- [Nor06] Nordström, F.L., Rasmuson, A.C., Solubility and Melting Properties of Salicylic Acid, *J. Chem. Eng. Data.* 51 (2006) 1668–1671. doi:10.1021/je060134d.
- [Nor99a] Nordhoff, S., Dümpelmann, R., Wagner, G., Ulrich, J., Vergrößerung der spezifischen Oberfläche von Kristallen durch gezieltes Nutzen von Pseudopolymorphen, *Chemie Ing. Tech.* 71 (1999) 487–490.
- [Nor99b] Nordhoff, S., Zur Pseudopolymorphologie unter Lösungsmiteleinfluss., Dissertation, Universität Bremen, Aachen: Shaker Verlag, 1999
- [Oma99] Omar, W., Ulrich, J., Application of Ultrasonics in the On-line Determination of Supersaturation, *Cryst. Res. Technol.* 34 (1999) 379–389.
- [Par12] Park, M.W., Yeo, S.-D., Antisolvent crystallization of carbamazepine from organic solutions, *Chem. Eng. Res. Des.* 90 (2012) 2202–2208. doi:10.1016/j.cherd.2012.05.001.
- [Pas12] Pastuszka, M., Kaszuba, A., Status of combination drugs with betamethasone dipropionate and salicylic acid in the treatment of skin diseases, *Postep. Dermatologii i Alergol.* 29 (2012) 196–204.
- [Pau13] Paulino, A.S., Rauber, G., Campos, C.E.M., Maurício, M.H.P., de Avillez, R.R., Capobianco, G., Cardoso, S.G., Cuffini, S.L. Cuffini, Dissolution enhancement of Deflazacort using hollow crystals prepared by antisolvent crystallization process, *Eur. J. Pharm. Sci.* 49 (2013) 294–301. doi:10.1016/j.ejps.2013.03.014

- [Pen06] Pena, M.A., Reillo, A., Escalera, B., Bustamante, P., Solubility parameter of drugs for predicting the solubility profile type within a wide polarity range in solvent mixtures, *Int. J. Pharm.* 321 (2006) 155–161. doi:10.1016/j.ijpharm.2006.05.014.
- [Per13] Perry, A.R., Peruffo, M., Unwin, P.R., Quantitative Plane-Resolved Crystal Growth and Dissolution Kinetics by Coupling In Situ Optical Microscopy and Diffusion Models: The Case of Salicylic Acid in Aqueous Solution, *Cryst. Growth Des.* 13 (2013) 614–622. doi:10.1021/cg301282q.
- [Prz15] Przybyłek, M., Cysewski, P., Pawelec, M., Ziółkowska, D., Kobierski, M., On the origin of surface imposed anisotropic growth of salicylic and acetylsalicylic acids crystals during droplet evaporation, *J. Mol. Model.* 21 (2015) 1–12. doi:10.1007/s00894-015-2599-z.
- [Ras92] Raskin, I., Role of salicylic acid in plants, *Annu. Rev. Plant Physiol. Plant Mol. Biol.* 43 (1992) 439–463. doi:10.1146/annurev.pp.43.060192.002255.
- [Riz13] Rizkalla, C.M.Z., Aziz, R.I., Soliman, I.I., Microencapsulation of hydroxyzine HCl by thermal phase separation: in vitro release enhancement and in vivo pharmacodynamic evaluation, *J. Microencapsulation*, 18 (2013) 196-209.
- [Rod99] Rodríguez-Hornedo, N., Murphy, D., Significance of controlling crystallization mechanisms and kinetics in pharmaceutical systems, *J. Pharm. Sci.* 88 (1999) 651–660. doi:10.1021/js980490h.
- [Sai99] Saito, N., Yokota, M., Sato, A., Kubota, N., Growth enhancement and liquid-inclusion formation by contacts on NaCl crystal, *AIChE J.* 45 (1999) 1153–1156. doi:10.1002/aic.690450522.
- [Sat14] Sato, T., Hamada, Y., Sumikawa, M., Araki, S., Yamamoto, H., Solubility of Oxygen in Organic Solvents and Calculation of the Hansen Solubility Parameters of Oxygen, *Ind. Eng. Chem. Res.* 53 (2014) 19331–19337. doi:10.1021/ie502386t.

- [Say02] Sayan, P., Ulrich, J., The effect of particle size and suspension density on the measurement of ultrasonic velocity in aqueous solutions, *Chem. Eng. Process. Process Intensif.* 41 (2002) 281–287. doi:10.1016/S0255-2701(01)00143-X.
- [Sch10] Schuster, A., Stelzer, T., Petersen, S., Ulrich, J., Closed Crystalline Tubes as a Container System, *Chem. Eng. Technol.* 33 (2010) 787–790. doi:10.1002/ceat.200900618.
- [Sch11a] Schuster, A., Stelzer, T., Ulrich, J., Generation of Crystalline Hollow Needles: New Approach by Liquid-Liquid Phase Transformation, *Chem. Eng. Technol.* 34 (2011) 599–603. doi:10.1002/ceat.201000511.
- [Sch11b] Schuster, A., Stelzer, T., Ulrich, J., Hollow Crystalline Needles: Filled and Closed, in: B. Biscans, M. Mazzotti (Eds.), *Proc. 18th ISIC, Zürich (Switzerland)*, 2011: pp. 369–370.
- [Sch13] Schuster, A., Investigations on the Formation of Hollow Acicular Crystals and their Usage as Container Systems, PhD-thesis, Martin Luther University Halle-Wittenberg, Shaker Verlag, 2013.
- [Sei15] Seidel, J., Ulrich, J. Generation of Crystalline Microcontainers of Salicylic Acid, *Chem. Eng. Technol.* 38 (2015) 984–990. doi:10.1002/ceat.201400716.
- [Sei16] Seidel, J., Ulrich, J., Encapsulation of Agents inside Crystals as Liquid Inclusions, *Chem. Eng. Technol.* 39 (2016) 1237–1241. doi:10.1002/ceat.201600031.
- [Sei17] Seidel, J. Ulrich, J., Effects of solution degassing on solubility, crystal growth and dissolution—Case study: Salicylic acid in methanol, *J. Cryst. Growth* 459 (2017) 153-158.
- [Sha08] Shalmashi, A., Eliassi, A., Solubility of Salicylic Acid in Water, Ethanol, Carbon Tetrachloride, Ethyl Acetate, and Xylene, *J. Chem. Eng. Data.* 53 (2008) 199–200.

- [Sim05] Simon, C, Männle, F., High performance coating based on hybrid-organic-inorganic Polymers, *PCI*, 201 (2005) 10, 104-110.
- [Sim07] Simon, C. Designer packaging, *Eur. Coatings J.* 49 (2007) 2, 32-44.
- [Tav79] Tavaré, N.S., Chivate, M.R., Growth and Dissolution Kinetics of Potassium Sulphate Crystals in a Fluidised Bed Crystalliser, *Trans. Inst. Chem. Eng.* 57 (1979) 35–42.
- [Til91] Tiller, W.A., *The Science of Crystallization, Macroscopic Phenomena and Defect Generation*, first ed., Cambridge University Press, Cambridge, 1991.
- [Tok75] Tokunaga, J., Oxygen, Nitrogen, and Carbon Dioxide in Aqueous, *J. Chem Engin Data.* 20 (1975) 41–46. doi:10.1021/je60064a025.
- [Tsu01] Tsuji, K., Microencapsulation of pesticides and their improved handling safety, *J. Microencapsulation* 18 (2001) 2, 137-147.
- [Udd01] Uddin, M.S., Hawlader, M.N.A., Zhu, H.J., Microencapsulation of ascorbic acid: effect of process variables on product characteristics, *J. Microencapsulation* 12 (2001) 2, 199-209.
- [Ulr13] Ulrich, J., Schuster, A., Stelzer, T., Crystalline coats or hollow crystals as tools for product design in pharmaceutical industry, *J. Cryst. Growth.* 362 (2013) 235–237. doi:10.1016/j.jcrysgro.2011.10.060.
- [Wac11] Wachsmuth, A., Stelzer, T., Ulrich, J., Decreasing the Diameter of Crystalline Tubes and an Approach to Explain its Nucleation, *Chem. Eng. Technol.* 34 (2011) 578–582. doi:10.1002/ceat.201000518.
- [Wal11a] Waldschmidt, A., Couvrat, N., Berton, B., Dupray, V., Morin, S., Petit, S., Coquerel, G., Impact of Gas Composition in the Mother Liquor on the Formation of Macroscopic Inclusions and Crystal Growth Rates. Case Study with Ciclopirox Crystals, *Cryst. Growth Des.* 11 (2011) 2463–2470. doi:10.1021/cg200245m.
- [Wal11b] Waldschmidt, A., Rietveld, I., Couvrat, N., Sanselme, M., Berton, B., Mahé, N., Petit, S., Céolin, R., Coquerel, G., About Aged Heterogeneous Liquid

- Inclusions Inside Organic Crystals in Relation to Crystal Formation, Structure and Morphology, *Cryst. Growth Des.* 11 (2011) 2580–2587.
- [Wan06] Wang, W., Liu, X., Xie, Y., Zhang, H., Yu, W., Xiong, Y., Xie, W., Ma, X., Microencapsulation using natural polysaccharides for drug delivery and cell implantation, *J. Mater. Chem.* 16 (2006) 32523267. doi:10.1039/b603595g.
- [Wan07] Wang, Z., Chen, J.F., Le, Y., Shen, Z.G., Yun, J., Preparation of ultrafine beclomethasone dipropionate drug powder by antisolvent precipitation, *Ind. Eng. Chem. Res.* 46 (2007) 4839–4845. doi:10.1021/ie0615537.
- [Wik08] Wikström, H., Rantanen, J., Gift, A.D., Taylor, L.S., Toward an Understanding of the Factors Influencing Anhydrate-to-Hydrate Transformation Kinetics in Aqueous Environments, *Cryst. Growth Des.* 8 (2008) 2684–2693. doi:10.1021/cg070629e.
- [Wil77] Wilcox, W.R., MORPHOLOGICAL STABILITY OF A CUBE GROWING FROM SOLUTION WITHOUT CONVECTION, *J. Cryst. Growth.* 38 (1977) 73–81.
- [Woh09] Wohlgemuth, K., Kordylla, A., Ruether, F., Schembecker, G., Experimental study of the effect of bubbles on nucleation during batch cooling crystallization, *Chem. Eng. Sci.* 64 (2009) 4155–4163. doi:10.1016/j.ces.2009.06.041.
- [Woh10] Wohlgemuth, K., Ruether, F., Schembecker, G., Sonocrystallization and crystallization with gassing of adipic acid, *Chem. Eng. Sci.* 65 (2010) 1016–1027. doi:10.1016/j.ces.2009.09.055.
- [Xu06] Xu, Y., Yin, H., Lu, Y., Yin, S., Wu, H., Jiang, T., Wada, Y., Size- and morphology-controlled preparation of extra fine salicylic acid crystallites by organic modifiers, *Mater. Lett.* 60 (2006) 2873–2876. doi:10.1016/j.matlet.2006.02.005.
- [Yos01] Yoshinaga, T., Tsuchida, M., Toyose, Y., Hiratsuka, H., Yamaye, M., Polyvinyl alcohol as a useful indicator on iodometry. (II): Temperature dependence of iodine recovery and the correction method of iodine

- concentration in the lower detection limit region., *Anal. Sci.* 20 (2004) 549–552. doi:10.2116/analsci.20.549.
- [Zha99] Zhang, G.G.Z., Grant, D.J.W., Incorporation Mechanism of Guest Molecules in Crystals: Solid Solution or Inclusion?, *Int. J. Pharm.* 181 (1999) 61–70.
- [Zha05] Zhang, G.G.Z., Grant, D.J.W., Formation of Liquid Inclusions in Adipic Acid Crystals during Recrystallization from Aqueous Solutions, *Cryst. Growth Des.* 5 (2005) 319–324. doi:10.1021/cg049868h.

12. Appendix

12.1. Crystallization behavior of SA

12.1.1 Saturation curve

Tab. 12.1: SA mass fraction of saturated solutions measured at different temperatures.

Temperature [°C]	Non-degassed		Degassed	
	Mass fraction	Confidence interval (95%)	Mass fraction	Confidence interval (95%)
	[%]	[%]	[%]	[%]
5	31.4	0.2	31.4	0.1
10	34.08	0.06	33.8	0.2
15	36.11	0.03	36.1	0.1
20	38.36	0.05	38.3	0.2
25	40.19	0.09	40.1	0.1
30	41.3	0.2	41.2	0.3

12.1.2 Solubility and MZW

Tab. 12.2: Nucleation and solubility temperatures depending on solution mass fraction of SA in MeOH measured by means of US-technique using heating rates of 2 K h⁻¹.

Non-degassed			Degassed		
Nucleation temperature [°C]	Solubility temperature [°C]	Mass fraction [%]	Nucleation temperature [°C]	Solubility temperature [°C]	Mass fraction [%]
24.10	27.37	39.57	24.37	28.43	40.22
24.29	27.46	39.57	22.24	24.68	38.68
23.95	28.37	40.11	17.51	21.95	37.65
21.05	25.76	38.74	11.34	17.77	34.98
18.80	22.35	37.00	6.93	14.91	33.26
19.15	22.12	36.93			
19.03	22.01	36.90			
14.03	17.99	35.03			
10.91	15.38	33.84			

Tab. 12.3: Nucleation and solubility temperatures depending on solution mass fraction of SA in MeOH measured by means of US-technique using heating rates of 5 K h⁻¹.

Non-degassed			Degassed		
Nucleation temperature [°C]	Solubility temperature [°C]	Mass fraction [%]	Nucleation temperature [°C]	Solubility temperature [°C]	Mass fraction [%]
22.55	27.60	39.56	23.99	28.75	40.21
23.39	27.46	39.58	16.79	26.14	38.58
23.18	28.94	40.11	20.31	25.33	38.65
19.29	26.71	38.74	16.94	22.28	37.02
17.16	21.69	36.69	10.47	17.63	34.99
11.79	18.10	35.01	6.81	13.91	33.36
8.78	15.54	33.82			

Tab. 12.4: Nucleation and solubility temperatures depending on solution mass fraction of SA in MeOH measured by means of US-technique using heating rates of 10 K h⁻¹.

Non-degassed			Degassed		
Nucleation temperature [°C]	Solubility temperature [°C]	Mass fraction [%]	Nucleation temperature [°C]	Solubility temperature [°C]	Mass fraction [%]
22.61	27.80	39.54	24.22	29.30	40.20
22.93	27.77	39.57	16.85	26.10	38.57
23.70	29.60	40.10	20.08	25.76	39.33
19.17	27.75	38.71	15.81	23.00	37.00
15.95	23.10	36.68	17.03	23.34	37.07
11.69	18.85	35.00	8.74	18.73	34.96
8.95	15.95	33.76	4.46	16.80	33.56
			3.66	14.57	33.32

Tab. 12.5: Nucleation and solubility temperatures depending on solution mass fraction of SA in MeOH measured by means of US-technique using heating rates of 15 K h⁻¹.

Non-degassed			Degassed		
Nucleation temperature [°C]	Solubility temperature [°C]	Mass fraction [%]	Nucleation temperature [°C]	Solubility temperature [°C]	Mass fraction [%]
20.66	28.47	39.53	22.73	30.42	40.21
22.23	28.33	39.55	19.78	25.91	38.84
24.01	30.27	40.10	19.93	26.19	38.64
18.81	28.26	38.71	16.71	23.83	37.06
15.29	23.43	36.69	16.62	23.93	37.00
11.55	19.23	34.98	9.76	19.61	34.86
9.48	16.49	33.82	4.58	17.44	33.57
			5.54	15.98	33.30

12.1.3 Growth rate

Tab. 12.6: Growth rates of SA in MeOH measured at 10 °C.

Non-degassed		Degassed	
Supersaturation	Growth rate	Supersaturation	Growth rate
[-]	m s ⁻¹	[-]	m s ⁻¹
0.0065	1.26E-07	0.0059	1.12E-07
0.0002	2.73E-09	0.0056	4.51E-08
0.005	9.35E-08	0.0092	1.34E-07
0.0086	1.01E-07	0.0058	8.93E-08
0.0012	1.28E-08	0.0019	2.49E-08
0.0013	1.60E-08	0.0032	4.19E-08
0.0046	6.95E-08	0.0037	5.83E-08
		0.0082	2.03E-07

Tab. 12.7: Growth rates of SA in MeOH measured at 30 °C.

Non-degassed		Degassed	
Supersaturation	Growth rate	Supersaturation	Growth rate
[-]	m s ⁻¹	[-]	m s ⁻¹
0.0258	9.57E-07	0.0104	1.93E-07
0.0263	1.40E-06	0.0082	1.94E-07
0.0022	3.02E-08	0.0204	9.12E-07
0.0036	6.26E-08	0.0179	8.43E-07
0.0063	9.65E-08	0.0186	4.28E-07
0.007	1.22E-07	0.0166	5.31E-07
0.0145	3.77E-07	--	--
0.0174	4.42E-07	--	--

12.1.4 Dissolution rate

Tab. 12.8: Dissolution rates of SA in MeOH measured at 10 °C.

Non-degassed		Degassed	
Saturation degree	Dissolution rate	Saturation degree	Dissolution rate
[-]	$\Delta\% \text{ s}^{-1}$	[-]	$\Delta s(-1)$
1.473	6.00E-05	1.0625	1.33E-04
1.0798	1.10E-04	1.2207	1.32E-04
1.2515	1.00E-04	1.358	1.07E-04
1.3804	9.00E-05	1.4848	1.81E-04
1.5463	6.00E-05	1.7424	8.80E-05
1.2801	7.00E-05	1.0903	1.71E-04
1.4409	9.00E-05	1.2464	1.32E-04
1.6055	6.00E-05	1.3865	2.04E-04
1.7511	7.00E-05	1.5158	9.96E-05
		1.6469	7.76E-05
		1.7924	7.39E-05
		1.9827	9.96E-05

Tab. 12.9: Dissolution rates of SA in MeOH measured at 30 °C.

Non-degassed		Degassed	
Saturation degree	Dissolution rate	Saturation degree	Dissolution rate
[-]	$\Delta\% \text{ s}^{-1}$	[-]	$\Delta\% \text{ s}^{-1}$
1.0572	5.20E-04	1.0622	6.00E-04
1.2196	1.00E-04	1.2191	1.90E-04
1.3533	1.30E-04	1.3458	1.90E-04
1.478	1.30E-04	1.4666	1.40E-04
1.5957	1.20E-04	1.5878	1.40E-04
1.8152	8.00E-05	1.802	1.20E-04
1.0753	0.00139	1.9011	1.80E-04
1.2087	5.00E-04	1.0605	3.40E-04
1.3248	1.10E-04	1.2186	1.70E-04
1.4385	6.00E-05	1.4667	9.00E-05
1.5442	1.00E-04	1.5877	1.70E-04
1.6465	1.00E-04	1.6978	7.00E-05
1.7439	1.10E-04	1.5455	1.10E-04
1.9251	5.00E-05	1.7386	1.20E-04

12.2. Ternary phase diagram

Tab. 12.10: Experimental values of water, EtOH and SA content from investigations of SA solubility in EtOH-water-mixtures.

Sample	No.	Water content [%]	EtOH content [%]	SA content [%]
Distilled water saturated with SA	I	97 ± 33	2. ± 33	0.6 ± 0.1
	II	98 ± 21	1 ± 21	0.6 ± 0.4
	III	97 ± 33	2 ± 33	0.6 ± 0.2
5% SA in EtOH	I	68 ± 1	30 ± 2	1.7 ± 0.5
	II	67 ± 26	30 ± 29	2 ± 3
	III	68 ± 29	30 ± 30	1.9 ± 0.2
	IV	65 ± 2	34 ± 3	1.9 ± 0.2
	V	66 ± 4	32 ± 5	1.9 ± 0.5
	VI	70 ± 8	29 ± 8	1.6 ± 0.2
10% SA in EtOH	I	70 ± 7	29 ± 7	1.4 ± 0.4
	II	54 ± 71	40 ± 71	3.4 ± 0.06
	III	63 ± 6	34 ± 7	2.8 ± 0.3
	IV	58 ± 3	37 ± 3	4.8 ± 0.3
	V	61 ± 24	30 ± 24	5.0 ± 0.1
	VI	61 ± 1	34 ± 2	4.7 ± 0.4
20% SA in EtOH	I	60 ± 8	37 ± 9	3 ± 1
	II	49 ± 10	42 ± 22	10 ± 12
	III	49 ± 4	43 ± 4	7.6 ± 0.3
	IV	42 ± 21	45 ± 21	12.51 ± 0.08
	V	43 ± 1	44 ± 1	12.84 ± 0.06
	VI	44.6 ± 0.2	42 ± 0.6	13.4 ± 0.4
25% SA in EtOH	I	32 ± 4	50 ± 15	19 ± 12
	II	32 ± 4.0	53 ± 6	15 ± 2
	III	33 ± 2	50 ± 3	17.0 ± 0.9
EtOH saturated with SA	I	0.64 ± 0.06	75.5 ± 5.4	23.9 ± 5.3
	II	0.6 ± 0.2	69.4 ± 0.6	29.9 ± 0.5
	III	0.60 ± 0.08	69.2 ± 0.4	30.2 ± 0.4

Eigenständigkeitserklärung

Hiermit erkläre ich, dass ich die vorliegende Arbeit selbstständig verfasst und keine anderen als die angegebenen Quellen und Hilfsmittel benutzt habe. Die Stellen meiner Arbeit, die wörtlich oder inhaltlich aus anderen Werken entnommen sind, habe ich in jedem Fall kenntlich gemacht. Dasselbe gilt sinngemäß für Tabellen und Abbildungen.

Berlin, den 29.10.2017



Julia Seidel

Lebenslauf

Julia Seidel

Geb. am 05.06.1989 in Annaberg-Buchholz

Seit 12/2016

Referentin

Bundesamt für Verbraucherschutz und Lebensmittelsicherheit

05/2013 – 09/2016

Wissenschaftliche Mitarbeiterin

Martin-Luther-Universität Halle-Wittenberg, Zentrum für Ingenieurwissenschaften am Lehrstuhl für Thermische Verfahrenstechnik

10/2008 – 04/2013

Studium der Lebensmittelchemie

Martin-Luther-Universität Halle-Wittenberg

09/2005-07/2008

Berufliches Schulzentrum für Ernährung und Hauswirtschaft Schneeberg

Publikationsverzeichnis

Peer-review-Artikel

- 2017 J. Seidel, J. Ulrich Effects of solution degassing on solubility, crystal growth and dissolution—Case study: Salicylic acid in methanol, *Journal of Crystal Growth* 459, 2017, 153-158..
- 2016 J. Seidel, J. Ulrich: Encapsulation of Agents inside Crystals as Liquid Inclusions, *Chemical Engineering and Technology* 39 (7), 2016, 1237-1241.
- 2016 L. Nemdili, O. Koutchoukali, J. Seidel, J. Ulrich: Crystallization Kinetics of Citric Acid Anhydrate, *Crystal Growth* 451, 2016, 88-94.
- 2015 J. Seidel, J. Ulrich: Generation of Crystalline Micro Containers of Salicylic Acid, *Chemical Engineering and Technology* 38 (6), 2015, 984-990.

Proceedingbeiträge

- 2016 J. Seidel, J. Ulrich Effects of solution degassing on solubility, crystal growth and dissolution—Case study: Salicylic acid in methanol, *Proc. of ACTS 2016*, edited by David. H. Wei, 107-109.
- 2015 J. Seidel, J. Ulrich: Encapsulation of Agents inside Crystals as Liquid Inclusions, *Proc. of BIWIC 2015*, edited by Kwan-Joo Kim and Kyeongsill Lee, Deajon, 222-228.
- 2015 L. Nemdili, O. Koutchoukali, J. Seidel, J. Ulrich: Crystallization Kinetics of Citric Acid Anhydrate, *Proc. of BIWIC 2015*, edited by Kwan-Joo Kim and Kyeongsill Lee, Deajon, 327-334.
- 2014 J. Seidel, J. Ulrich: Generation of Crystalline Micro Containers of Salicylic Acid, *Proc. of BIWIC 2014*, edited by Gérard Coquerel, Yohann Cartigny and Nicolas Couvrat, Rouen, 1-10.
- 2014 J. Seidel, J. Ulrich: Influence of solved gases on solubility and crystallization behavior – Case study salicylic acid, *Proc. of ISIC 2014*, edited by Béatrice Biscans and Marco Mazzotti, 412-414.